Prospects For Direct Air Capture Onboard Floating Offshore Wind Turbines

by

Ryan Foxall
B.Eng., The University of Victoria, 2020

A Thesis Submitted in Partial Fulfillment of the
Requirements for the Degree of

Master of Applied Science

in the Department of Mechanical Engineering

Prospects For Direct Air Capture Onboard Floating Offshore Wind Turbines

by

Ryan Foxall
B.Eng., The University of Victoria, 2020

Supervisory Committee

Dr. C. Crawford, Supervisor
(Department of Mechanical Engineering)

Dr. H. Struchtrup, Committee Member
(Department of Mechanical Engineering)

Dr. A. Rowe, Committee Member
(Department of Mechanical Engineering)

ABSTRACT

Direct air capture (DAC) is a method for removing CO_2 directly from air. To date, no studies have considered installing DAC offshore. This thesis explores offshore implementation, and the changes that may be necessary in order to complete it.

First, a design using modular solid sorbent DAC units is proposed onboard the deck of a floating offshore wind turbine. The main objective is to understand detailed flow characteristics, and CO_2 dispersion around air contactors when placed in close proximity to one another. Two dimensional (2D) and three dimensional (3D) computational fluid dynamics is used. The pressure drop through a representative commercial scale unit was found using 2D simulations. Various adsorbents commonly used in practice are examined, with a pressure loss curve obtained for each one. 3D simulations analyze the impact of ambient wind conditions for local CO_2 mixing, as well the reduction in necessary fan work. Wind speeds at hub height (150m) greater than 24m/s, allowed fans to be turned off in upstream contactors; passively blowing air through the contactors using ambient wind. Thermal energy had a similar relationship; high wind speeds induced increased CO_2 mixing, thus greater concentration entering downstream units.

Second, design and energy demand changes from operating DAC offshore were explored. Parallel technologies offered insights, and further experimental work is suggested to bridge knowledge gaps. A configuration for air pre-treatment to remove aerosol salt particles contained in sea air is examined. Using a wire mesh demister pad to capture salt particles contained in the air, liquid solvent DAC systems had a greater change in pressure loss and fan energy requirement. An additional 79% pressure loss, and 194.4kWh/t-CO_2 of fan energy was incurred. Air pre-treatment is more pertinent with regards to solid sorbent DAC, resulting in an additional pressure loss of 20-28%, and fan energy input of 38.1kWh/t-CO_2. Solid sorbent DAC is likely more susceptible to performance changes as a result of aerosol salt particles contained in sea air, and aqueous based DAC more sensitive to dynamic motions encountered on floating platforms. Size, modularity, and lack of feed stock requirements lend solid sorbent DAC better to implementation far offshore, onboard floating platforms. Aqueous based DAC systems are likely restricted to shore/shore side deployment due to large unit sizes; and feed stock and waste transportation limitations.

Contents

List of Tables

List of Figures

Nomenclature

Constants

Symbol	Description	Value
c_μ	Turbulent viscosity constant	0.09
K	Von Karman constant	0.41
$\overline{R}$	Universal gas constant	8.314 J/mol-K

Greek Symbols

Symbol	Description	Unit
α	Separation efficiency of gas species	-
α	Toth fitting Parameter	-
β	Modified Toth isotherm parameter	kg/mol
ϵ	Dissipation rate of turbulent kinetic energy	m^2/s^3
η_{fan}	Fan efficiency	%
η_{II}	Second law efficiency	%
η_{s,CO_2}	Solid efficiency of CO_2 adsorption	%

η_{s,H_2O}	Solid efficiency of H_2O adsorption	%
γ	Modified Toth isotherm parameter	kg/mol
μ	Dynamic viscosity	kg/m s
Φ	Total concentration flux of "c" across surface area	mg/m^3s
ϕ	Void fraction/ porosity of bed	-
ρ_p	Demister packing density	kg/m^3
ρ_{ref}	Density of gas used in CFD analysis	kg/m^3
σ	Cross sectional area	m^2

Roman Symbols

Symbol	**Description**	**Unit**
A	Fixed media coefficient porous media model coefficient Alpha	-
B	Fixed media coefficient porous media model coefficient Beta	-
b	Toth affinity coefficient	1/MPa
b_0	Toth affinity coefficient at reference temperature	1/MPa
c	Passive scalar concentration	mg-CO_2/m^3
C_G	GAB isotherm parameter	-
C_m	GAB isotherm parameter	mol-H_2O/kg-sorbent
C_p	Specific heat capacity	J/kg K
c_p	Molar specific heat capacity	J/mol K

D	Diffusion coefficient/diffusivity	m^2/s
d	Distance in the direction of flow	m
D_p	Spherical particle diameter	m
D_w	Demister wire diameter	mm
ΔH	Heat of adsorption	J/mol
ΔH_{iso}	Isoteric heat of adsorption	J/kg K
ΔH_{vap}	Heat of vaporization	J/kg K
Δq_i	Equilibrium adsorption capacity of species "i"	mol/kg
F_{fan}	Force applied by the fan	N
j	Total mass flux of "c" across surface area	mg/m^2s
j_m	Volumetric mass flux	mg/m^3s
k	Turbulent kinetic energy	m^2/s^2
K_{ads}	GAB isotherm parameter	-
k_{LDF1}	Kinetic constant of the first order linear driving force model	-
k_{LDF2}	Kinetic constant of the second order linear driving force model	-
k_s	Sand grain roughness height	m
k_{toth}	Kinetic constant of the Toth rate equation	-
L	Length of bed in the direction of gas flow	m
$\dot{m}$	Mass flow rate	mg-CO_2/s

M_i	Molecular weight of species "i"	g/mol
m_i	Mass of species "i"	kg
n_i	Moles of species "i"	mol
n_s	Maximum adsorption capacity	mol-CO_2/kg-sorbent
n_{s0}	Maximum adsorption capacity at reference temperature	mol-CO_2/kg-sorbent
P_{fan}	Power requirement of the fan	W
p_{CO_2}	Partial pressure of CO_2	MPa
Δp	Pressure drop	Pa
p_{des}	Desorption pressure	MPa
∇p	Pressure gradient	Pa/m
$Q_{reaction}$	Reaction thermal energy	J/kg-CO_2
$Q_{sensible}$	Sensible thermal energy	J/kg-CO_2
$Q_{eq,th}$	Equilibrium thermal energy demand	J/kg-CO_2
q_e	Equilibrium loading	mol/kg
q_s	Maximum loading at any condition	mol/kg
RH	Relative humidity	%
S	Momentum source term	kg/m^2s^2
S_R	Reaction source term	mg-CO_2/m^3s
S_S	Pure source term	mg-CO_2/m^3s
T	Ambient temperature	K

t	Time	s
t	Toth exponent	-
T_0	Reference temperature	K
t_0	Toth exponent at reference temperature	-
T_{ads}	Adsorption temperature	K
T_{des}	Desorption temperature	K
U	Velocity	m/s
u	Fluid velocity	m/s
u^*	Friction velocity	m/s
u_{ref}	Velocity at reference height z_{ref}	m/s
V	Control volume	m^3
$\dot{V}$	Volumetric flow rate	m^3/s
v_s	Superficial gas velocity	m/s
$\bar{w}_{rev}$	Minimum thermodynamic work/Reversible work	J/mol-CO_2
X	Initial mole fraction of CO_2	-
X	Toth isotherm Parameter	-
x_i	Mole fraction of species "i"	-
z	Height	m
z_0	Aerodynamic roughness height	m
z_{ref}	Reference height of velocity u_{ref}	m

ACKNOWLEDGEMENTS

I would like to thank my:

family and friends for sticking with me and supporting me through the many years of my studies. It sure hasn't been the shortest route through, but it has been worth it in the end. I couldn't have done it without your continued support.

supervisor, Dr. Curran Crawford for inspiring me to work on climate solutions, mentoring, supporting, and encouraging me throughout my degree. I appreciate your patience and understanding and focus on balancing mental and physical health with work.

committee members, Dr. Andrew Rowe, and Dr. Henning Struchtrup for providing feedback on my thesis and engaging in insightful conversations to strengthen my research.

the Pacific Institute of Climate Solutions for funding my research work, and giving me the opportunity to take part in a dynamic team of researchers across multiple universities.

the Solid Carbon team for providing an engaging project to be apart of. It has been a pleasure to work with each and everyone of you, and I am excited to see the next deployment of the Solid Carbon concept in the future.

Chapter 1

Introduction

Climate change is one of the most pressing issues to be solved by society today. Although caused by a number of greenhouse gasses (GHG), the most commonly discussed is carbon dioxide (CO_2) due to its extremely long lifetime in the atmosphere. Rapid decarbonization is required across all sectors, and beyond this, it is now well understood that carbon dioxide must also be actively removed from the atmosphere. This is known as carbon dioxide removal (CDR), and technologies to assist in this are commonly referred to as negative emission technologies (NET). Virtually all scenarios modelled by the Intergovernmental Panel on Climate Change (IPCC) for reaching net-zero CO_2 emissions includes some form of CDR to offset anthropogenic emissions [1, 2]. Simple arithmetic shows that any leftover positive emission that can not be otherwise reduced, will need to be matched with an equal or greater negative emission to reach net-zero emissions. This is exemplified further in figure 1.1. Ambient CO_2 concentrations must fall below current levels experienced today, which is approximately 414 ppm as of 2021 [3].

Many options exist to remove CO_2 from the atmosphere, utilizing photosynthetic mechanisms or engineered approaches. The most common photosynthetic mechanisms include: coastal blue carbon, soil carbon management; and afforestation, reforestation, and improved forest management. It should be noted that many of the "nature-based" processes involve a great deal of engineering to implement. They also raise concerns about longevity/durability of storage. Carbon captured by means of photosynthesis can later be released, such as forest fires or decomposition of organic material. Its highly unlikely the scale of carbon removal required can be met solely

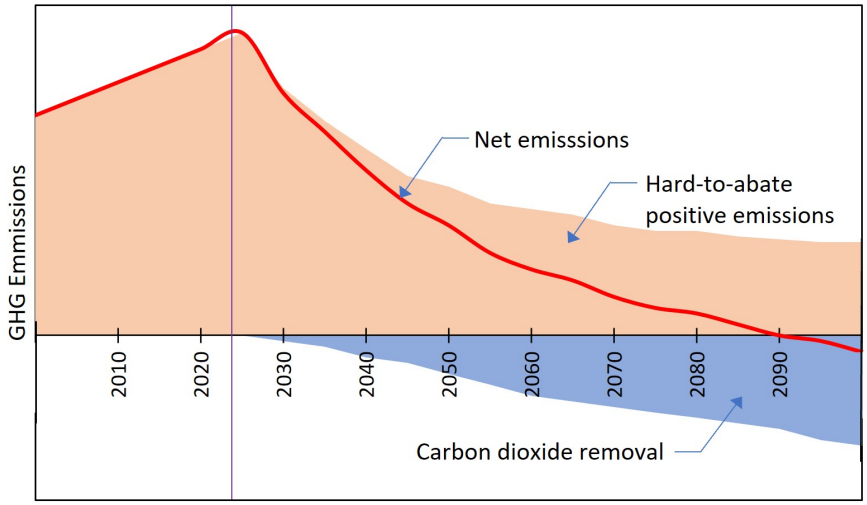

Figure 1.1: Emission projection for keeping global temperature rise below 2°C. Current year (2023) marked with vertical purple line. Carbon dioxide removal (blue) to offset hard to abate positive emissions (orange), with net zero emissions achieved towards the end of the century. Re-created from [4]

using nature based methods, and engineered approaches are likely to contribute to the CDR portfolio. The predominant engineered approaches include accelerated chemical weathering of rocks, waste biomass processing with carbon capture and storage, and direct air capture (DAC). These approaches are discussed in great detail in a recent book, CDR primer [5], as well as a recent report for CDR pathways for British Columbia by Todd at the Pacific Institute for Climate Sciences [6].

To increase the technological readiness of existing carbon capture systems leading to increased overall adoption of NETs; one can envision a pathway for the utilization of CO_2 for useful purposes. Carbon capture and utilization (CCU) as it is referred to, can also be coupled with storage, known as CCUS. One common pathway currently being deployed is DAC to enhanced oil recovery (EOR). Although this may be better than traditionally mined CO_2 for EOR, this is not a long term climate solution, and is merely a stepping stone to provide revenue for de-risking and scale up of the technology. CO_2 can also be combined with hydrogen to form synthetic fuels, as well as added to various products such as concrete, and plastics. Synthetic fuels are attractive in that if produced using purely renewable energy, the fuels are in a sense net-zero emission; as long as the carbon released through combustion, is then captured again from the atmosphere. This provides an opportunity to chemically

store energy that is difficult to transport, such as far offshore wind energy. Ishaq, Foxall, and Crawford [7] explored the generation of monoethanolamine (MEA), a chemical used for carbon capture, utilizing far offshore wind energy coupled with DAC and seawater electrolysis. Using 20 MW of offshore wind power, the designed system produces 8.7 kt/yr of monoethanolamine, 2.75 kt/yr of diethanolamine and 0.47 kt/yr of triethanolamine. Although these methods can provide a pathway to increase adoption while providing a revenue source; to provide real climate impact, CO_2 must be permanently removed from the atmosphere at large (gigatonne) scale.

Each carbon removal approach possess a unique opportunity and none are appropriate in every situation. One thing that is certain, is that as the world population increases, so will the competition for resources (land, water, feed stocks, and energy), alongside the need to remove carbon emissions that cannot be reduced by other means.

1.1 Background

As discussed, CO_2 must first be removed from the atmosphere, and then stored away permanently. The capture process is described in 1.1.1, and storage mechanisms are described in 1.1.2.

1.1.1 Capture

The atmosphere, and oceans are constantly equilibrating with one another, with carbon fluxes going between them to adjust for changes in the other. CO_2 can be captured from either carbon sink using a number of different methods. Capture can be done through biological means, relying on photosynthesis, or through technologically engineered solutions such as synthesized chemicals. Engineered approaches require a means of stripping the CO_2 off the capture material, which is typically done through the use of heat, pressure, or electrochemical means. Hybrid approaches have been developed to bridge the gap, using biogenic process alongside engineering processes.

DAC is a method that uses large fans to pass vast quantities of atmospheric air over chemical substances, to then concentrate into a pure stream of CO_2. This can be combined with storage to provide CDR, or utilized for other purposes through CCU/CCUS.

Direct air capture

Currently, two DAC technologies exist on a commercial scale: solid sorbent (SS), and liquid solvent (LS) approaches. These methods differ in design and implementation, but follow similar overall processes. First, CO_2 is absorbed/adsorbed onto either a solid or liquid chemical substance by passing air over it using fans; second, the CO_2 is released into a concentrated stream and the capture material is regenerated for further use. This has been detailed in a recent review by McQueen et al. [8]. LS DAC is designed to be run as a continuous process, whereas SS DAC is a batch process that can be run with multiple units in parallel to make a pseudo-continuous process. A mixture of heat and pressure are used to release the CO_2 from the capture material. LS DAC typically relies on very high temperature heat, around 900°C, which is currently met using the combustion of natural gas, with CO_2 concurrently captured in the process. SS DAC uses much lower heat, typically around 100°C, and can be met using a variety of heat sources, including direct electrical heating, heat pumps, and combined with low grade waste heat and geothermal.

LS systems, such as that of Canadian company, Carbon Engineering, rely on large scale, existing industrial equipment, and reach economies of scale by increasing unit size. Their baseline configuration is approximately 1 MT CO2/year. This approach combines two chemical loops, and commonly found inexpensive feed stocks [9]. Fans pass large volumes of air through an air contactor, which has an aqueous capture solution pumped over a structure packing material. Once CO_2 has been dissolved in solution, pellets are formed, and then sent to a calciner to pull CO_2 off and regenerate the solvent for further use. Cost estimates are in the range of \$94-232 USD/t CO_2.

The SS DAC approach has been more widely adopted, with historically two major companies, Climeworks out of Switzerland, and Global Thermostat out of the United States. Recently, many more companies have started up using this approach. SS DAC takes advantage of modular units, which can be scaled out, rather than scaled up. A typical unit is approximately the size of a standard shipping container, and can capture 500 t-CO_2/y. Since they are individual units of a particular size, the cost of scaling is more or less linear. Solid sorbent systems require the whole contactor to periodically be sealed off, to desorb the CO_2, which requires manufacturing processes that may not be well developed. Current cost are estimated to be around \$600 USD/t-CO_2, however, advancements are progressing quickly, and \$100 USD/t-CO2 is not far

off in the opinions of many [10]. The sorbent is commonly the most expensive piece, with the sum of capital and operational expense at about 92-93% of the total levelized cost [11]. As the rate of deployment increases and larger scales are reached; as well as refinements to the processes, sorbent/solvent synthesis techniques, and supply chains mature; cost are expected to come down the cost curve aggressively.

Land use is an important metric when comparing NETs. Current estimates for DAC have quite a broad range. Solid sorbent systems have a total land impact of 730,000-5,000,000 m2/Mt CO2 (180-1,235 acres), and a direct impact of 36,500- 250,000 m2/Mt CO2 (9-62 acres) [4]. Aqueous systems have a total land impact of approximately 7×10^6 m2/Mt CO2 (1,730 acres) and a direct land use of 24,000 m2/Mt CO2 (6 acres) [4]. Direct land use accounts for the process equipment itself, whereas indirect land use accounts for the spacing between contactors to allow tropospheric CO_2 mixing. Spacing between contactors increases direct land use by about 300 times to allow adequate re-equilibration to atmospheric CO_2 concentrations. The current study aims to understand if this spacing is required in practice, or is an overly conservative estimate. Further land area is required to build power generation equipment to run the plants, which is not included in the above mentioned land impacts.

Detailed life cycle analysis (LCA) must be conducted on a case by case basis to ensure net negative carbon as a result of a DAC plant. This is beyond the scope of this study, and has been conducted elsewhere for individual technologies comprising the design within this thesis. Deutz et al. [12] conducted a detailed LCA for a solid sorbent based DAC plant located in Iceland operated by Climeworks. They state that the plant can already achieve net negative carbon emissions today with carbon removal efficiencies of 85.4% to 93.1%. Major emission sources of the process are associated with the plant construction and absorbent choice. Plant construction can induce up to 15 g-$CO_{2_{eq}}$ per kg-CO_2 captured, and adsorbent choice up to 45g-$CO_{2_{eq}}$ per kg-CO_2 captured. Renewable power generation required to run the plant also contributes significantly. This DAC plant has combined thermal and electrical demand of 2000 kWh/t-CO_2. The choice of energy used to power the plant plays a significant role in the overall climate impact. The current analysis couples DAC with floating offshore wind. Floating offshore wind global warming potential (GWP) was determined by Garcia-Teruel et al. [13] by analyzing case studies, finding a GWP of 25.6-45.2 g-CO_2/kWh, mostly dependant on operation and maintenance (O&M) strategy and vessels. In order to meet the 2000kWh/t-CO_2, power generation from offshore wind

power would emit about 51.2-90.4g-CO_2 per kg-CO_2 captured. Summing these three emission sources results in 111.2-150.4 g-CO_2 per kg-CO_2 captured. Many other aspects of an offshore DAC plant would need to be considered to capture the total carbon removal efficiency, but from an energy, plant construction, and adsorbent procurement perspective, it remains feasible to operate with net-negative emissions.

1.1.2 Storage

Most CCS projects today inject CO_2 into sedimentary basins, using an impermeable cap rock to contain CO_2. Another option is to inject into reactive rocks, such as mafic or ultramafic formations, where CO_2 mineralizes to permanently fix the carbon [14]. The trapping mechanism changes over time from structural, to solubility, to mineral. As the trapping mechanism progresses from one to the next, so does the permanence and decreased risk of leakage as shown in fig. 2.4 of CDR primer [15]. In reactive rocks, the progression from one trapping mechanism to the next is much faster than in sedimentary basins, on the order of thousands of years quicker. This has been demonstrated in conjunction with DAC at a geothermal plant in Iceland, at a project called Carbfix [14, 16, 17]. Building upon a similar idea, a feasibility study was conducted off the coast off British Columbia and Washington state to store 50 Mt-CO_2 into sub seafloor basalt called CarbonSAFE [18]. Following on this geological feasibility study, the SolidCarbon project [7, 19–27] began to investigate sub seafloor basalt injection from an engineering, geologic, social, regulatory and investor acceptance perspective. Tutolo et al. [22] and Awolayo et al. [23] modelled the reactive transport of this site prior to injection to better understand the geology, and expected time for mineralization to occur. This drives the groundwork to develop the measurement, reporting, and verification (MRV) plan.

1.2 Research questions

The overarching goals of this work is to assess the viability of designing DAC to be built offshore, onboard floating wind turbines. The physical implications of building in such an environment are explored as well as the performance impacts.

The work of chapter 2 is to investigate three main research questions:

1. What is the pressure drop through an commercial scale direct air capture device?

2. How do ambient wind speed and direction effect overall fan power requirement?

3. How does CO_2 mix in the atmosphere as it exits an air contactor? What is the energy impact of decreased CO_2 concentrations entering downstream contactors? How close to one another can air contactor units be placed without causing detrimental energy impacts?

As DAC is just becoming commercially available, publicly available data on commercial scale operations is very limited. The pressure drop of the system has a significant impact on the overall system energy demand, so a two dimensional computational fluid dynamics (CFD) model was developed to predict the pressure loss of a system based on patent information scaled up to a commercial scale. Three dimensional CFD was then utilized to model the atmospheric mixing of CO_2 nearby air contactor units to determine the CO_2 concentrations entering adjacent units, and ultimately the energy impacts. The CFD result was also used to analyze the impact of wind direction and speed on fan energy requirement.

The main research questions for chapter 3 include:

1. What are the operational implications of operating DAC offshore?

2. What are the performance impacts of operating in this environment?

3. What modifications can be made to to current DAC designs to allow operating in this environment?

Currently, no experimental work has been completed for DAC in an offshore environment. This makes estimating energy requirements and costs difficult, so further work is described to facilitate future development.

1.3 Contributions

The main contributions of this thesis directly address the research questions listed above. The contributions from chapters 2 and 3 are listed below.

The main contributions of chapter 2 are:

1. Pressure drop curves using a commercially deployed air contactor design. Curves obtained for four common solid sorbents used for DAC, including: APDES-

NFC, Tri-PE-MCM, MIL-101(Cr)-PEI-800, and Lewatit VP OC 106. This can be used for further energy studies, increasing the accuracy of estimation of fan work on what remains mostly proprietary within the DAC industry.

2. A simplified CFD model of solid sorbent DAC units to understand the implications of contactor arrangement on flow, fan work, and CO_2 inlet concentration. The configuration can be further modified to test alternate arrangements placed in varying environments. This model could be adapted for both onshore, and offshore applications.

The main contributions from chapter 3 are:

1. Insights to the changes necessary to implement DAC in an offshore environment. Highlighting key areas for exploration and suggestions of future work to de-risk technology, prior to deployment under new operating conditions.

2. Propose design configurations which show promise for future development to push NET installations further from shore.

1.4 Document Structure

This thesis follows a paper based format. The presented work has been prepared, and submitted as two separate journal papers, and are presented here as two independent chapters. The complete structure of this thesis is as follows:

Chapter 2 presents a design case study on direct air capture built on board a floating offshore wind turbine. Computational fluid dynamics is utilized to find system pressure losses, and local CO_2 concentrations entering downstream units. These outputs are fed into an energy model to predict the electrical energy requirements of the fans based on pressure gradients, as well as an the impacts to the thermal energy impacts based on CO_2 concentrations.

Chapter 3 explores the implications of operating direct air capture in an offshore marine environment. A review of the current research landscape is presented, as well as discussion of the open research questions that must be solved. The pre-treatment of air prior to coming into contact with the capture material is assessed. The additional fan power required to overcome the pressure loss

induced by the pre-treatment components is analyzed. Pressure loss curves obtained in chapter 2 were used for further analysis in this chapter.

Chapter 4 contains a summary of the claims and results of the thesis and how they relate to the advancement of offshore direct air capture. Avenues of future work for further development of the concept and its applications are also discussed.

Chapter 2

Research paper- 'Ambient Wind Conditions Impact on Energy Requirements of an Offshore Direct Air Capture Plant'

This chapter is prepared as a standalone journal article to be submitted for publication at a to be determined (TBD) journal. Its main author is also the author of this thesis, having done its research, calculations and writing in consultation with Dr. Curran Crawford as the primary advisor. All section, equation, and reference numbering has been modified to integrate it with this thesis.

The citation for this article [28] is as follows:

R. Foxall and C. Crawford, "Ambient Wind Conditions Impact on Energy Requirements of an Offshore Direct Air Capture Plant," Journal TBD, Jan. 2023.

Abstract

This study proposes an off-grid direct air (carbon) capture (DAC) plant installed on the deck of an offshore floating wind turbine. The main objective is to understand detailed flow characteristics, and CO_2 dispersion around air contactors when placed in close proximity to one another. A solid sorbent DAC design is implemented using a

commercially deployed air contactor configuration and sorbent. Computational fluid dynamics is used to determine the local conditions entering each unit based on varying wind speed and angle. Two-dimensional simulations were used to determine the pressure drop through a detailed air contactor design. Three dimensional simulations were used to model flow patterns and CO_2 dispersion using passive scalars. A worst case scenario is analyzed; all DAC units are in adsorption mode with fans running simultaneously. Two dimensional simulations show an under utilization of contactor length, and quantify pressure loss curves for four common sorbents. One commercially deployed sorbent is considered for further analysis. A pressure drop of 390.62 Pa is experienced for a flow velocity of 0.73m/s through a 1.5m x 1.5m x 1.5m contactor. Using three dimensional simulations, fan energy demands are computed based on flow velocities and applied pressure gradients. There is found to be a decrease in overall fan power demand as wind speed increases. At high wind speeds, fans can be shut off at certain wind directions, allowing sufficient airflow to passively drive the adsorption process. This occurs at an average contactor inlet velocity of 17.5m/s, correlating to a hub height (150m) wind speed of 24m/s. Thermal energy demands are computed based on inlet CO_2 concentrations entering downstream units. Contactor arrangement, wind angles, and wind speeds have a significant impact on flow patterns experienced, and resulting CO_2 dispersion. High wind speeds assist in CO_2 dispersion, resulting in higher inlet concentrations to downstream DAC units, thus decreased thermal energy requirement.

2.1 Introduction

Meeting the climate targets set out in the Paris agreement will require an aggressive global effort to decarbonize, both in terms of carbon emission reductions, as well as direct or indirect carbon removal from the atmosphere. It is well understood among the scientific community that carbon dioxide removal (CDR) is now a necessary component to meeting climate goals [6]. Direct air capture (DAC) is a method for directly capturing carbon dioxide (CO_2) from atmospheric air and has a number of distinct advantages over alternative approaches. A significant advantage of DAC is that it is location independent. CO_2 is well mixed within the atmosphere so its concentration variations are small when comparing different locations. Changes in performance are expected as a result of varying ambient conditions, such as temperature and humidity. Choosing optimal locations for DAC is dependant on proximity to resources including

energy, water, and sufficient CO_2 storage. So although locationally independent, it cannot be placed just anywhere. As the worlds population continues to increase, competition for land and resources become stronger. This, along with utilization of vast offshore wind resources and technologies, drives the motivation to explore locations where direct land use competition is not an issue, such as far from shore.

Beyond capturing CO_2, it must also be physically stored permanently to deliver its long term climatic benefit. One approach to ensure durable storage, meaning there is no risk of leakage back into the atmosphere, is mineralization in basalt rocks. This technique has successfully been demonstrated at Carbfix [14, 16] in Iceland and is gaining attention elsewhere [18, 29, 30]. CO_2 mineralization is one of the most robust forms of carbon storage, as once the CO_2 has reacted with the rock, and mineralized into a solid state, the risk of leakage is removed [15]. Thus, mineralization likely does not require as extensive of monitoring programs as required for other types of sequestration relying on cap rock as a trapping mechanism such as saline aquifer, and storage in depleted oil and gas fields. Awalayo et al. [23] and Tutolo et al. [22] quantified the reactive transport of CO_2 in basalt crusts, and their results show significant carbonation can be expected in relatively short timescales. Although previous estimates from Carbfix had suggest about two years to mineralization [31], this is likely site specific, and other sites may require slightly longer timescales to ensure complete mineralization. Nevertheless, mineralization within tens of years timescale is significantly shorter duration than traditional monitoring, reporting and verification (MRV) schemes required for traditional saline aquifer or depleted reservoir storage which typically require 100 plus years of plume monitoring to ensure its stability in the geologic formation. Basalt rocks are plentiful across the globe, and cover large portions of the ocean floor [32]. This drives the motivation for the Solid Carbon project [7, 19–27], which is focused on sub sea floor CO_2 injection and mineralization in basalt rocks in the Cascadia basin, off the west coast of Canada.

Along with having plentiful basalt, many offshore sites are also in close proximity to renewable energy resources. This provides an opportunity to use an otherwise difficult to capture and transport renewable energy to drive a negative emissions process, such as DAC plus sequestration. Building DAC offshore allows for a site to be chosen that is in close proximity to renewable energy resources, as well as a storage location, eliminating the need to transport CO_2 from shore.

Normally, in onshore installations and modelling, DAC units are placed adequately far from one another to allow re-equilibration to atmospheric CO_2 concentrations entering adjacent units. However, due to space constraints onboard offshore wind turbines, units need to be placed in close proximity to one another. Regardless whether onshore or offshore, footprint should be minimized/optimized. As a result of placing units in close proximity, local CO_2 concentrations entering downstream units will be decreased by the upstream contactors. A small decrease in CO_2 concentration entering a DAC unit has a significant impact on overall energy demand. This is governed by thermodynamics, which shows an exponential increase in energy demand to separate gas species with decreasing CO_2 concentration. Additionally, to meet the same overall capture rate, more air must be passed through the contactors when concentration is decreased. This can be done by increasing the inlet cross sectional area, or increasing fan speed, both of which will increase overall fan power requirement. For example, a drop in inlet concentration by 50%, would require fan speed to be doubled, or the cross sectional area to be doubled in order to meet the same capture rate. This in turn, this would double the fan power requirement. So far in literature, studies considering plant wide energy estimates for DAC assume a constant ambient concentration of CO_2 entering each unit. On land, where space limitations are commonly less of an issue and contactors may be placed adequately far from one another to allow re-equilibration, this may be a reasonable assumption. However, for most offshore applications, deck space is very limited, and local decreases in CO_2 concentrations will likely have play a larger role in overall energy demand.

The minimum/reversible thermodynamic work required for separating gas species is useful to understand how energy demand changes with concentration. Energy demand increases exponentially as concentration decreases, shown in fig. 2.1 using a capture fraction of 90% at 100% CO_2 purity. As high a purity as possible is desired/necessary for further utilization or geologic storage. The concentration levels relevant to DAC, mole fractions between $[0 - 5 \times 10^{-4}]$ (0-500ppm) are found in the leftmost region-the steepest portion of the curve; where small changes in concentration, result in large changes in energy requirement. This represents the theoretical minimum work, whereas to understand the real work from an actual plant, one may consider a second law thermodynamic efficiency. This is discussed further in future section 2.3.4.

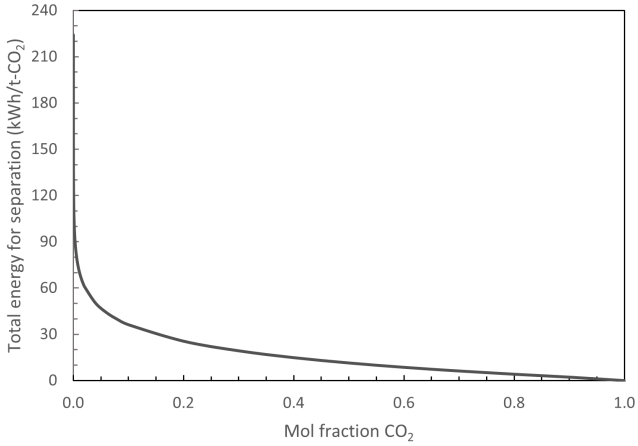

Figure 2.1: Minimum thermodynamic work for gas separation at 25° C with a CO_2 capture fraction $\alpha = 0.9$ from air, and output purity of 100% CO_2. Solved using eq. (2.15)

An opportunity for energy savings can be found in using the ambient wind conditions to decrease the fan power required to overcome the large pressure drops encountered by DAC devices. The proposed design is placed onboard floating offshore wind turbines, which by nature are placed in regions with steady high wind speeds. Current studies estimating plant wide energy consumption assume zero ambient wind [33–36], computing a fan power required to overcome a certain reactor pressure drop to meet a designed volumetric flow rate. Fan power has been found to account for approximately 3-57% of the total plant energy requirement [9, 33, 34]. Typical wind speeds for floating offshore wind show annual averages of 6-11.3m/s at 100m hub height [37].

During times of low power availability, one could envision operational schemes for DAC where fans are left turned off, allowing air to passively pass through the contactors. Although sufficient volumetric flow may not be achieved to reach the desired capture rate, cycle times for adsorption could be modified to allow a longer period for air to contact sorbent. All power available could then be directed to the desorption process of as many units as possible, allowing for the plant to continue running at a lower output. Sufficient power would be assessed on a unit by unit basis to ensure that average thermal power supplied to a single unit is not lowered. Rather, fewer individual units are run at full capacity if sufficient power is available, else, all are left off and the small power available is curtailed or stored depending on available storage capacity. Continuing to run parts of the process during times where total plant de-

mand cannot be met contributes to a higher overall capture rate, which is beneficial for capital intensive pieces of equipment, lowering the overall cost per tonne.

2.1.1 Motivation, objectives, and paper structure

This study is motivated by the opportunity to provide a CDR solution by: harnessing currently unused but abundant renewable energy far offshore, not contributing to land competition, while choosing a cite adjacent to plentiful and secure CO_2 storage. Its important to note that this does comes with additional complexities of offshore operation. This means that the energy used in the process does not directly remove clean electricity capacity that could be used elsewhere to decrease the carbon intensity of the grid. Of course, conducting any project requires financial investment, so competition exists regardless. DAC is an energy expensive process, and should be driven by renewable power to maximize the climate impact.

Plant wide energy estimates for solid sorbent DAC have been completed, but to the best knowledge of the author, none have taken into account the local atmospheric conditions such as varying CO_2 concentration downstream of other contactors and incoming wind speed. The goal of the present study is to build an understanding of the effects of varying wind speeds and angles on total energy consumption of a plant. Additionally, the present study aims to produce pressure loss curves for a commercially deployed air contactor design using CFD which is not available in literature. Due to DAC technology's relatively nascent nature, most detailed information remains proprietary. The pressure drop through solid sorbent DAC units is currently only available at a lab scale, very little detail is given about operation at commercial scale [38]. As such, a 'generic DAC contactor geometry' is applied and tuned to industry stated values using various sorbents. Energy estimates are sensitive to the chosen sorbent and configuration in which they are laid out. This makes producing accurate energy estimates at scale difficult, especially for academic studies.

The three main contributions from this paper include analysis of: 1) 2D pressure loss curves using different adsorbents of a commercially deployed contactor design and scale, 2) 3D CO_2 dispersion model of a DAC plant installed onboard a floating offshore wind turbine, and 3) the change in energy consumption due to inlet CO_2 concentration and local wind speed.

The paper is structured as follows. A literature review is conducted in section 2.2.

Section 2.3 discusses the methodology and design setup for the analysis. Section 2.4 presents the results alongside discussion from the CFD and energy modelling, and section 2.5 presents the summary of the major findings.

2.2 Background

A literature review of the current landscape in DAC, and atmospheric dispersion modelling is carried out in sections sections 2.2.1 and 2.2.2 respectively.

2.2.1 DAC

Two main DAC technologies exist on a commercial scale, solid sorbent (SS), and liquid solvent (LS)/aqueous approaches. A detailed summary of the technology was conducted by McQueen et al. [8]. The two methods follow a similar overall process, but differ in design and implementation. In either case, CO_2 is absorbed/adsorbed onto a chemical capture material, either liquid or solid, by using fans to pass large volumes of air over the capture material. Once the substance has reached a saturated state, heat and pressure are used to drive the CO_2 off into a concentrated output stream and the capture material is regenerated for further use. LS DAC is designed to be run as a continuous process, whereas SS DAC runs as a batch-wise process, using multiple units in parallel to enable continuous operation. LS DAC historically has relied on scaling up unit size, taking advantage of economies of scale based on unit size to drive cost reductions. SS DAC uses small modular units and scales out to drive cost reductions using economies of scale based on number of units produced.

The temperature requirements of the processes also differ. LS DAC requires heat around 900° C, which is typically met using combustion of natural gas. Temperatures at this level can achieved using electrical heating as well, but is far more challenging, and until recently has not been available at industrial scale. Long-Innes [39] explored a LS DAC system run entirely using electricity. They conclude that on an energy basis, an all electric configuration appears ideal, however, due to uncertainty regarding pellet fluidization in the reactor and ability to consistently reach 900° C, this option appears more difficult in practice than using fossil fuel powered reactors. Electric calciners have been used in the production of steel, ceramic, and glass since around the 1920's and offer benefits over combustion of fossil fuels in terms of efficiency, process control, and emissions [40]. Recent developments have allowed electric kilns

to reach temperatures up to about 1700° C [41]. SS DAC requires heat on the order of 100° C. Heat transfer is commonly done using direct electrical heating; jacket heating, by passing heat transfer fluid through internal tubes surrounding sorbents; or passing steam through the contactor. LS DAC may also use electrochemical methods to regenerate solvent, which negates the high temperature thermal demand. Due to unit size, and feed stock requirement for heating, SS DAC is explored for further analysis in this offshore application.

SS DAC rely on extremely large surface areas of sorbent material to contact with the ultra dilute air. Solid sorbents are commonly comprised of amines and may be physically bound to a porous backbone structure, sometimes visualized as a honeycomb structure; or arranged into packed sheets. Commonly, this arrangement is refereed to as a packed bed, or a structured adsorbent bed. These structures allow for extremely large surface areas to contact with the air. Particles are often arranged in a manner to minimize pressure drop through the unit. Many sorbents are being examined for feasibility, which possess high affinity for CO_2, while minimizing energy demand to pull CO_2 off. Four adsorbents are discussed by Sabatino et al. [35], which show good promise, have a large amount of experimental data available, and appear to be used by industrial DAC companies. These adsorbents are APDES-NFC [42], Tri-PE-MCM-41 [43], MIL-101(Cr)-PEI-800 [44], and Lewatit VP OC 106 [45, 46]. The sorbent APDES-NFC appears to be commercially used [12, 47, 48], and is the sorbent used for further analysis in the present study.

As a result of dealing with such dilute concentrations, very large volumes of air must be passed through DAC units. Significant work has gone into the optimization of airflow through the reactors to minimize pressure losses within the system as seen in patented designs by Gebald et al. [47] and Sauerbeck et al. [48]. Clever designs have been implemented in industrial application, however, few public details can be found, so researchers must rely on lab scale implementations. These pressure losses do not necessarily translate to a commercial scale.

Once the solid sorbent has reached near saturation with CO_2 by passing air over the capture material, the entire unit is closed to the atmosphere, and temperature and/or pressure are introduced to release the CO_2. A five step process is commonly used to describe the adsorption desorption cycle as per Sinha et al. [34]. The process is as follows: 1) adsorption using fans to pass air through, 2) evacuation of oxygen using

a vacuum pump, 3) pressurization using steam, 4) desorption through heating of sorbent material, and 5) cooling to return to ambient temperatures before beginning a new cycle. This technology is receiving significant attention from both academia as well as industry. Industrially, units are typically thought of to be the size of a standard shipping container, and capture on the order of 500 t-CO_2/y [38]. The sorbents region comprises the bulk of the volume of the unit, and fans are placed at the outlet to pull air through the device, over the sorbent particles.

Multiple studies have examined the energy consumption of DAC at a plant level. Steady state analysis is done in many cases [33, 34, 36] to study the energetic and economic performance of DAC plants. Many studies [35, 46] have also examined from a transient analysis perspective to understand further the operational implications such as adsorption/desorption times, as well as pressure, temperature and mechanism of heat transfer.

The pressure losses within the contactor overcome by the use of fans contribute significantly to the overall electricity consumption. As stated previously, fans can account for between 3-57% of the total plant energy requirement. Carbon Engineering, a commercial liquid solvent DAC company, reports in a study by Keith et al. [9], an electricity consumption of 61 kWh/t-CO_2. This is 16.7% of the total electrical consumption, and 3.3% of the total energy consumption (electrical plus thermal energy). In the case of SS DAC, Bos et al. [33] reports fan electrical consumption of 31.9% of the total energy consumption. Sinha et al. [34] reports a fan energy consumption of 44.4% to 57.0% of total plant energy use. Conventional point source capture makes use of deep contactor beds as they draw from a much higher concentration, thus less air must be passed through. In the case of DAC, these beds must be much thinner to allow large volumes of air through, while minimizing pressure drop. The pressure drop through the contactor is a function of the porosity of the membrane, the thickness, and the velocity at which air is passed through.

The pressure drop through solid sorbent contactors has been experimentally tested in a number of studies but no public data is available for a commercial plant. Bajamundi et al. [49] experimentally measured the average pressure drop through a bench scale reactor (1m diameter, 0.2m thickness), finding a pressure drop of 450 Pa. In the patent by Gebald et al. [47], a table of pressure loss with respect to volumetric flow rate is presented on page 23 for a lab scale set-up utilizing an accordion style arrangement of

sorbent sheets. The scale of the contactor is much smaller than a commercial design, but gives good insight into the design configuration, geometric details, and volumetric flow rates expected. Analytically, McQueen et al. [36] calculated a pressure drop of 480 Pa through a similar 1.5m length reactor using amines bound to monolithic channels. Using the Ergun equation, Stampi-Bombelli et al. [50] computed a pressure drop of less than 100 Pa for all scenarios. From this, lab scale pressure losses are expected in the range 100-450 Pa, and very few details can be found for contactors with applicable size for commercial operation.

One of the major implications of operating SS DAC units in an offshore environment, is an increase in the humidity. As the humidity increases, water adsorption in the contactor also increases. Co-adsorption of water severely impacts the energy requirements of the system. Using a conservative estimate for CO_2 to H_2O desorption ratio of 1:4, the heat energy requirement for desorption per mol of CO_2 is more than tripled ($\sum_i \Delta H_{ads,i} = 75 + 4 \cdot 41 = 239$ kJ/mol-CO_2) [51]. As humidity increases, there is also an enhancing effect on CO_2 adsorption as shown by Wurzbacher et al. [52]. Few studies have quantified this effect because co-adsorption measurements are complex. Experimental data is available for only select sorbents, and as a result in modelling of DAC, humidity enhancing effects on CO_2 adsorption are often neglected. Different approaches have been used to capture this effect when modelling DAC energy requirements. Wurzbacher et al. [53] used an empirical enhancing factor dependant on the relative humidity and CO_2 partial pressures. Stampi-Bombelli et al. [50] built on this by embedding the H_2O isotherm within the CO_2 isotherm, but this requires extensive experimental data on the sorbent of interest. Sabatino et al. [35] overcame this lack of data by developing a hybrid approach, where they solve for an equivalent temperature dependant on the humidity and ambient temperature. The Toth isotherm model is typically used to describe the capacity with regards to CO_2, and the Guggenheim, Anderson, de Boer isotherm (GAB) isotherm is typically used to describe water adsorption. Bos et al. [33] discuss how further heat reductions are possible by reducing the amount of water co-adsorbed by increasing the relative humidity during desorption by using steam, however, from their previous work, they determined that this does not result in an net reduction in energy. Elfving et al. [54] explored the implications of ambient temperature, and humidity on CO_2 adsorption capacity and found that cold humid air had the highest adsorption capacity. Sanz-Pérez et al. discusses the implications of temperature and humidity on both LS DAC

and SS DAC [55].

2.2.2 Atmospheric dispersion modelling

Computational wind engineering (CWE) is the application of computational methods to wind engineering problems, and is mostly conducted using CFD [56]. Dispersion modelling of particles is commonly conducted in urban environments as well as indoor spaces to monitor pollution or contaminant distribution. As per Holmes et al. [57], dispersion modelling can be grouped into the following subgroups: box models, Gaussian models, Lagrangian models, and CFD models. The present study analyzes the latter. As per Loomans et al. [58], CFD dispersion models are divided into passive scalar models, Euler models, and Lagrange models. Euler models account for particle settling velocity, and presents an attractive alternative to more precise Lagrange models. Passive scalars are the simplest of the three model types.

At 15° C and at sea level, CO_2 gas has a density of $1.87 kg/m^3$ [59], about 1.5 times that of atmospheric air under the same conditions. Thus, as a pure stream, CO_2 should be treated as a heavy gas. Heavy gas modelling deals with substances released to the atmosphere with a density greater than atmospheric air. This type of model is commonly conducted for dispersion from concentrated sources such as leakage from a pipeline, a gas storage location, or the output of an exhaust stack. These models are summarized by Markiewicz [60], and can be broken down into four groups: simple/empirical models, intermediate/integral and shallow layer models, advanced/Lagrangian particle trajectory and Lagrangain puff models, and CFD models. However, in the case of this analysis, CO_2 is present at extremely low concentrations in the bulk air, and is included as a constituent in the density of air. Dry air is comprised of about 21 vol% oxygen, 78 vol% nitrogen, and only about 0.0412 vol% CO_2 (0.063 wt%). As this study is concerned with CO_2 removal, overall density of air leaving the contactors would be decreased. Additionally, small changes in CO_2 concentration (400ppm) result in an insignificant change in the overall density of air. As a result, heavy gas dispersion modelling is not used in the current study.

In the case of the analysis at hand, a steady state Reynolds Averaged Navier Stokes (RANS) model supplemented with a Eulerian advection-diffusion dispersion model of passive scalars is used to model the dispersion of CO_2. Passive scalars are not actively involved in the flow physics of the simulation; rather they are tracked and analyzed

during post processing after solutions to other flow variables are solved. This assumes the species present is in low concentration, and is considered a fluid. Passive scalars are commonly seen in dispersion studies, however, the majority of studies examine a passive scalar source in pollution dispersion applications rather than a passive scalar sink (removal) as is used in the current study.

Labovsky et al. [61] studied the pollutant dispersion of gas and liquid particles from a concentrated output stream of liquefied chlorine gas in an urban environment. They used a Eulerian approach for the air and pollutant particles, and a Lagrangian approach for the dispersion of liquid particles. They compared their results to a simpler integral dispersion model, and found that the CFD result performed better in complex urban environments where many obstacles are present.

Ramponi et al. [62] conducted a study on outdoor ventilation in urban areas with varying street widths. They used steady RANS CFD simulations and passive scalars as a tracer gas in there studies. They conducted an extensive literature search and concluded that although LES simulations are intrinsically superior, they have a higher computational cost as well as require greater user expertise. As such, they find that vast majority of studies in this area are conducted using steady RANS simulations, and the results show good to very good performance.

Nottrott et al. [63] studied atmospheric dispersion of GHG's from heavy emitters, and used LES models and passive scalar dispersion. Passive scalars solved the filtered advection-diffusion equation for the atmospheric boundary layer (ABL), and their study accurately modelled the mean plume trajectories and concentration fields. An ABL model is commonly applied in the field of wind engineering to approximate the velocity profile encountered near earths surface as a result of ground roughness.

2.3 Methods

CFD is utilized, and its outputs are fed into an energy consumption model using Microsoft Excel. CFD is used to determine: 1) the pressure loss curve for an air contactor, 2) the local CO_2 dispersion around air contactors, and 3) pressure gradient applied by each fan/momentum source and volumetric flow rate. The initial plant design is discussed in section 2.3.1. Then, the CFD methodology is discussed in sections 2.3.2 and 2.3.3. Following this, the energy modelling is described in sec-

tion 2.3.4. The CFD model solves the steady RANS equations as mentioned earlier. Further details of the RANS equations are given in appendix A.

2.3.1 Initial plant design

Currently, the largest DAC installation is 4000 $t - CO_2/y$, located in Iceland, known as the Orca plant [38] from the solid sorbent DAC company, Climeworks. It uses eight shipping container sized units, each capturing about 500 $t - CO_2/y$ using a mixture of electrical and geothermal heat. The combined thermal and electrical energy consumption is estimated to be about 2000 kWh/t-CO_2 [12], equal to a constant load of 127 kW at 500t-CO_2/y if run with a 90% capacity factor to allow for maintenance and shutdowns. Thermal energy is about 75% of the total energy, 1500 kWh/t-CO_2, and is assumed to be met using electrical means.

The floating offshore platform for the 15 MW IEA reference turbine [64] developed at the university of Maine [65] in conjunction with the national renewable energy laboratory (NREL) was used for this analysis. Based on an average annual capacity factor of 45% [66], the average power output is 6750 kW. An approximation using a capacity factor, as opposed to a second-by-second dynamic power analysis, removes site specific attributes and wind profiles, and allows modelling takeaways to be applied more broadly to various locations. To assume continuous operation at this power output, sufficient energy storage is assumed to be installed on board. Efficiency losses due to the energy conversion are not accounted for in the present analysis; rather a conservative estimate of the number of contactors is used. Round trip efficiencies have a large range depending on the energy storage system, with estimates between 20-98% [67]. One attractive option for onboard logistics is energy storage using hydrogen, by conducting electrolysis of seawater. As DAC is a thermally expensive process, this could be combusted to meet the thermal demand, and potentially produce a greater round trip efficiency.

At 6750 kW average power output, and each DAC consuming an average of 127 kW, 54 DAC units could hypothetically be installed on board. It is hypothesized that due to the tight spacing of air contactors, local concentration will be decreased at the entrance to downstream contactors, thus they would have a larger energy requirement. Assuming this consequence is large, a conservative estimate of 30 DAC units (three contactor banks, each with five DAC units stacked vertically into two rows) are placed

symmetrically in a triangular arrangement around the base of the turbine. This configuration can be seen in fig. 2.2. In future analysis, if the consequences of CO_2 mixing are small, an additional three banks of contactors could be added in the same triangular configuration inside of the outer contactor banks. Each additional bank could contain eight units (two rows of four). The dimensions of the platform are adapted from the reference turbine developed by NREL at The University of Maine [65]. The floater design does not contain a deck, however the DAC units are assumed to be mounted on catwalks extending between the three outside floats. This would require further structural and stability design and analysis in order to be implemented in practice.

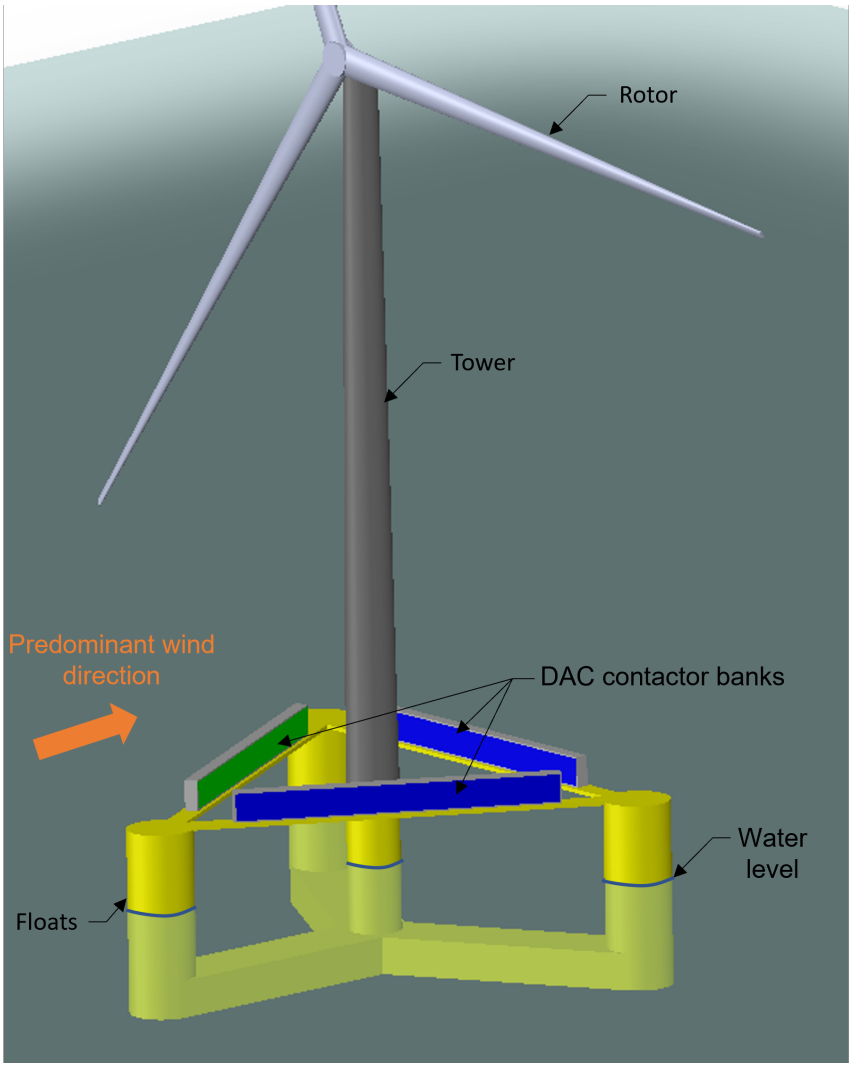

Figure 2.2: DAC air contactor configuration mounted on the platform of a 15MW floating offshore wind turbine. Sorbent zone shown in blue, and the fan zone shown in green. Contactor cross section can be seen in the appendix.

The DAC units are mounted to promote horizontal airflow as this allows ambient wind to assist in overcoming the pressure loss of the air contactor, thus reducing fan power required. This configuration can be seen deployed commercially in the Orca plant discussed earlier. Another possible configuration is to mount the fans vertically, drawing air in the top, and expelling CO_2 depleted air out the sides or visa versa [68,69]. A central vertical fan may be shared between multiple DAC units, which would decrease the capital cost of each unit. However, it does not take advantage of local wind conditions, as upstream contactors may be aligned with the wind direction,

but the downstream/opposite facing contactors will be forced to blow upwind. For the purpose of this study, the goal is to examine the extent that ambient wind can assist DAC, and reduce energy consumption, so the horizontal fan configuration was chosen.

The rotor at the top of the turbine was not included in current analysis. The main goal of the present study is to understand how fan work can be reduced by incoming horizontal wind flow, and to understand the order of magnitude of local CO_2 depletion in the region of DAC units. It can be seen in figure 15 from Uchida et al. [70], that the impacts to the ABL profile are minimal in the region immediately below the rotor. Majority of the impacts to velocity profile are seen downstream of the rotor within the stream tube. For the sake of this analysis, the impacts from the rotor acting overhead are deemed to be negligible. This is meant to serve as a worst case analysis. In reality the rotor may induce increased mixing, as it could transport un-depleted air from above down to the region of the DAC units, but this is beyond the scope of the current analysis and would require a further, more detailed investigation.

2.3.2 CFD Part 1- 2D modelling

The goal of this section is to obtain a pressure loss curve for a commercial scale and design SS DAC unit using a variety of sorbent materials. Gebald et al. [47] and Sauerbeck et al. [48] present a patent for a commercial design of a solid sorbent DAC air contactor. This design was re-produced for this analysis, with a cross sectional view shown in fig. 2.3a; employing horizontal sheets of solid sorbent particles arranged in an accordion manner. Simplification to a 2D analysis is completed by taking a 2D cross section through the center of the contactor, and applying symmetry in the vertical and transverse directions as shown in fig. 2.3b. Each sorbent sheet was modelled using a porous media model within the commercial software Simscale. The fixed coefficient porous media model [71] was used in the 2D analysis. The area averaged pressure was interpreted at the inlet and outlet to obtain to pressure drop through the contactor by applying numerous inlet velocities to produce a pressure loss curve. This result is then applied in part 2, section 2.3.3 to simplify the mesh complexity and computational effort when introduced into a larger 3D domain.

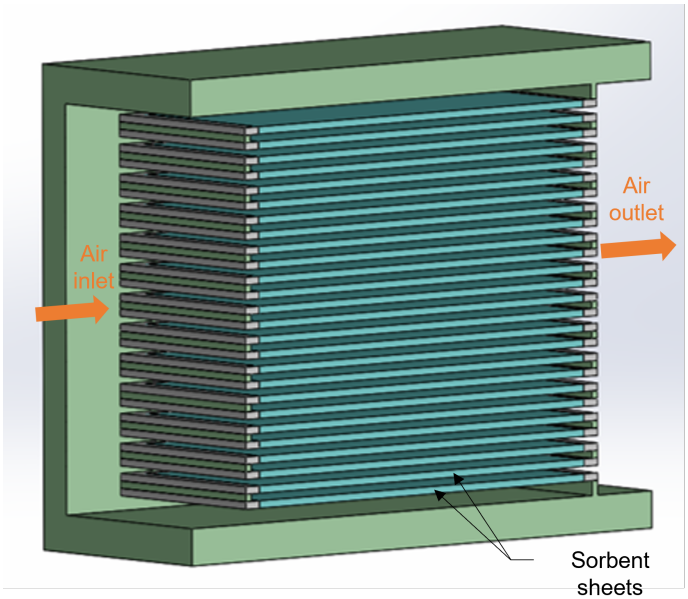

(a)

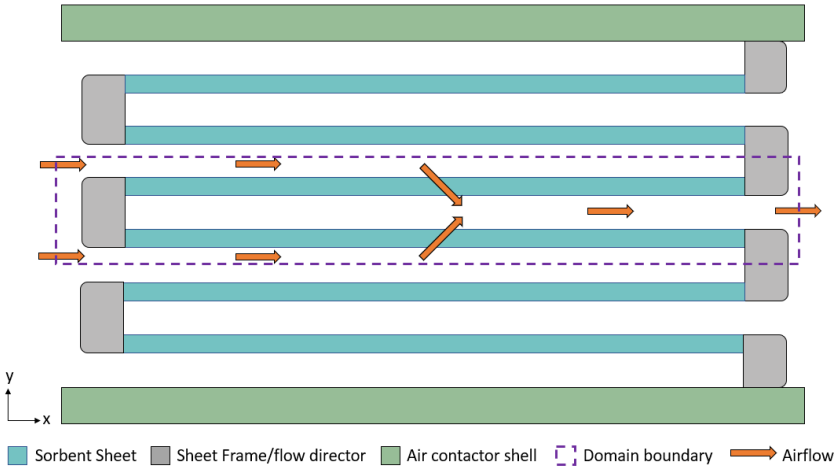

(b)

Figure 2.3: a) Cross section of a stack of sorbent sheets used in a solid sorbent air contactor. b) 2D cross section of a simplified geometry representing a DAC air contactor.

The fixed coefficient porous media model is applied to each sorbent sheet. This model adds a momentum source term to the governing RANS equations being solved in the back end of the commercial software. Users specify coefficients for all three directions, and the software internally solves a pressure gradient dependant on the flow velocity. The pressure gradient, ∇p, is described in eq. (2.1)

$$\nabla p = \rho_{ref} \left(A + B|v_s|\right) v_s \tag{2.1}$$

where ρ_{ref} is the density of the fluid, v_s is the superficial fluid velocity, and A and B are coefficients input based separately for each direction x, y, and z. In Simscale, the coefficients are specified as α, and β, however, to avoid confusion with other symbols used in this analysis, the variables are discussed as constants A and B instead. In this case, isotropic flow is expected so the coefficients are equal in all three directions.

In order to find appropriate values for these coefficients, the Ergun equation,eq. (2.2) is applied. The Ergun equation expresses a friction factor through packed beds with spherical particles based on a modified Reynolds number. The pressure drop through a packed bed of spherical particles is shown in equation 2.2.

$$\Delta p = \frac{150\mu L}{D_p^2} \frac{(1-\phi)^2}{\phi^3} v_s + \frac{1.75 L \rho}{D_p} \frac{(1-\phi)}{\phi^3} v_s |v_s| \tag{2.2}$$

Here, L is the length/thickness of the bed (L) in the direction of flow, D_p the spherical particle diameter of the packing, ρ is density of the fluid, μ the dynamic viscosity of the fluid, v_s the superficial velocity, and ϕ the void fraction/porosity of the bed. The parameters used for each sorbent are summarized in table A.1.

By matching terms in equation 2.1 and equation 2.2, the coefficients A and B are solved. The resulting equations are shown in equation 2.3 and equation 2.4.

$$A = \frac{150\mu}{\rho D_p^2} \frac{(1-\phi)^2}{\phi^3} \tag{2.3}$$

$$B = \frac{1.75}{D_p} \frac{(1-\phi)}{\phi^3} \tag{2.4}$$

The goals of incrementally increasing model complexity with 2D simulations was to first verify the coefficient porous media model worked as intended, apply it to a lab scale configuration with known pressure drop, and then scale the model up to a commercial size unit. This was done with the three incremental sub models:

1. Single vertical sheet, one sorbent (APDES-NFC).

2. Multiple horizontal sheets at **lab/patent scale** (0.55m x 0.55m x 0.65m (Wx-HxL)). Pressure drop compared at representative air velocities for one sorbent (APDES-NFC).

3. Multiple horizontal sheets at **commercial scale** (1.5m x 1.5m x 1.5m (Wx-HxL)). Pressure drop curve obtained for four sorbents at representative air velocities. One sorbent (APDES-NFC) used for further analysis in CFD-part 2.

First, to verify the validity of the coefficients, the outputs of the CFD model are compared with the results of the Ergun equation. This is done with a simple single vertical sheet of porous material. Particles of sorbent APDES-NFC are assumed to be packed into a 1cm thick sheet, and air is passed through perpendicular through the thickness. The pressure drop across the sheet is analyzed at the domain inlet and outlet. Once verified, this methodology is applied to other materials with known spherical particle diameter, and density and applied to other geometrical configurations.

Second, the fixed coefficient model is applied to a lab scale, air contactor configuration using a stack of horizontal sheets of APDES-NFC sorbent as shown in fig. 2.3. The pressure loss obtained from the CFD analysis was compared with the pressure loss curve presented in the patent [47].

Third, this geometric configuration, fig. 2.3, was then scaled up to an appropriate sizing for commercial operation, with dimensions suggested by Sabatino et al. [35]. Sorbent sheets with the same thickness and spacing were arranged in the same manner as described above, and a pressure drop curve was obtained for four sorbents of interest by applying the same representative inlet velocities to each one, matching the flow described in the patent. Four common sorbents discussed in the paper by Sabatino et al. [35] were modelled to find the pressure loss curves. The sorbents include APDES-NFC, Tri-PE-MCM, MIL-101(Cr)-PEI-800, and Lewatit VP OC 106.

The domain dimensions from the three scenarios discussed above are detailed in appendix A.

Model closure was obtained using the steady-state RANS equations, with the k-ω-SST turbulence model using commercial CFD software Simscale, run on the OpenFOAM framework. The k-ω-SST model is one of the most frequently used in industry, combining two common turbulent models; the k-ω for near wall, low Reynolds number flows; and switching to the k-ϵ model in the free stream. Outputs were evaluated

once residual values reached below 1×10^{-4}.

2D- Mesh generation

Simscale only supports 3D simulations, however, a 2D simulation can be performed by creating a thin mesh with a small number of cell depth in one direction and applying a periodic boundary condition at both faces. To obtain this, a mesh was created using the hex dominant parametric setting. A base mesh with perfect cubes for each cell was generated with a cell size of 1mm in all three directions. Five cells depth into the page produced the best results. For the single vertical sheet, a mesh was generated with 172.5k cells. For the 0.5m contactor, a mesh with 212.6k cells, and 442.4k cells for the 1.5m contactor simulations. Detailed domain dimensions can be seen in appendix A.

2D- Boundary conditions

Six boundary conditions were applied to the internal flow domain, shown in fig. 2.3b. A uniform velocity inlet is prescribed at the leftmost face, in the positive x-direction. Symmetry was applied in the positive-y direction on the top and bottom faces. A periodic boundary condition was applied on the sides into and out of the page (+-z). This results in a repeating slice of the sorbent sheets. This assumption ignores the no slip condition at the contactor edges, as this is deemed insignificant in the overall pressure drop. The gauge pressure was set to zero at the outlet face.

2D-Flow Regime

To determine the expected level of turbulence, the Reynolds number was computed in key areas. The largest Reynolds number is encountered at the inlet of the sheets where the flow is constricted, as shown in fig. 2.3b. In this region, a hydraulic diameter of a square duct is used, with a value of 2cm. The density of air is assumed to be 1.204 kg/m^3, and dynamic viscosity of 1.825×10^{-5} for air 20 $^\circ$ C. The average velocity in the constriction is 2.9m/s. This gives a Reynolds number of 3826. A critical Reynolds number of 2300 is generally accepted for internal flow in circular ducts [72], so the flow is expected to be in the transition region. As such, an appropriate turbulence model must be applied in the CFD analysis.

2.3.3 CFD Part 2- 3D modelling

The k-ϵ turbulence model is used for all 3D modelling discussed in the following sections. The k-ϵ model is commonly used for wind studies around buildings and dispersion flow problems using large external domains concerned with bulk flow characteristics [61, 62, 73–75]. A diffusion transport model utilizing passive scalars was supplemented using Eulerian advection-diffusion equations. Outputs were evaluated once residual values reached below 1×10^{-4}. The tools used in the 3D analysis are the pressure loss curve porous media model [71], momentum sources [76], and passive scalars [77].

The geometry shown in fig. 2.2 is used in this section, applied to the 3D domain as shown in fig. 2.4a. Each contactor bank consists of a sorbent region, represented with a porous media, and fan region, represented with a momentum source, as shown in fig. 2.4b. The sorbent region is assumed to have a depth of 1.5m as per Sabatino et al. [78], and the fan region is assumed a depth of 1m. The pressure drop curve obtained using the methods from part 1 is applied to the porous zone, utilizing the pressure loss curve model in Simscale. Momentum sources calculate the force required (ie. pressure gradient), and apply it to meet an average flow velocity through the applied geometry.

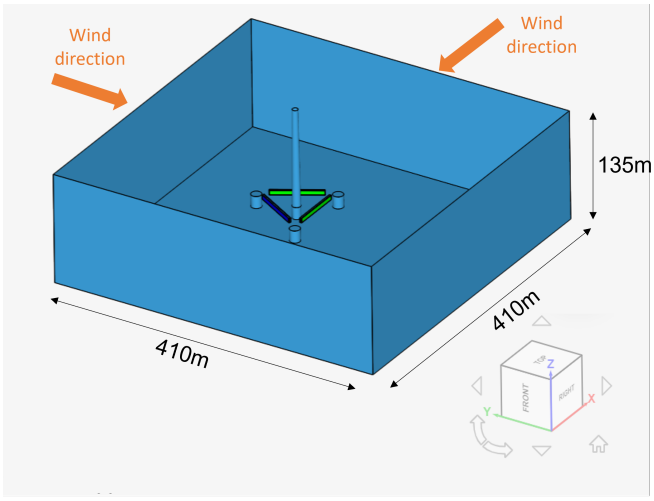

(a)

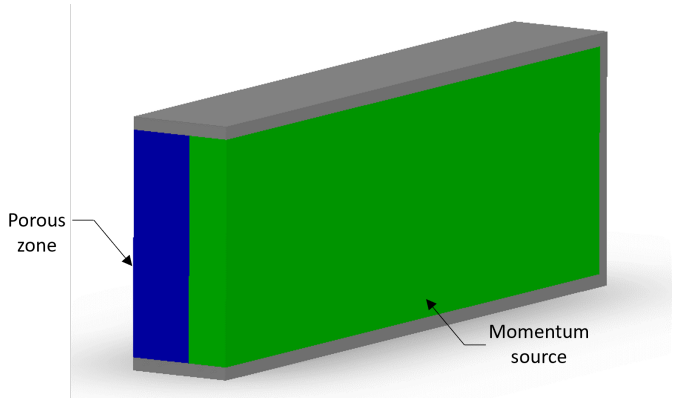

(b)

Figure 2.4: a) 3D CFD simulations domain for wind angles from 0-90°. Wind angles 91-180° shown in appendix A, b) Cross section of simplified air contactor.

A standard shipping container has dimensions 12.19m x 2.6m x 2.44m (LxHxW), which was used to roughly determine the size of the modelled units. Commercially, a shipping container sized DAC unit may be comprised of multiple adjacent units. However, in the case of this analysis, units were modelled by one fan region, and one sorbent region, neglecting any gaps between adjacent units to simplify meshing. The focus of the current study was analyzing gross flow characteristics at length scale of meters downstream. As a result, each contactor bank (two vertical rows of five DAC units) includes one fan region, and one sorbent region. A thin (0.3m) container shell contains both the sorbent and fan region to direct the flow through the two regions. Three contactor banks are placed symmetrically in a triangular arrangement around

the turbine base as shown in fig. 2.4a.

Passive scalars were used to model the dispersion of CO_2 depleted air exiting each DAC unit. Passive scalars are assumed to be transported in the flow, and do not actively change the flow physics of the simulation. Passive scalar transport can be described by the transport equation, also known as the convection-diffusion equation; which is a first order partial differential equation (PDE). This can be derived from the generalized form of the continuity equation which is shown in eq. (2.5).

$$\frac{\partial c}{\partial t} + \nabla \cdot j = S \tag{2.5}$$

Here c is the scalar field, j is the total (convective + diffusive) flux of c through the boundary, S is the source or sink term inside the domain. The flux, j, is divided into two terms, the diffusive, and convective terms respectively in the full transport equation, shown in eq. (2.6).

$$\frac{\partial c}{\partial t} - \nabla \cdot (D \nabla c) + \nabla \cdot (uc) = S_S + S_R \tag{2.6}$$

Here $\frac{\partial c}{\partial t}$ represents the time variation of the scalar quantity, D is the diffusivity $[m^2/s]$, c is the transported scalar quantity, u is the velocity of the means which transports this quantity [m/s], and S_S and S_R are the pure source term and the reaction source term respectively. S_R is often neglected in engineering applications.

In Simscale, the value of c, is tracked by the term T_1, but to avoid confusion with temperature, c is used throughout this analysis. The variable c can have any unit assigned to it, as long as it is kept consistent in all aspects of model setup, and post processing. In this analysis, c is considered as a concentration, with units of (mg-CO_2/m^3), which can be converted to more understandable units of concentration such as parts per million (ppm). An atmospheric concentration of 414.72 ppm CO_2 [3] corresponding to $758.55 mg/m^3$. A sample calculation for this unit conversion is shown in appendix A. This value is assigned as a fixed value at the velocity inlet along the inlet and top of the domain, at the bottom boundary condition as well as set as an initial condition in the entire domain.

In simulation set-up, values of the diffusion coefficient (D) is defined, as well as the

turbulent Schmidt number (Sc_t), representing the ratio between turbulent transport of momentum and the turbulent transport of mass. At 20° C, D for CO_2 in air is $0.16cm^2/s$ [79], and Sc_t is 0.7, based on the flow characteristic and is left at the default value.

Volumetric passive scalar sources (sinks) are assigned to the porous zone of each contactor. Passive scalar sources/sinks require a flux to be defined. In this case, a mass per volume flux ($\jmath_v$) is prescribed in units of ($mg/m^3 \cdot s$). The flux is back calculated based on a target outlet concentration of the contactor. Based on the adsorption breakthrough curve shown by Gebald et al. [47], and Bajamundi et al. [49], CO_2 concentrations at the outlet of the contactor range from 10-20 ppm at the beginning of an adsorption cycle, and reach levels close to ambient towards the end of the cycle. An average value was interpreted from the figures of 150 ppm. In practice, adjacent DAC units would be in different phases of adsorption and desorption, however, a worst case scenario of all units in adsorption is used in this analysis. With all units in desorption mode, an outlet concentration is set homogeneously across the entire sorbent region, and is assigned a value representative of the beginning of an adsorption cycle. Similar values are reported for Aqueous DAC systems, so this result could be applied to other systems as well. Keith et al. [9] reports an air contactor outlet concentration of about 105ppm CO_2 for aqueous based DAC process.

In order to calculate the concentration flux, one must understand the number of particles entering the contactor, and specify the amount that must be removed in order to achieve a desired outlet concentration. The amount of CO_2 particles (mg/s) entering the contactor ($\dot{m}_{enter}$) is described by equation 2.7.

$$\dot{m}_{enter} = \sigma_{contactor} \cdot u_{contactor} \cdot c \tag{2.7}$$

Here $\sigma_{contactor}$ is the cross sectional area of the contactor inlet, $u_{contactor}$ the velocity, and c the concentration entering.

The quantity of particles (mg/s) removed by the volumetric passive scalar source $\dot{m}_{removed}$), is solved by re-arranging equation 2.8.

$$c_{contactor,out} = \frac{\dot{m}_{enter} - \dot{m}_{remove}}{\dot{V}_{contactor,inlet}} \tag{2.8}$$

The volumetric mass flux value (j_v), in units ($mg/m^3 \cdot s$) is solved using equation 2.9.

$$j_v = \frac{\dot{m}_{removed}}{V_{contactor}} \tag{2.9}$$

Based on a contactor velocity ($u_{contactor}$) of $0.73m/s$ as used from part 1, and an inlet area ($\sigma_{contactor}$) of $316.94m^2$, a flux value of $-188.58mg/m^3 \cdot s$ is applied to each volumetric source. A constant flux value was specified for all cases based on a design velocity, however, in reality, the flux would vary depending on actual flow velocity through contactors. Results were post processed in Paraview, and presented in units of ppm as it is more readily understandable as it relates to atmospheric concentrations.

Three nominal wind speeds are analyzed at a hub height of 150m: cut-in (3 m/s), rated (10.59 m/s), and cut-out (25 m/s). The turbine is assumed to have fixed mooring direction, with 0° in the positive y-direction. This is expected to align with the predominant wind direction, however, as the wind direction varies, the turbine rotor will yaw about the tower to align with the wind direction, while the platform below remains fixed in place. Bidirectional fans are assumed to be used, so that fan direction will change to best align with the flow to minimize pushing air upstream. Wind angle is varied from 0-180° at 30° increments. The fan direction with respect to the flow can be seen in figure 2.5 below.

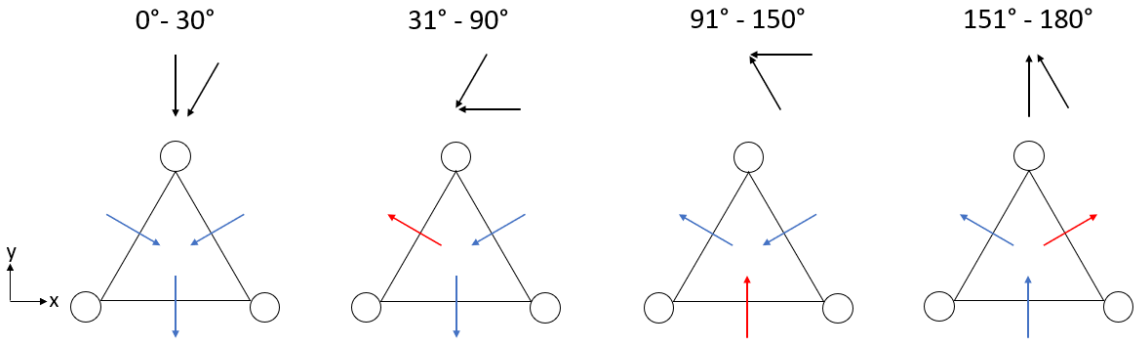

Figure 2.5: Fan directions with respect to incoming wind direction.

It is hypothesized that at high wind speeds, upstream contactor banks may experience strong enough wind speeds to enable them to run passively, without turning fans on to increase velocity through the sorbent region. To test this hypothesis, a single bank of

contactors, containing only a sorbent region is placed perpendicular to the incoming flow, and run at varying wind speeds from 3-25m/s defined at hub height (150m). The actual velocity experienced by the contactors is measured at contactor center height, 17.9m. Velocity at the outlet of the sorbent region is measured to investigate whether sufficient volumetric air flow is met. An average outlet velocity of 0.73m/s or greater is required to meet the volumetric flow rate to enable turning of the fans. As a result, the full scale simulation is modified accordingly, turning off fans where possible. The fan off configuration dependant on incoming wind flow angle is outlined in appendix A.

3D Domain size

The domain size of external aerodynamic simulations can have a large impact on model accuracy, but also has a large impact on the number of cells in the mesh, and as a result computational effort. A balance must be struck between computational grid size so that the boundaries do not interfere with the flow physics, but also not so big that the quantity of cells makes simulations too computationally heavy. Abu-Zidan et al. [80] aimed to optimize the domain size by comparing the results of many external simulations. They concluded that the previous recommendations by Franke et al. [81] seemed overly conservative in most cases. Franke et al. [81] recommends 5H upstream, 15H downstream, 5H in a lateral direction, and 6H a vertical direction. In this case, H refers to the tallest building height. Abu-Zidan et al. [80] recommends 3H upstream, 3H downstream, 3H laterally, and 4H vertically. To remain conservative, the recommended domain size from Franke was used in this study, based on the height of the contactor units from the bottom of the domain. Future analysis could explore making the domain smaller, in line with Abu-zidan.

The domain dimensions were determined using a height (H) of 20m from ocean surface to the top of the contactors. The recommendations from Franke et al. [81] were used, ensuring a minimum of 5H upstream, 5H in the lateral direction, 15H downstream, and 6H in the vertical direction. A Distance of 15H was applied to one side as well as downstream, to account for the change in wind direction. Two domains/meshes were created, one for 0-90°, and one for 91-180 °. For simulations from 0-90°, the domain has dimensions of 410m x 410m x 135m in the x-y-z directions respectively. For simulations from 91-180°, the domain has a size of 520m x 506m x 135m in the x-y-z direction respectively. The domain dimensions are highlighted in figs. 2.4a and A.4

for 0-90 °, and 91-180° respectively. The turbine tower base at water level is placed at the origin. The turbine tower extends far beyond the domain height, protruding through the top boundary. This may cause interference with the boundary conditions, however, modelling based on this height will make the domain excessively large. The area of interest is at the bottom of the domain, where the CO_2 mixing predominantly occurs, and does not interact with the flow near the top of the domain. The turbine tower may cause the residuals to not decrease as low as if the domain was extended to fully encompass it.

3D Mesh

A 3D mesh was generated using Simscale's automatic algorithm. This uses a mix of tetrahedral cells where necessary around key geometry, and hexahedral cells within the bulk flow. The global fineness was increased to seven out of ten. For simulations of the single contactor with porous region only, a mesh with 1.2M cells was generated. For the complete simulation, wind angles 0-90 ° used a mesh with 8.3 million cells,and 8.2 million cells for angles 91-180 °. Mesh refinements were added in key areas to improve the resolution around flow features. Region refinements were implemented in cell zones and Boundary layer inflation was implemented on all non-slip wall surfaces, discussed further in the following paragraphs.

Cell zones are used to group 3D regions of cells created in the CAD model. This allows properties to be applied to specified regions such. In this case, cell zones are used to define the porous media region, and the momentum source region. SimScale recommends having a minimum of five cells through the thickness of a cell zone, thus a region refinement was used to define a maximum edge length of 0.2m inside the porous region and momentum source cell zones.

To achieve a horizontally homogeneous ABL profile with a sand grain roughness applied at the bottom of the domain, Blocken et al. [74] suggests four basic requirements: 1) A sufficiently high mesh resolution in the vertical direction at the bottom face, 2) A homogeneous ABL upstream and downstream of the objects of interest, 3) The vertical distance from the center of the wall adjacent cell should be less than k_s, and 4) k_s and z_0 are related by equation 2.10.

$$k_s = 30 \cdot z_0 \tag{2.10}$$

In this case, $z_0 = 6.1 \cdot 10^{-3}m$, equal to $k_s = 0.183m$. As a result the first layer cell height adjacent to the bottom plane needs to be greater than 0.366m. This is obtained by adjusting the first layer height for the inflate boundary layer refinement.

3D Boundary conditions

A variety of boundary conditions are commonly used in literature. Typically six boundary conditions are applied to the six sides of the rectangular domain: Inlet, outlet, bottom, top, and two sides. Domain boundaries can be seen in figs. 2.4a and A.4.

A logarithmic atmospheric boundary layer (ABL) velocity profile is applied at the inlet. This resolves the expected wind velocity profile near earths surface, and is assumed to be fully developed over a sufficient upstream distance with the same ground roughness that is applied within the domain. This ensures that an internal boundary layer profile does not develop within the domain. A wind angle of 0 ° is in the negative y-direction. Wind angle increases in a clockwise rotation. This is shown in figs. 2.4a and A.4. The ABL profile follows the form of equations eqs. (2.11) to (2.14) as per Blocken et al. [74].

$$u^* = K \cdot \frac{u_{ref}}{\ln\left(\frac{z_{ref}+z_0}{z_0}\right)} \tag{2.11}$$

$$u = \frac{u^*}{K} \cdot \ln\left(\frac{z+z_0}{z_0}\right) \tag{2.12}$$

$$k = \frac{u^{*2}}{\sqrt{c_\mu}} \tag{2.13}$$

$$\epsilon = \frac{u^{*3}}{K(z+z_0)} \tag{2.14}$$

where u^* is the wall function friction velocity (m/s), u is the velocity (m/s), u_{ref} is the reference free stream velocity (m/s) at reference height z_{ref} ($z_{ref} = 150m$), K is the Von Karman constant equal to 0.41, z_0 is the aerodynamic roughness length ($z_0 = 6.1 \times 10^{-3}$ m), z is the height at which the velocity is calculated, k is the

turbulent kinetic energy (m^2/s^2), ϵ is the rate of dissipation of turbulent kinetic energy (m^2/s^2), and c_μ is the turbulent viscosity constant equal to 0.09. The variables u, k, and ϵ are entered directly in CFD as a custom boundary condition, applying a fixed value then inputting the above equations, while leaving pressure as zero gradient.

The bottom of the domain is defined by the no slip wall function, more specifically applying a sand grain roughness height (k_s). The relationship between z_0 and k_s is given by equation 2.10 as per Blocken et al. [74]. Golbazi et al. [82] recommend a median surface roughness height of 6.1×10^{-3}, representative of a rough sea state. This corresponds to $k_s = 0.183m$. First layer height of the mesh along the bottom boundary is imperative to achieving a horizontally homogeneous BL as discussed in the previous section.

The outlet of the domain commonly has different boundary conditions applied. In some studies [61, 75], the normal gradients of all variables are set to zero, whereas in others [73, 80] the static pressure, or in other words the gauge pressure is set to 0. In the case of this simulation, the former is applied, setting outlet pressure to the free stream value, and all other parameters set to zero-gradient. Setting zero gauge pressure across the outlet of a large external domain caused issues as it induces a small artificial pressure gradient. Applying the software solved free stream pressure at the outlet face effectively gets rid of any artificial pressure gradient caused by applying a strict zero gauge pressure.

For the top and side boundary conditions, different combinations are also applied in literature. Abu-zidan et al [80], and Blocken et al. [73] apply symmetry planes to the top and sides. Labovsky et al [61, 75] use a periodic boundary condition on the sides, and apply the same inlet velocity profile along the top plane. They discuss using symmetry planes for the sides, however, conclude that the result are better in their case when using periodic boundary conditions as when fluid (air) escapes from one side boundary, an equal amount is let in through the opposite. As such, a periodic boundary condition is applied to both side walls. Labovsky follows the best practices from Franke et al. [81], applying a constant shear stress to the flow along the top boundary. This is done by applying the same ABL velocity profile to the top plane. This best practice is also adhered to in this study.

Horizontal homogeneity of the ABL velocity profile was ensured by running an empty domain with the same boundary conditions applied. This result can be seen in ap-

pendix A.

To simulate different wind directions, unit vectors were applied to the velocity inlet boundary conditions. Instead of using periodic side boundary conditions, identical velocity inlet BC's were applied to two adjacent faces, and the free stream outlet boundary condition applied on the opposite adjacent faces. Effectively this allows flow in and out through all four vertical faces of the domain.

2.3.4 Energy model

The minimum thermodynamic work is calculated to obtain a baseline of minimum plant wide energy demand based on inlet CO_2 concentration. Computing the real work based on a second law efficiency includes both electrical and thermal energy requirements, and is used as a baseline comparison. However, the work computed in this manner is only a function of the inlet inlet CO_2 concentration, and does not account for ambient wind conditions.

Total plant energy is composed of electrical and thermal energy. Further analysis is conducted to assess the estimated change in electrical and thermal energy demand as a result of ambient wind conditions. They are discussed in section 2.3.4, and section 2.3.4 respectively. All calculations in this section were conducted using Microsoft Excel.

Minimum thermodynamic work and second law efficiency

The minimum thermodynamic work (J/mol-CO_2), $\bar{w}_{rev}$, for separating gas species can be computed using equation 2.15 as per Struchtrup [83].

$$\bar{w}_{rev} = -\overline{R}T \frac{\ln(1-\alpha X) + \frac{\alpha X}{1-\alpha X} - \ln(1-X) - \frac{X}{1-X}\ln(X)}{\frac{X}{1-X} - \frac{\alpha X}{1-\alpha X}} \tag{2.15}$$

where $\overline{R}$ is the universal gas constant, T is the ambient temperature, α is the separation efficiency, and X is the initial CO_2 mole fraction. Remaining air has CO_2 content αX.

In 2021, the global average concentration of CO_2 in the atmosphere was 414.72 ppm [3]. In the results section to follow, a hypothetical worst case of inlet CO_2

concentration scenario are analyzed,as well as two middle scenarios. In the worst case, an upstream contactors outlet is directly connected to a downstream contactors inlet giving an inlet concentration of roughly 100ppm. In the middle scenarios, 200ppm and 300ppm CO_2, downstream contactors are placed some distance from upstream units and the downstream units experiences some decreased level of concentration between 100 and 414.72ppm. These outlet concentrations are described previously in section 2.3.3.

An estimation of the actual work($\bar{w}$) can be computed using the second law thermodynamic efficiency (η_{II}), described by $|\bar{w}| = \frac{|\bar{w_{rev}}|}{\eta_{II}}$. The second law efficiency is computed through detailed analysis of specific plants. Long-Innes and Struchtrup [84] compute a second law efficiency of 7.8% using aqueous based DAC. Solid sorbent systems are believed to fall within this range as per the National Academy of Sciences report on negative emissions [4], with middle-range scenarios between 7.6-11.4%. In this analysis, $\eta_{II} = 7.6\%$ is assumed as a conservative estimate.

Electrical energy

The electrical energy consumption of the plant is composed of the fan/blower to push air through the contactor over the adsorbent material; the vacuum pump to evacuate oxygen from the air contactor before heat is applied to avoid sorbent degradation; and the CO_2 compression to bring output CO_2 a desired pressure. The energy for the vacuum pump, and CO_2 compression is based on design choices and does not vary greatly as a result of ambient conditions. This is assumed to be constant based on the designed setup, thus is not analyzed further in this study.

The fan power is a function of the pressure drop, and the volumetric flow rate through the contactor. As a result, the fan power is dependant on the ambient conditions entering the contactor. Conducting unit analysis along with laws of force, momentum, and power, an expression can be derived for the work from each fan. The force exerted on the flow represented by equation 2.16, and then the power required by equation 2.17.

$$F_{fan} = \int_V S_x dV \tag{2.16}$$

$$P_{fan} = \int_V S_x \cdot u_x dV \tag{2.17}$$

where S_x ($\frac{kg}{m^2 \cdot s^2}$) represents a direct momentum source term in the RANS momentum equations in the direction of the flow, V (m^3) is the volume of the momentum source, and u_x (m/s)) is the normal velocity in the direction of flow. In this case, the average value of u_x is obtained by integrating the normal flow velocity about the surface area the normal flow through the inlet area to each fan.

The momentum source used to simulate this in the CFD model solves for the momentum source strength to meet a prescribed velocity. At each iteration, the pressure gradient applied to the momentum source volume is outputted as a result. The pressure difference, Δp, experienced through the contactor, can be solved by $\Delta p = \nabla p d$, where ∇p is the pressure gradient, and d is the distance in the direction of flow. This can be used to compute the power consumed by the fan. Equation 2.17, is simplified to be used with the output from the CFD results, as equation 2.18. From the CFD result, the area integral applied to the cross section perpendicular to the flow direction of the normal velocity across the fan inlet plane is taken to obtain the volumetric flow rate. A fan efficiency of 60% is assumed as per Sabatino et al. [35].

$$P_{fan} = \frac{1}{\eta_{fan}} \Delta p \cdot \dot{V}_{air} \tag{2.18}$$

Where η_{fan} is the fan efficiency, Δp is the pressure Difference (Pa), d is the distance in the flow direction (m), and $\dot{V}_{air}$ is the volumetric flow rate (m^3/s).

Thermal energy- Isotherm method

Thermal energy is required to strip the CO_2 molecules from the capture material. Typically this is met by passing steam through the module. The total equilibrium thermal energy ($Q_{eq,th}$) for desorption is comprised of the sensible ($Q_{sensible}$) and reaction heat ($Q_{reaction}$). It is described in eq. (2.19). The sensible and reaction heat is further broken down into the components for CO_2, H_2O, and the sorbent. The sorbent chosen for analysis in this study is the APDES-NFC sorbent, which has seen significant experimental work, and includes isotherms for CO_2 and H_2O, in both dry and humid conditions.

$$Q_{eq,th} = \sum Q_{reaction} + \sum Q_{sensible} \tag{2.19}$$

The reaction heat for CO_2 is shown in equation 2.20, and for H_2O in equation 2.21. The sorbents reaction heat is zero.

$$Q_{reaction,CO_2} = \frac{\Delta H_{iso,CO_2}}{M_{CO_2}} \tag{2.20}$$

$$Q_{reaction,H_2O} = \Delta H_{iso,H_2O} \frac{\Delta q_{H_2O}}{\Delta q_{CO_2} M_{CO_2}} \tag{2.21}$$

Here, ΔH_{iso} is the isoteric heat of adsorption, Δq is the equilibrium adsorption capacity, and M is the molar mass of each species.

The isoteric heat of adsorption can be solved using the Van't Hoff equation, which is a function of the temperature, and gas partial pressures during adsorption and desorption. This relationship is discussed in appendix A.

The equilibrium adsorption capacity, Δq_{CO_2}, and Δq_{H_2O} describe the difference in the quantity of species adsorbed during the adsorption phase, q_{ads}, and the quantity of species re-adsorbed during the desorption phase, q_{des}. This is highlighted below in eq. (2.22).

$$\Delta q = q_{ads} - q_{des} \tag{2.22}$$

Adsorption of CO_2, and re-adsorption of CO_2 during the desorption phase, is described by the modified Toth isotherm equation, with parameters fit using experimental data from literature. Water adsorption, and re-adsorption during desorption phase, is described by the Guggenhein-Anderson de Boer (GAB) isotherm model, also with parameters fit using experimental data obtained from literature.

The CO_2 loading capacity is enhanced by increased water uptake, however, multi-component isotherms are not available in literature for the sorbents at hand. Majority of literature to date has ignored this phenomenon, however, it has a significant impact on the overall energy demand and capture capacity of a plant. Various methods

have been presented in literature to capture the enhancing effect with the presence of increased humidity. Wurzbacher et al [53] used an enhancing factor to increase the equilibrium loading based on empirical results, however, this was only accurate within a small range of values, and produced errors beyond the bounds of the experiments. Stampi-Bombelli improved this by embedding the water loading within the CO_2 isotherm. The methods of Stampi-Bombelli are used in the current analysis. The adsorption models are described in further detail in appendix A.

The concentrations/partial pressures during desorption can be computed, assuming all CO_2 and H_2O adsorbed, is desorbed in the subsequent phase. The partial pressures can be computed using Dalton's law of partial pressures. This allows the computation of the desorption capacities, $q_{H_2O,des}$ and $q_{CO_2,des}$, and further the equilibrium loading capacities, Δq_{H_2O} and Δq_{CO_2}.

The sensible heat for CO_2 is shown in equation 2.23, for H_2O in equation 2.24, and for the sorbent in equation 2.25.

$$Q_{sensible,CO_2} = c_{p,CO_2} \left(T_{des} - T_{ads}\right) \cdot \frac{1}{M_{CO_2}} \tag{2.23}$$

$$Q_{sensible,H_2O} = \left(c_{p,H_2O} \left(T_{sat} - T_{ads}\right) + c_{p,vap} \left(T_{ads} - T_{sat}\right)\right) \frac{\Delta q_{H_2O} M_{H_2O}}{\Delta q_{CO_2} M_{CO_2}} \tag{2.24}$$

$$Q_{sensible,sorbent} = c_{p,sorbent} \left(T_{des} - T_{ads}\right) \frac{1}{\Delta q_{CO_2} M_{CO_2}} \tag{2.25}$$

Here c_p is the molar specific heat capacity. The values for the specific heat capacity of CO_2, c_{p,CO_2} are interpolated from values in the National Institute of Standards and Technology (NIST) webbook [85]. The c_{p,H_2O} is comprised of liquid and vapor phases, and values are interpolated from Struchtrup [83] for the vapor phase, and the engineering toolbox for the liquid phase [86]. The $c_{p,sorbent}$ for APDES-NFC used the value from Wurzbacher et al. [53].

2.4 Results and discussion

The results obtained from the CFD model are fed into the energy model. CFD results are shown in section 2.4.1, and the energy modelling results are shown in section 2.4.2. Further analysis, including the full scale model to explore the impacts of CO_2 mixing, and fan work were completed based on the sorbent APDES-NFC, as this sorbent has received significant attention in literature, as well as likely been commercially deployed.

2.4.1 CFD results

The three main sections of the CFD model are the pressure drop modelling, wind driven fan energy decrease, and CO_2 dispersion modelling.

2D CFD Pressure drop simulations

This section produced a pressure loss curve for a contactor with realistic dimensions for commercial scale. In order to do this, the porous media was first verified by comparing the CFD results from a 2D vertical sheet, and the calculated pressure loss from the Ergun equation. The results matched very closely, summarized in table A.3.

Next, the fixed coefficient model was applied to the configuration in the patent by Gebald et al. [47] discussed earlier, to verify that the modelled geometry and sorbent properties, produced similar pressure drops to the pressure loss curve given in the patent. The modelled results closely matched the pressure loss curve, indicating the model accurately described the configuration used in the patent. The results are summarized in table 2.1. At low velocity, the largest error was found, with a 51% difference, however, the velocity of interest showed a decent correlation with an error of 6.1%. The CFD model uses periodic boundary conditions on the side walls, and symmetry on the top and bottom and thus ignores the pressure loss associated with the friction from the wall at the sides and top of the contactor. This is likely a source of deviation between the results, and thus some large errors associated with it. This is more significant at lower velocities, where friction losses make up a larger portion of the overall pressure loss through the system.

Velocity (m/s)	Patent pressure loss Δp (Pa)	CFD pressure loss Δp (Pa)	Percent error (%)
0.18	16	7.9	51
0.37	31	27	13
0.55	58	55	5.2
0.73	98	92	6.1

Table 2.1: Comparison of patent [47] pressure loss through a 0.5m contactor length with geometry shown in fig. 2.3b.

This verification provided good confidence that the model was accurately describing a realistic air contactor, and was then scaled up to a length of 1.5m. The pressure loss data for APDES-NFC, Tri-PE-MCM, MIL-101(Cr)-PEI-800, and Lewatit VP OC 106 is shown in table 2.2. Only the sorbent APDES-NFC was considered for the following 3D simulations.

	APDES-NFC	Tri-Pe-MCM	MIL-101(Cr)-PEI-800	Lewatit VP OC 106
Velocity (m/s)	Pressure drop (Pa)	Pressure drop (Pa)	Pressure drop (Pa)	Pressure drop (Pa)
0.18	38.9	46.8	46.9	58.2
0.37	122	149	149	192
0.55	239	294	295	383
0.73	391	479	481	626

Table 2.2: Pressure loss data obtained by 2D modelling a 1.5m long contactor, 1cm thick sorbent sheets, and 1 cm flow channels.

The flow through the sorbent sheets follows a typical jet pattern as expected. Air enters the domain on the left, is accelerated as it enters the flow channels/constrictions, diffuses through the porous material, and accelerates again through the outlet. This behaviour can be observed in fig. 2.6a for the 0.5m contactor length simulation. A non-symmetric flow pattern is encountered at the outlet, which could be due to many reasons. The turbulence encountered in the wake will have oscillations of a certain frequency, which may cause the jet to favour one side or another.

It can be seen in fig. 2.6b that the most of the flow diffuses through the porous zone only at the ends of the channel. This means that majority of the sorbent is not having air convectively passed over it, and thus is relies purely on diffusion to adsorb CO_2. This can be understood from looking at the transport equation from earlier, eq. (2.6). The two terms of interest are the diffusive flux, $\nabla \cdot (D\nabla c)$, and the convective flux, $\nabla \cdot (uc)$. At 20° C, D for CO_2 in air is $0.16cm^2/s$ [79]. The concentration gradient (∇c) from the flow channel to the adjacent particles is also expected to be relatively small. This results in a small change of overall concentration as a result of diffusive transport. With zero velocity through the sheet, the convective term is zero. The present 2D modelling does not account for CO_2 adsorption, and this could be explored in future work to gain a better understanding of the sorbent usage efficiency.

This suggests that alternate sorbent sheet configurations should be considered to maximum convective air flow past all particles in the sheet. If only the ends are coming into contact with the air, they will lose their adsorption capacity much quicker than the rest of the sheet, and will require replacement earlier. The whole sheet would likely be replaced at once, resulting in sorbent usage less than its full capacity. Sorbents are known to contribute the largest cost to DAC installations as they typically need replacement every 0.5-2 years. The uniform pressure buildup through the contactor length can be seen in fig. 2.6c.

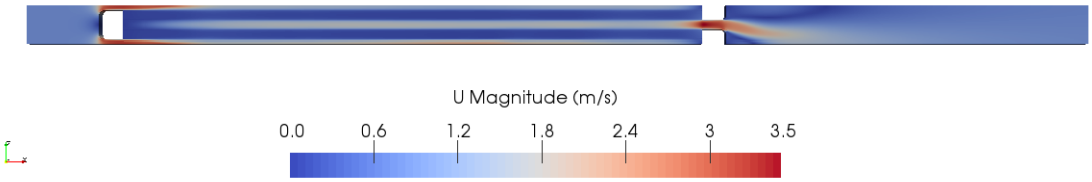

(a)

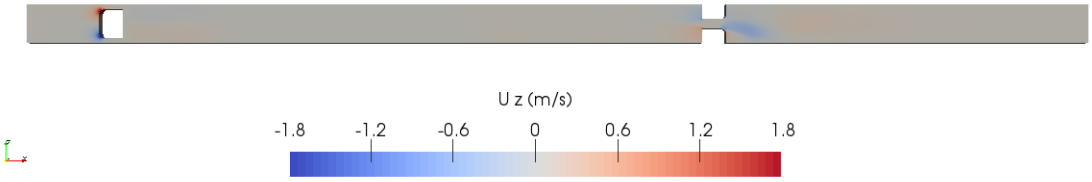

(b)

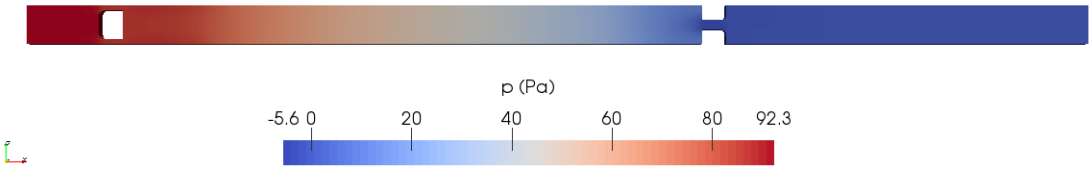

(c)

Figure 2.6: 2D CFD result of contactor with length of 0.5m, sorbent sheet thickness of 1cm, and air flow channels of 1cm. Shown is the a)velocity magnitude (m/s), b)velocity in the vertical direction (m/s), and c)the uniform pressure buildup through the reactor (Pa).

3D CFD- Wind driven velocity increase

The velocity throughput results of the single contactor bank with a porous region only placed perpendicular to incoming wind flow can be seen in fig. 2.7.

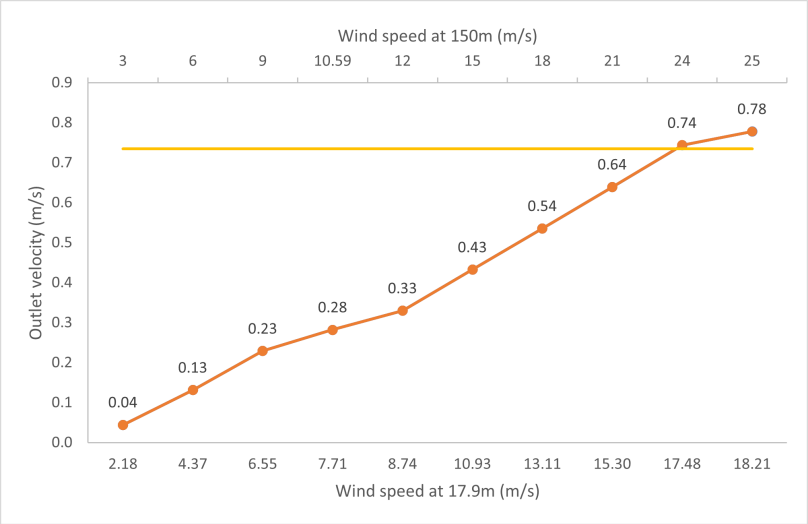

Figure 2.7: Porous zone output velocity as a function of wind speed with a contactor bank mounted 15m above ground/water. Wind speed is measured using an upstream probe point at a height of 17.9m, the center of the contactor bank. Target throughput velocity is 0.73 m/s, shown with the horizontal yellow line.

It is clear from fig. 2.7 that the desired output velocity of 0.73m/s is not reached until an input velocity of roughly 17.48 m/s at contactor center height, representing 24 m/s at hub height. With a cut-out wind speed of 25 m/s, majority of the operating zone of the turbine will require additional fan work. Above 24 m/s, the unit should still pass the required volume of air through the contactor to meet the desired capture rate, thus fans could be turned off, and the energy required to power the fans could be saved. As a result, in following simulations, at cut-out wind speed, upstream fans are turned off, and the units are assumed to passively contact with the air.

For a land based scenario, contactors may be mounted at or near ground level. Sufficient wind speed is never met before cut out wind speeds as seen in fig. A.6, thus fans would always need to be turned on to some extent. A contactor inlet wind speed of about 17.48m/s is required to allow turning off the fans. The wind speed required at a certain height to achieve this could be calculated using the ABL velocity profile, and appropriate ground roughness using eqs. (2.11) and (2.12).

Based on this conclusion, certain fans were turned off based on the velocity inlet angle when run at the cut-out wind speed of 25 m/s. The upstream fans are assumed to be turned off, whereas the downstream fans are left on as the upstream fans disrupt the local wind speed entering downstream units below the point at which they meet the

required flow velocity. The on/off configuration of each fan is shown in appendix A.

3D CFD- Concentration entering contactor

The local mixing of CO_2 at cut-in wind speed (3m/s) can be seen on a cutting plane from above through the center of the contactor bank in fig. 2.8. A wind angle of 0° is shown in fig. 2.8a, 90° in fig. 2.8b, and 180° in fig. 2.8c.

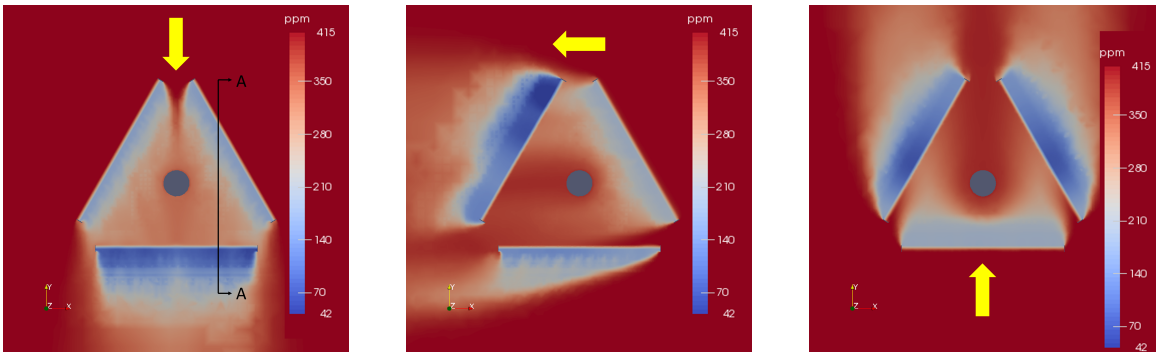

(a) (b) (c)

Figure 2.8: CFD result showing dispersion of CO2 in domain at cut in wind speed (3 m/s) with inflow angle of wind angle a) 0°, b) 90°, and c) 180°. Wind direction shown with yellow arrow. Shown projected on the top plane (x-y plane) through the center of the air contactor bank, at height z = 17.9m. Cut plane A-A shown in fig. 2.8a, and further cut planes are shown in appendix A

Average CO_2 concentration entering downstream contactors can reach levels as low as about 280 ppm. This occurs in the case with a 3m/s at 30 °. As wind speed increases, the concentration entering downstream units also increases. At higher wind speeds, more CO_2 is brought into the domain, mixing with the depleted region at the contactor outlet. A top view plane of 0°, 90°, and 180° wind angles at cut-in, rated, and cut-out wind speeds are shown in appendix A. This clearly shows the relationship of increasing CO_2 dispersion with increasing wind speed. Increased CO_2 dispersion means higher concentrations entering downstream units, thus decreased thermal energy demand.

A side view of CO_2 concentration leaving one contactor, and entering a downstream contactor is shown in fig. 2.9. Majority of the CO_2 depleted air leaving the upstream contactor does not have CO_2 diffuse vertically into it from the surrounding air. Note that the upstream contactor is cut on an angle, whereas the downstream contactor is

cut perpendicular to the flow direction.

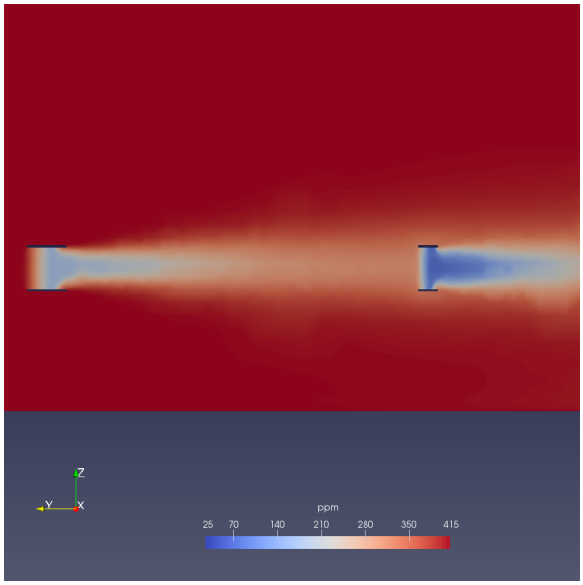

Figure 2.9: CO_2 mixing shown on a side view orientation. Cutting plane placed 15m in the x-direction, parallel with the y-z plane. Cutting plane shown as A-A in fig. 2.8a Wind enters at 3m/s with an angle of 0° (negative y-direction).

2.4.2 Energy modelling results

From the CFD model, the pressure drop curve, discussed in section 2.4.1, and the wind driven velocity through the contactor, discussed in section 2.4.1, effect the energy consumed by the fan. The CO_2 dispersion, discussed in section 2.4.1, effects the thermal energy requirement.

Second law efficiency work

With $\eta_{II} = 7.6\%$, the real work required for 100ppm, 200ppm, 300ppm, and 414.72ppm is shown in fig. 2.10.

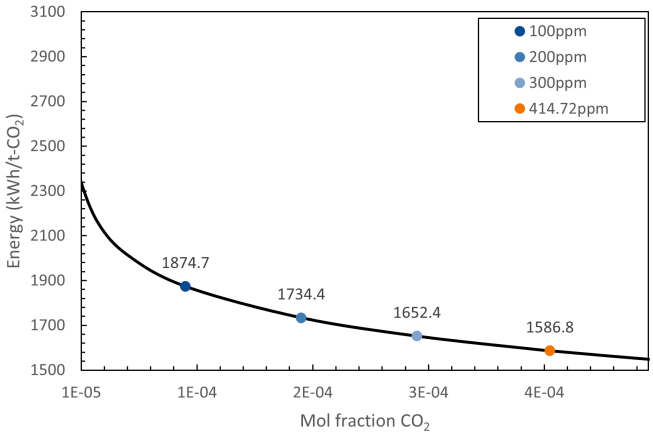

Figure 2.10: Real thermodynamic work using $\eta_{II} = 7.6\%$ for gas separation at 25° C with a capture fraction $\alpha = 0.9$. Shown for the region applicable to DAC, 10-500ppm. Results highlighted for 100ppm, 200ppm, 300ppm, and 414.72ppm CO_2.

This change in energy is non-negligible, especially as DAC is typically considered to be deployed at very large scales. Commercial DAC plants have been proposed on the order of 1Mt-CO_2/y. Under a worst case scenario with CO_2 concentration of 100ppm entering downstream units, an additional 287.9×10^6 kWh/t-CO_2 is required, an increase of 18% from 400ppm. This is not practical as one would not expect to install units in this manner. However, some level of CO_2 depletion is expected to enter enter downstream units- assume 300ppm for arguments sake. This results in an additional 65.6×10^6 kWh/t-CO_2 (4% increase). To put this into perspective, in 2020 the average household in the US consumed 10,715 kWh/y of electricity [87]. At 300ppm inlet concentration, the energy difference is equivalent to the annual electricity consumption of almost 6,000 households for 1Mt-CO_2/y removal. Studies suggest DAC deployment in the multiple Gt-CO_2/y level by about mid century, potentially reaching 10-20 Gt-CO_2/y by the centuries end [4]. At this level, the additional energy requirement can certainly not be ignored, especially for a technology whose biggest criticisms lies in its high energy demands compared to other decarbonization approaches.

Electrical energy- Fans

The total fan power for all wind speeds and directions is shown in fig. 2.11. A hypothetical fan power for zero velocity is shown, where the average contactor velocity is 0.73m/s through an area of $316.9m^2$, with a pressure drop of 391 Pa as per table 2.2.

This results in a fan power of 455 kW. It is clear from the figure that there is a decrease in overall fan power at all three wind speeds. There is a slight increase in total power required from 3m/s to 10.59 m/s, but this is likely due to negative pressures at the contactor outlet due to the contactor wake region. As a general trend, there is a drop in power requirement with increasing wind speed. At 25m/s, upstream fans can be turned off as per fig. 2.7, allowing the contactor to passively contact with air. Downstream contactors are kept on as they are within the wake region of the upstream contactors, thus will not be at the required inlet velocity.

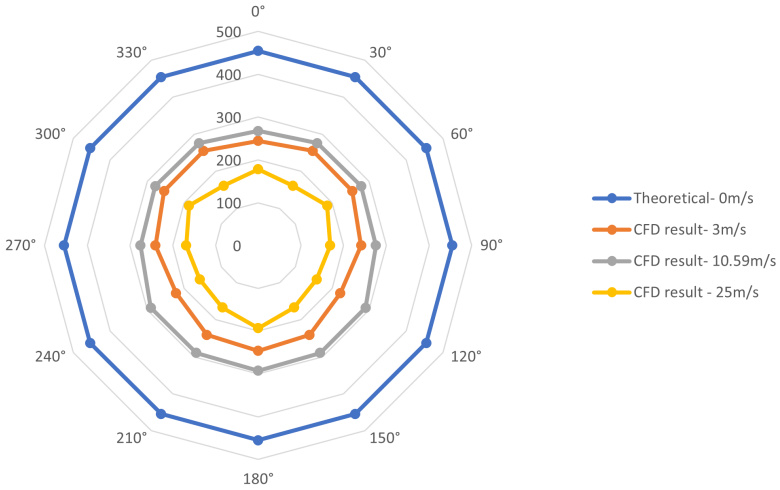

Figure 2.11: Total fan power (kW) for all three contactor banks at zero (theoretical), cut-in, rated, and cut-out wind speeds.

Further details for contactor banks 1-3 can be seen in figs. 2.12a to 2.12c. At high wind speeds, wind angles perpendicular to the upstream contactors allow the fans to be turned off, and the minimum overall power is consumed. This becomes a control problem where based on the wind direction and speed, fans can be ramped up and down appropriately.

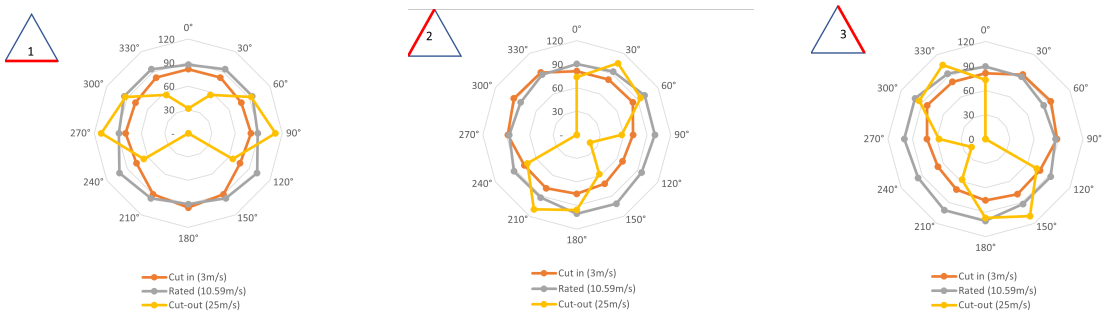

(a) (b) (c)

Figure 2.12: Total Fan power (kW) of each contactor bank at cut-in, rated, and cut-out wind speeds for a) contactor 1, b) contactor 2, and c)contactor 3.

Thermal energy- Isotherm method

The thermal energy breakdown computed using the isotherm data is presented in fig. 2.13.

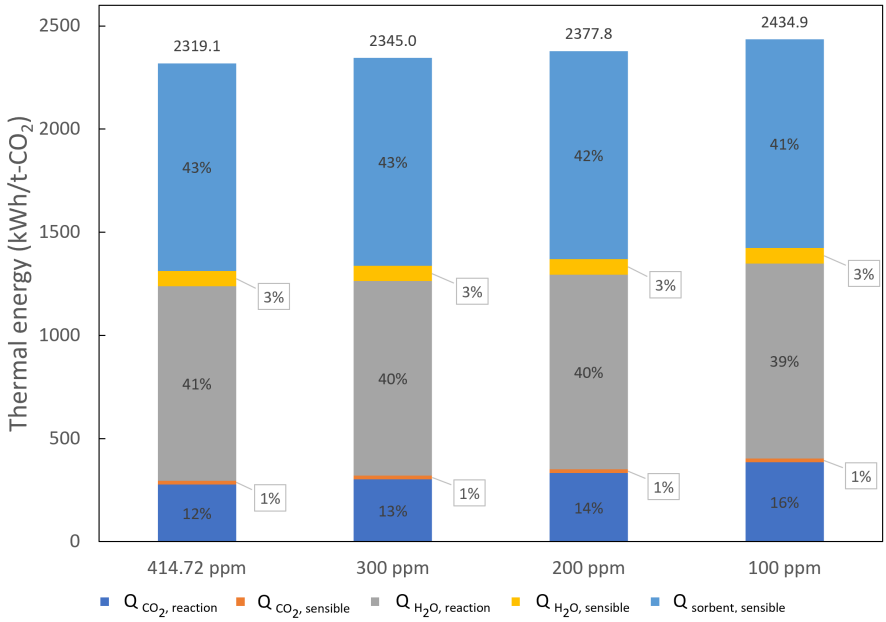

Figure 2.13: Breakdown of thermal energy requirement for sorbent APDES-NFC at varying CO_2 inlet concentrations using isotherm method. Relative humidity of 66% assumed [88]. Operating conditions reported in table A.4.

It can be seen that the sorbent sensible heat comprises majority of the thermal requirement of the plant (41-43%). This aligns with values stated in literature using

solid sorbents [33, 35]. The mass of sorbent required for capture, as well as its specific heat capacity have a large impact on the overall thermal energy requirement. Minimizing the mass of sorbent required as well as specific heat capacity are areas of major focus as the next generation of solid sorbents are developed. Materials with high affinity for CO_2 allow for less sorbent to be used as a result. Recovery of sensible heat is discussed by Bos et al [33]. Recovery of sensible heat in fixed bed operation is difficult, and can be done by recovering heat from a hot bed at the end of a desorption cycle, and a cold bed at the beginning of a desorption cycle. Gebald et al. [89] present an invention to recover sensible heat using a glycol loop and external thermal energy storage in a stratified tank. In their particular case, thermal energy demand decreases from 3334 kWh/t-CO_2 to 2245 kWh/t-CO_2 by recovering sensible heat.

The real thermodynamic work computed in section 2.4.2 is based on total plant energy which includes both electrical and thermal energy. Electrical energy does not vary greatly with a change in concentration as it is comprised of fan energy, and compression energy which is more a related to mass flow. As such, a comparison can be drawn between the two methods. Computed using the real work method, there was a change of energy from 414.72 ppm to 300ppm of 63.9 kWh/t-CO_2. Using the Isotherm method, there is a change in thermal energy of 25.9 kWh/t-CO_2. Although the thermal energy requirement is higher when computed using the isotherm method than with the second law efficiency approach, the values are still well within the bounds presented in The National Academy of Sciences report on negative emissions [4]. It is outside of the middle range, but within the full range of η_{II} = 2-24%. The higher energy values are likely a result of not accounting for thermal heat recovery and varying isotherm parameters by using different sorbents.

2.5 Conclusions

The results show that there is a clear impact on overall DAC plant energy consumption based on ambient wind conditions. Increased wind speeds decrease fan power requirement, as well as induce increased CO_2 mixing near air contactors. As a result of increased CO_2 mixing, plant wide thermal energy requirement is decreased. Wind approach angle also effects the fan power requirement, and local CO_2 dispersion. When the wind angle is perpendicular to upstream contactors, they have a decreased fan energy requirement. This is particularly predominant at high wind speeds; where

upstream contactors can be shut off entirely at wind speeds above 24m/s at hub height (150m), correlating to an average contactor bank inlet velocity of 17.5m/s.

Using CFD, pressure loss curves for a commercially deployed air contactor design are generated for four sorbents of interest, which can be used to improve future energy analysis of DAC. A pressure loss of 391 Pa was found for a flow velocity of 0.73m/s through sheets of APDES-NFC sorbent arranged in an accordion manner with a length of 1.5m.

Further iteration of contactor layouts could be completed in future work to better understand impacts from alternate configurations. Iterating on the current methodology to include alternate arrangements, as well as simulating various phasing of adsorption/desorption cycles would give a broader insight in future studies. Ultimately, the phasing and operation of the plant could be optimized based on the power available at different wind speeds.

DAC is an energy intensive process, so all efforts should be made to optimize energy use, and plants should be carefully designed to allow for maximum CO_2 dispersion between air contactors.

Chapter 3

Research paper 2- 'Marinisation for offshore direct air capture- Design evaluation for air pre-treatment to remove aerosolized salt particles'

This chapter is prepared as a standalone journal article to be submitted for publication at a to be determined (TBD) journal. Its main author is also the author of this thesis, having done its research, calculations and writing in consultation with Dr. Curran Crawford as the primary advisor. All section, equation, and reference numbering has been modified to integrate it with this thesis.

The citation for this article [90] is as follows:

R. Foxall and C. Crawford, "Marinisation for offshore direct air capture- Design evaluation for air pre-treatment to remove aerosolized salt particles," Journal TBD, Jan. 2023.

Abstract

Direct air capture is a method for removing carbon dioxide (CO_2) directly from atmospheric air. To date, only land based installations have been considered, but with growing competition for land and resources, offshore locations are beginning to be

contemplated. Offshore locations offer close proximity to vast renewable energy potential, and robust CO_2 storage locations, but come with a large degree of uncertainty on performance and cost. The current study explores considerations to take into account for offshore operation, and reviews parallel technologies that have undergone similar transitions to use in offshore environments. A baseline energy calculation is completed under the assumption that air would need to be pre-treated prior to entering conventional DAC units. A design is proposed using wire mesh demister pads to collect and remove liquid particles containing salt from the air prior to entering the air contactor and coming into contact with capture materials. The pressure loss, and additional fan power required to overcome this is computed. Demister pads increase overall pressure drop by 20-28% for solid sorbents, and 79% for aqueous based DAC, resulting in an additional fan energy requirement of 38.1 kWh/t-CO_2 and 194.44 kWh/t-CO_2 respectively. Until further experimental studies are completed to better understand the impacts, this design serves as a worst case to compare to. Once further experimental data becomes available, it can be determined whether the additional components for pre-treatment of air are necessary.

3.1 Introduction

Carbon dioxide removal (CDR) is now known to be an essential component to meeting climate goals as it is an imperative component to net zero arithmetic. Virtually all scenarios assessed by the IPCC include some form of CDR to reach net zero CO_2 to compensate for residual anthropogenic emissions [1]. Direct air capture (DAC) is a method for directly removing carbon dioxide (CO_2) from the atmosphere and has a number of distinct advantages over alternative approaches. As the global population increases, so will the competition for land and resources [91]. This drives the motivation to explore locations where direct land use competition is not an issue, such as offshore locations. DAC can be implemented anywhere that has access to energy, water, and a suitable storage mechanism.

Offshore DAC may be sited in close proximity to vast renewable energy resources which are otherwise difficult to harness and transport to shore, as well as to vast storage resources such such as basalt rock which covers large portions of the ocean floor. Figure 3.13 of the CDR primer [92] highlights potential sites with good energy resources, such as offshore wind, in close proximity to CO_2 storage. There is an

immense energy potential of offshore wind power. According to the IEA [66], global offshore wind potential is greater than 420 000 TWh per year worldwide, more than 18 times the present global electricity demand. Offshore average annual capacity factors range from about 29-52%, compared with onshore of 23-44%. Typical offshore wind speeds show an annual average of 6-11.3m/s at 100m hub height [37]. New onshore installations built in 2021 showed an average wind speed of around 8m/s at 100m [93]. Beyond resource potential, going offshore ensures power is not directly removed from the grid, that could be used for decarbonization elsewhere.

Historically, DAC has only been discussed for onshore applications. As such, the costs, and implementation requirements are highly uncertain when moving a nascent technology into a new operating environment. This paper aims to explore the implications of operating offshore, modifications required, and highlight future experimental work that could de-risk the technology.

Offshore environments expose equipment to corrosive conditions, unsteady dynamic movement from waves, and power limitations due to grid isolation. High humidity levels, as well as increased salt content in the air due to sea spray are often encountered in marine environments. Marinisation can be described as the "modification of equipment normally used onshore to be suitable for use in an offshore environment" [94]. The three main factors that must be considered for a product to be truly marinised are corrosion resistance, vibration resistance, and the ability to function with constantly changing attitude (an objects orientation about its center of gravity) [95]. Further considerations for design include bio fouling, increased humidity, isolated power generation, and changes in operation and maintenance routines. Material selection, protective coatings, or the inclusion of sacrificial components as part of the design can likely address corrosion and biofouling. Ability to handle vibrations and changes to the center of gravity may require redesign to whole processes dependant on each specific process considered. Humidity may be addressed through material selection, process changes, or just having an understanding of how plant wide energy will change as a result. Isolated power generation requires energy buffering and storage capability, as well as a diverse set of energy production methods to allow production from an alternate when another is unavailable. This is commonly done in micro-grid applications.

Ultimately, the question is if each factor will affect performance, or simply impose

additional operational and design ramifications resulting in additional costs. The elements which are most likely to affect the performance are dynamic movement, increased humidity, and the presence of salt and other contaminants in the sea air. Major cost changes are likely to be attributed to typical marinisation activities such as corrosion resistance, bio fouling, and increased power production and storage.

Beyond capturing CO_2 from the air, it can also be captured from the ocean, sometimes referred to as direct ocean capture (DOC) or more generally, ocean based CDR. Three main approaches for ocean based CDR are: electrochemical, ocean alkalinity enhancement, and macroalgae cultivation and carbon sequestration [96].

When conducting carbon capture offshore, one may consider also consider removal of CO_2 directly from seawater. Electrochemical approaches pass seawater through a membrane, apply electricity, capturing a pure stream of CO_2 [97–100]. Two major electrochemical sea water CO_2 extraction methods exist: one driving the pH down to more acidic conditions, thereby driving CO_2 off in a gaseous state; and the other driving pH up to more basic conditions, and precipitating CO_2 out in the form of calcium carbonate. In either case, effluent seawater must be neutralized prior to putting back into the ocean. This requires significant volumes of water to be pumped, roughly 200 times that required for the CO_2 capture itself, causing a significant energy expense. This is one of the major drawbacks to this approach, and as such, in order to obtain better process economics, is often coupled with desalination plants in order to take advantage of free pumping work. Alkalinity enhancement changes the seawater chemistry by adding a source of alkalinity to drive off and capture CO_2. This is mined onshore, and transported to site. Methods have been developed to use mine tailings waste to produce a source of alkalinity [101–103]. Due to transport costs and logistics, this is likely more appropriate for nearshore applications. Macroalgae cultivation captures and stores CO_2 using seaweed. Approaches have been developed to cultivate seaweed, and sink it to deep depths in attempt to permanently store the CO_2 found in the plant material [104].

Further approaches are summarized by the National Academies of Sciences, Engineering, and Medicine report on ocean based CDR [105]. These approaches include: artificial down welling, deep sea storage, marine ecosystem restoration, and microalgae cultivation. Ocean based CDR will certainly become part of the overall CDR solution, but at this point in time, projects are still in their infancy stages, and re-

quire further development to reach commercial scale. As a result, the current study considers capture from air, as it has a higher technological readiness level (TRL).

3.1.1 Motivation, and objectives

To the best knowledge of the author, no studies have examined the practical implications of building DAC units offshore. This study aims to provide insight to important considerations that should be looked into prior to deploying DAC in marine environments. Further, this study will identify future experimental work that could assist in providing better energy and cost estimates, to inspire confidence prior to deployment. This study reviews the current landscape of DAC, and draws parallels to other technologies that have undergone similar transitions. A baseline energy estimate on an air pre-treatment design for solid sorbent and liquid solvent DAC systems is conducted.

A review on existing literature, identification of knowledge gaps, and suggestions for experimental work to help fill these gaps are identified in section 3.2. The methodology for the pressure drop calculation and additional energy requirement for air pre-treatment are discussed in section 3.3, and the results and discussion in section 3.4. After which, conclusions and major takeaways be drawn in section 3.5.

3.2 Existing research

The following sections review current literature on process and energy modelling for onshore DAC, parallel technologies that may undergone similar transitions to offshore operation, and alternatives to DAC.

3.2.1 DAC

Currently, two main DAC technologies exist on a commercial scale, solid sorbent (SS), and liquid solvent (LS) approaches. The two main steps in either process are: 1) adsorption/absorption- where CO_2 is absorbed/adsorbed onto a chemical substance, either liquid or solid until it reaches a saturated state; 2) desorption- where heat/pressure is applied to release CO_2 into a pure stream and regenerate the capture material for further cycles. In LS DAC, air is contacted with liquid potassium hydroxide (KOH) or sodium hydroxide (NaOH). Solid sorbent systems typical rely on solid micro/mesoporous materials bound to amine groups. LS DAC is a contin-

uous process, whereas SS DAC is a batch-wise process,relying on multiple units run in parallel to make a pseudo-continuous process. In both cases, a mixture of heat and pressure is used to release the CO_2 from the capture material. SS DAC units are commonly about the size of a standard shipping container, 12m x 2.4m x 2.6m (LxHxD), and capture about 500t-CO_2/y. At 1 Mt-CO_2/y, 2000 SS DAC units of this size would be required. Currently the largest plant in operation uses eight SS DAC units, capturing 4000t-CO_2/y [38]. For LS DAC, the air contactors are the biggest component. To capture 1Mt-CO_2/y, ten air contactors, roughly 200m x 20m x 7m (LxHxD) are required [4]. Other components of the process require roughly an additional 20% of the land area of the air contactor units. The first commercial scale plant, with a plant size of 0.5-1Mt-CO_2/y, has broken ground for construction as of Q3 2022 [106].

LS DAC systems, such as that done by Canadian company, Carbon Engineering, rely on scaling up existing industrial equipment size to reach competitive unit economics. This approach is comprised of four main sub processes/components: 1) air contactor, 2) pellet reactor, 3) calciner, and 4) slaker. This process is shown in fig. 3.1. These four sub-processes can be described by two chemical loops, and are summarized in by Keith et al. [9]. The air contactor uses an aqueous capture solution actively pumped over a structured PVC based packing material. The pellet reactor precipitates solid calcium carbonate pellets, which are then sent to a fluidized bed calciner producing CO_2. To achieve the 900°C temperature requirement, natural gas gas is combusted, and CO_2 released through combustion is co-captured in the process.

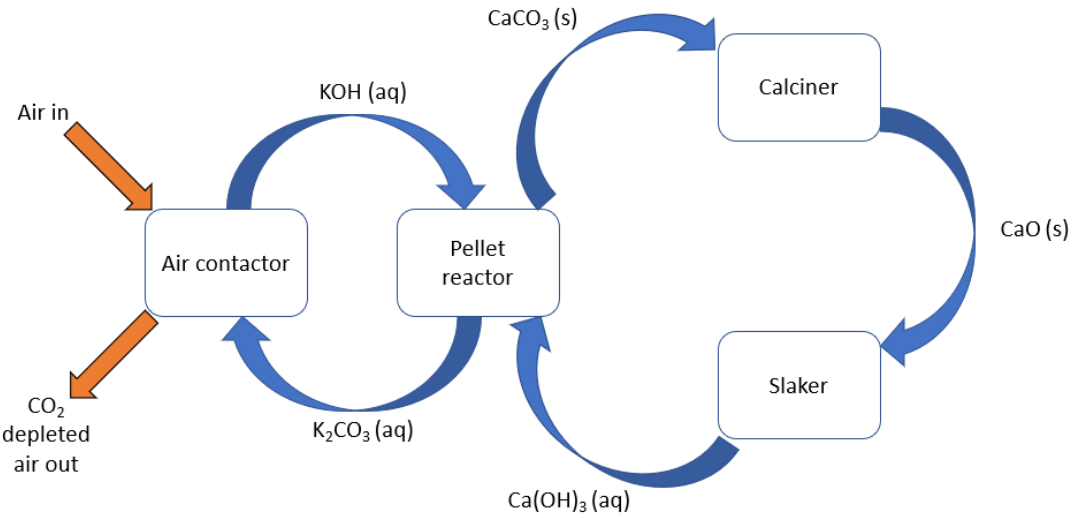

Figure 3.1: Liquid solvent DAC process flow diagram re-created from Keith et al. [9].

The SS DAC approach has received more attention than LS DAC from academia as well as industry. Historically this is adopted by major DAC companies Climeworks, located in Switzerland; and Global Thermostat, located in the United States. Many more companies have recently been started in the SS DAC realm, and show promise to scale up, while decreasing costs [10]. This approach takes advantage of modular units, which can be scaled out, rather than scaled up. The units commonly undergo a five-step process as described by Sinha et al. [34]. The process first undergoes adsorption by passing air over a solid sorbent using fans, then evacuation by vacuum pump to remove oxygen from the chamber, pressurization then desorption through heating (typically steam) to about 100°C, and finally cooling to ambient conditions before starting the cycle again. A process flow diagram for SS DAC is shown in fig. 3.2. Thermal requirements can be met purely using electricity or upgrading some form of waste heat if available using heat pumps. Steam can be generated using electric powered, or fossil powered boilers; the latter of which requires subsequent co-capture or it will lower the overall CO_2 removal rate of the unit.

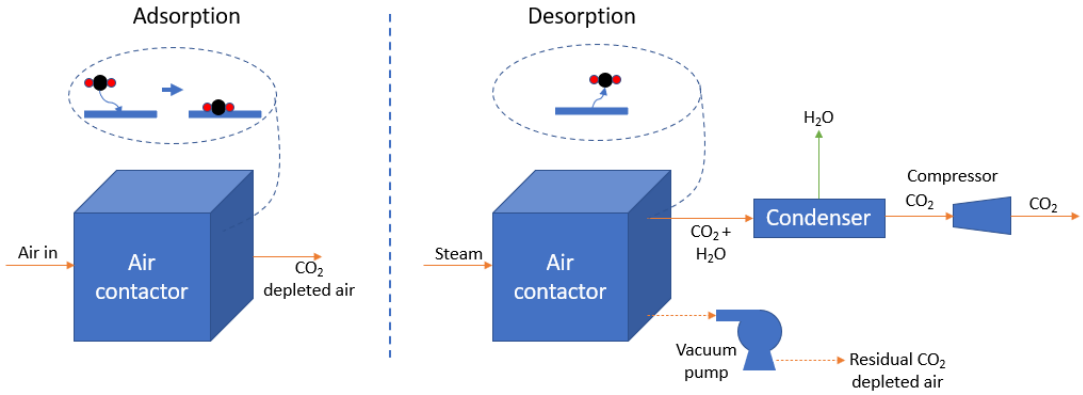

Figure 3.2: Process flow diagram for SS DAC. Re-created from McQueen et al. [8].

DAC is commonly known to have an energy split of about 80% thermal energy, and 20% electrical energy. Thermal energy modelling can be conducted from a steady state, or dynamic analysis perspective.

Steady state analysis for SS DAC relies on the use of isotherm equations to model experimental adsorption data [33,34]. The Toth isotherm is commonly used to model CO_2 adsorption on amine based sorbents. The Guggenhein-Anderson de Boer (GAB) isotherm model is commonly used to describe H_2O adsorption. The equilibrium loading (Δq_i) is computed based on the difference between the quantity of CO_2 and H_2O adsorbed during the adsorption phase ($q_{i,ads}$), and the quantity re-adsorbed during the desorption phase ($q_{i,des}$). This is shown in eq. (3.1).

$$\Delta q_i = q_{i,ads} - q_{i,des} \tag{3.1}$$

Three common approaches for SS DAC dynamic modelling are summarized by Bos et al. [46] as: Pseudo-first order linear driving force (LDF) model, Pseudo-second order LDF model, and the Toth rate equation model. The first order LDF does not accurately describe the adsorption profile, whereas the second order LDF is more accurate to experimental results. The most accurate model for describing adsorption is the Toth rate equations All use mass and energy balances to model adsorption in a specific column. This is seen in many studies examining ambient conditions and operating conditions to evaluate performance and cost [35, 46, 50, 107–110]. Dynamic models rely on kinetic constants describing the rate of reaction, and equilibrium

loading capacity. Elfving et al. [108] expanded on these kinetic models to include the enhancing effect of increased humidity on CO_2 loading. This was done by generating rate constants specific to the reaction pathways under dry and humid conditions. This enhancing effect is crucial to understanding the real performance of a plant under humid conditions, such as those experienced near the ocean.

In equilibrium or dynamic analysis, the equilibrium loading must first be calculated using experimental data. Currently, only a handful of sorbents have data available for both CO_2 and H_2O loading, with even fewer having co-adsorption data. Increased humidity leads to higher H_2O adsorption, but also has an enhancing effect on CO_2 adsorption, causing an increase in CO_2 loading in the presence of humidity. CO_2 loading has been seen to double in the presence of high humidity levels [108]. This is often neglected, but has a large impact on overall energy demand and loading capacities. This has been captured in a few analysis by including an empirically derived enhancing factor [53], an equivalent temperature based on humidity [35], and by embedding the H_2O adsorption directly in the CO_2 isotherm equations [50]. The latter method from Stampi-bombelli et al. is the most consistent across a range of operating conditions, but relies on having extensive experimental adsorption data on both CO_2 and H_2O. Rim et al. [111], study sorbent MIL-101(Cr) under a large range of operating conditions, including temperatures down to -30°C under a range of humidity conditions as well as using very small temperature swings. They see a significant increase in adsorption capacity compared to ambient conditions (20°C). Elfving et. [54] al. found that cold humid air had the highest adsorption capacity. Sanz-Pérez et al. [55] explore the effects of temperature and humidity on both solid sorbent, and liquid solvent DAC systems. An et al. [112] study LS DAC at different ambient conditions. They suggest that estimations on DAC should consider ambient conditions rather than relying on generic performance figures.

3.2.2 Parallel technologies

A technology that possesses potential parallel issues that have been addressed for use in a marine environment, is the gas turbines used on board ships, in particular navy vessels. The air intake must include air purification to remove water droplets containing sea salt prior to entering the engine. In a naval ships technical manual from the US Navy [113], air pre-treatment is discussed. If excessive salt particles are permitted to enter the engine, a buildup of solid particles on compressor blades will

gradually reduce the efficiency The associated maintenance routine is also discussed, such as emptying water collector traps, and cleaning of demister pads. Prior to air entering the combustion chamber, demister pads are used to capture water droplets containing salt particles.

Dashliborun et al. [114] conducted a thorough review of ship based CO_2 capture systems. On board CO_2 capture is considered by the following two experimental studies. Dashliborun et al. [115] examined the effects of motion on a packed bed, MEA based CO_2 absorber. Six degree's of freedom were simulated to examine the effects of ship movement on mass transfer performance. They concluded that the absorption performance would deviate under offshore conditions with conventional stationary packed bed reactors. Effective gas-liquid interfacial area was found to decrease with increasing tilt angle for both structured and random packing's. Packed beds onboard floating vessels under varying inclination and oscillations saw decreased mass transfer efficiency. As such, Dashliborun recommends that the effect of offshore conditions and their impacts on performance be carefully considered in the design of scrubber units in use under these conditions. Issa et al. [116] also investigated MEA based absorption of CO2 in a packed bed scrubber, attached to a diesel generator. Their goal was to evaluate the SO_X and CO_2 concentration with $NaOH$ pre-treatment and without.

Packed bed columns used for LNG processing plants have also been examined for use in a marine environment. Schultes et al. [117] experimentally compared structured and unstructured packing's performance during column motion. Previously, only structured collumns were considered applicable for use onboard vessels under moving conditions, but Schultes et al. conclude that either type may be appropriate.

3.3 Methodology- Air pre-treatment

To serve as a baseline assumption that air would need to be pre-treated prior to entering DAC air contactors to avoid performance changes from contaminants, specifically salt particles in sea air, additional components are added to the current designs for SS DAC and LS DAC. A proposed method for pre-treatment is to pass air through wire mesh demister pads, similar to what are used in marine gas turbine engines [113]. Simplified configurations for pre-treatment on marine turbines/generators and DAC units is shown in figure 3.3a and figure 3.3b respectively. Demisters, also known as

wire mesh mist eliminators, are commonly used in gas/liquid operations such as distillation, absorption, and evaporation and have a low cost, low pressure drop, and high efficiency of droplet capture. The additional pressure loss is overcome by increasing the fan power. As air passes through demister pads, small liquid particles contained in incoming air are coalesced into larger particles and removed from the stream. The rest of the process is be assumed to remain unchanged. These liquid particles contain the salt particles within the air. The additional pressure loss imposed, and associated energy demand is analyzed further for LS DAC and SS DAC.

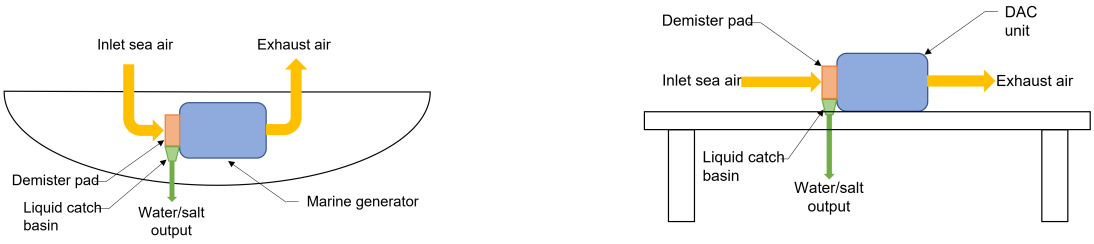

(a) (b)

Figure 3.3: Simplified schematic of demister pads used for air pre-treatment for a) marine gas turbines/generators, and b) DAC units.

Fan power is calculated using equation 3.2.

$$P_{fan} = \frac{1}{\eta_{fan}} \Delta p \cdot \dot{V}_{air} \tag{3.2}$$

where η_{fan} is the fan efficiency, Δp is the pressure drop, and $\dot{V}_{air}$ is the volumetric flow rate of air. η_{fan} is assumed to be 70% as per Keith et al. [9].

Typical SS DAC units are thought to be about the size of a standard shipping container, capturing 500t-CO_2/y, each containing 6 individual DAC modules [38]. Sabatino et al [35] estimates that each module is about 1.5m x 1.5m x 1.5m. Air velocity through the contactor is estimated to be about 0.73m/s based on the patent information from Gebald et al. [47]. This results in a volumetric flow rate $\dot{V}_{air} = 9.855 m^3/s$. Previous work from the author of the current study [28] estimated the pressure drop through a SS DAC unit with 1.5m length for four common adsorbent materials. A 2D CFD model was used to examine pressure loss through sheets of

tightly packed, spherical adsorbent particles arranged in a horizontal stack as per the patent by Gebald et al. [47] and Sauerbeck et al. [48]. Adsorbent sheets with thickness of 1cm, were place one 1cm apart from one another, forming alternating layers of sheets and flow channels, each 1cm thick. The four sorbents analyzed were APDES-NFC, Tri-PE-MCM, MIL-101(Cr)-PEI, and Lewatit VP OC 106. The physical properties used for the pressure loss simulation are summarized in appendix B. The pressure drop associated with each one at a flow velocity of 0.73m/s are summarized in table 3.1 below.

Adsorbent material	Pressure drop (Pa)
APDES-NFC	390.62
Tri-PE-MCM	479.13
MIL-101(Cr)-PEI	480.54
Lewatit VP OC 106	625.67

Table 3.1: Pressure drop through SS DAC unit with 1.5m long contactor from previous CFD study.

For LS DAC, Keith et al. [9] state a pressure loss per packing depth of 9.7 Pa/m at a air velocity of 1.4m/s. This results in a pressure drop of 67.9 Pa through their contactor with 7m depth. To capture 112t-CO_2/h, 251,000 t-air/h are required to be passed through the air contactor. At 21°C, air has a density of 1.2kg/m^3 [118], resulting in a volumetric flow rate of 58,101.9 m^3/s. Solving equation 3.2 provides the fan power, which can be normalized by the annual capture rate to present the energy intensity in kWh/t-CO_2.

Rahimi and Abbaspour [119] examined the pressure loss through demister pads using a CFD study. Results are compared with experimental results of El-Dessouky et al. [120]. El-Dessouky developed an empirical relationship for the wet pressure drop shown in equation 3.3. The dry pressure drop refers state where water droplets are not present on the demister pad. The wet pressure drop refers to the state where water particles are retained within the pad, and on the surface of the wire mesh. This is the likely operating state after the unit has been run for some time. Al-Dughiather et al. [121] experimentally studied pressure losses through wire mesh, building on prior experimental work of El-Dessouky by extending the operation range.

Al Dughaither et al. determined that the dry pressure drop was nil, and derived an empirical relationship for the wet pressure drop. The derived empirical relationship from El-Dessouky is used in this analysis, shown in equation 3.3.

$$\Delta p = 3.88178 \rho_p^{0.375798} v_s^{0.81317} D_w^{-1.56114147} \tag{3.3}$$

where ρ_p is the packing density (kg/m^3), v_s is the superficial gas velocity (m/s), and D_w is the wire diameter (mm). El-Dessouky et al. used a demister with a thickness of 15cm, packing density $\rho_p = 180.518$kg/m^3, and a wire diameter of $D_w = 0.28$mm. The same dimensions are used in this analysis, and the pressure drop at 0.73m/s flow velocity is calculated for SS DAC, and 1.4m/s for LS DAC. Flow velocity is a design choice, and ultimately impacts capture rate. For SS DAC, 0.73m/s is the maximum velocity tested in the patent by Gebald et al. [47], and for LS DAC, 1.4m/s is stated as the design velocity by Keith et al. [9]. The change in total fan power with this additional pressure drop is then calculated using equation 3.2.

3.4 Results and discussion

Baseline energy consumption assuming pre-treatment of air with demisters is conducted in section 3.4.1. Then the the design considerations to implement each type of DAC offshore are discussed in section 3.4.2. Offshore operation and maintenance (O&M) is discussed in section 3.4.3. Alternate design configurations are shown in section 3.4.4. Knowledge gaps and further experimental work are identified in section 3.4.5.

3.4.1 Air pre-treatment energy demand

In the case of SS DAC, the demister pad induces a wet pressure drop of 154.5 Pa at 0.73m/s. Based on a capture rate of 500t-CO_2/y, this results in a change in energy of 38.1kWh/t-CO_2. LS DAC using a demister pad with the same properties will experience a wet pressure drop of 262.4 Pa at a flow velocity of 1.4m/s. This results in an additional energy requirement of 194.4 kWh/t-CO_2. This is a direct result of the increased velocity that LS DAC is run at as can be seen from eq. (3.3). Velocity is a design choice and drives the overall capture rate. If decreasing volumetric air flow is not feasible; one could consider increasing the inlet cross sectional area to slow

the flow as it passes through the demister, and then converging it again through the DAC unit. Space constraints are however an issue, and in doing so, the inlet area would need to be almost doubled in order to maintain the capture rate for LS DAC, while slowing velocity through the demister to equal SS DAC.

A comparison can be drawn between the four solid sorbents, and the liquid solvent DAC. The pressure loss associated with the demister pad, and the air contactor is shown in figure 3.4. The fan power normalized by the annual capture rate and is summarized in figure 3.5. It is seen that if pre-treatment is applied to both types of DAC, LS DAC experiences a much larger change in pressure drop and energy intensity. The demister pad accounts for 79% of the total pressure drop, and 75% of the energy requirement in LS DAC. For SS DAC, the demister pad accounts for 20-28% of the pressure drop, and 22-31% of the energy requirement.

When appropriate experimental data becomes available for DAC operating in marine conditions, an energy comparison can be made to scenarios including air pre-treatment, and without. If the modelling reveals a change in energy greater than that imposed by air pre-treatment, 38.1 kWh/t-CO_2 in the case of SS DAC, and 194.4 kWh/t-CO_2 for LS DAC, then the additional equipment for air pre-treatment is justified. This is of course from an energy perspective. If degradation/loss of useful life is experienced as a result of not pre-treating air, then a analysis would need to be conducted which has greater impact on overall cost.

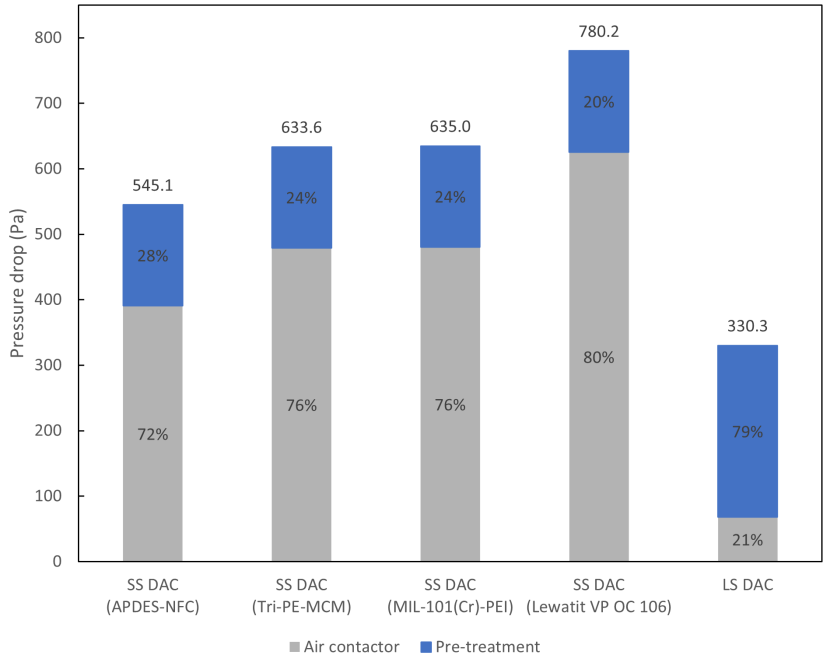

Figure 3.4: Pressure drop for SS DAC and LS DAC as a result of demister pad and air contactor.

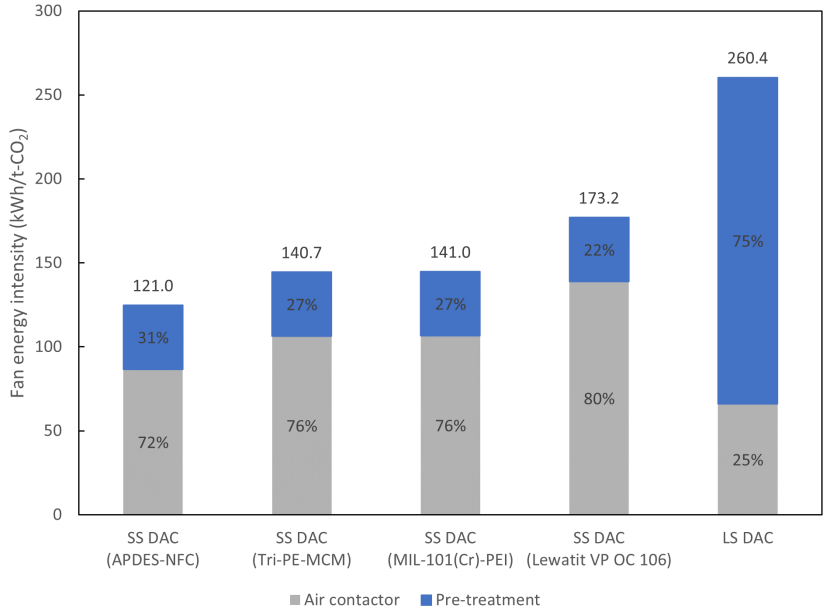

Figure 3.5: Fan energy required by LS DAC and SS DAC units as a result of demister pad and air contactor.

3.4.2 Design considerations of offshore DAC

LS DAC and SS DAC are both discussed in the following paragraphs as they relate to size and modularity, feed stock requirements, interaction with aerosol salt particles, energy modelling, and effects of motion.

Size and modularity

Due to the size difference between each DAC type, they require vastly different design conceptualizations when envisioning deployment offshore. SS DAC having a more modular approach, lends itself better to space limited situations, such as on-board floating offshore wind turbine structures. LS DAC requires large unit sizes, so one possible configuration that can be envisioned is larger offshore hubs, built on platforms, or potentially re-using container ship hulls or offshore oil and gas infrastructure. One could also envision a near shore/shore side deployment that would also be exposed to marine conditions. LS DAC is comprised of multiple independent pieces of equipment, the air contactor, pellet reactor, calciner, and slaker. Each process unit must be placed in close proximity to one another and may not allow stacking on top of one another. This would result in an uneven mass distribution, and require precise stability modelling and design. SS DAC modular units have all equipment for capture houses within a single unit. As they are repeatable units of the same dimensions, multiple units may be easier to stack on one another, while ensuring stability from an equal mass distribution perspective.

Feed stock requirements

SS DAC provides more flexibility in the range of applications they can be deployed on party due to the size and modularity, but also due to the feed stock requirement. LS DAC currently requires natural gas as a feed stock for combustion to meet the thermal energy demand. When placed in an offshore location, this would require co-location with an natural gas processing plant, or transporting natural gas via ship or pipeline. Though the technology claims to be able to run fully electrically, this has yet to be proven publicly at a commercial level. LS DAC also requires constant replenishment of process chemicals due to evaporate losses, and incomplete pellet reactions. Feed stocks must be transported to site, and wastes transported away for disposal. The plant discharges 1% of circulating calcium per cycles as waste. Calcium carbonate ($CaCO_3$) is replenished at a rate of 3.4t/h to capture 112 t-CO_2/h, or in

other words 0.03t-$CaCO_3$/t-CO_2 [9]. This capture rate results in 0.98Mt-CO_2/y from the atmosphere, and requires almost 30,000 t-$CaCO_3$/y. Unless ample storage was available on board, this would need to be delivered in smaller increments. LS DAC consumes water, 4.7t-H_2O/t-CO_2, whereas SS DAC can have net water production. Process water would need to be produced on site via sea water purification, likely using reverse osmosis, or shipped to site and stored on board. Transport to and from offshore structures adds significant operational costs and complexities. As such, LS DAC may be limited to near shore applications.

Energy modelling

Under the current process, the electrical energy for SS DAC is less likely to vary greatly from onshore operations. A caveat is that adsorption times may vary due to the change in environmental conditions, changing the length of time the fans must be run. Also, offshore environments typically have relative humidity, which would increase the water co-adsorption, and thus increase the thermal energy required for desorption. The thermal energy is more likely to be impacted from the change in operating conditions. Further equilibrium and dynamic analysis using experimental data appropriate to a marine environment is necessary to confirm this hypothesis. In LS DAC, the electrical energy is more likely affected than the thermal energy. The liquid solvent contacts the air, but thermal energy is not added to the process until further downstream. The CO_2 suspended in capture fluid is first precipitated into a solid calcium carbonate particle, then inputted to the calciner; the main thermal energy consumption of the plant. Downstream processes are likely unaffected by upstream processes, and thermal energy is a function of design parameters of the calciner.

Interaction with aerosol salts

SS DAC systems are likely more sensitive to higher concentrations of aerosol salt contained in inlet sea air. The highly porous solid sorbent comes directly into contact with the air. In post combustion capture, Li et al. [122] has discussed pore blockage as a barrier to mass transport and it is estimated it will also impact SS DAC. No experimental studies have considered the impacts of salt particles or other contaminants contained in the air on SS DAC. Pore blockage is hypothesized to decrease mass transport, and lower equilibrium loading levels. This would as a result directly

impact the thermal energy demand of the plant. LS DAC air does not rely on the solvent material itself to be highly porous, but uses its structured packing material fluid is passed over to achieve high surface areas. The transport of CO_2 into the capture solution within the air contactor is limited by a reaction diffusion process occurring in the liquid film. The mass transfer coefficient is mostly a function of hydroxide concentration and temperature and assumes well-wetting of the packing material liquid interface. Aerosol salt particles are unlikely to block mass transport in this configuration, and sodium chloride and the capture solution (KOH or NaOH) are not expected to react with one another, so there should be no change in the net reaction. The effects of salt on capture materials for DAC are unknown, and not well studied, however, Weiland and Hatcher [123] studied the effects of contaminants, including salts such as NaCl, on aqueous amines in point source CO2 capture. These salts are often referred to as heat stable salts (HSS), and accumulate in solvents and cause performance changes. These changes are sometimes positive, but majority of the time, they have a negative impact. Often strong bases such as sodium hydroxide (NaOH), or potassium hydroxide (KOH) are added to neutralize salts. This is the capture solution used in LS DAC, and as a result, the incoming salt particles are expected to be neutralized and have little to no impact. As salt accumulates in the capture solution, causing dilution, overtime this could impact overall reactivity.

Motion effects

LS DAC systems are likely susceptible to issues caused by motion, as multiple physical phases are encountered within the process. Although no studies have examined this specific to LS DAC as of yet, parallels can be drawn to other technologies such as ship bound aqueous CO_2 capture [114], and floating liquefied natural gas (FLNG) processing plants [117]. As the air contactor relies on liquid capture solvent passing over a structured packing material, one can predict that the transport parameters will be affected by induced motions. As seen in both cases, gas-liquid interfacial area is impacted by motion, likely decreasing the CO_2 adsorption rate. The pellet reactor, calciner, and steam slaker have potential to be affected by motion as well. In the pellet reactor, as calcium carbonate is precipitated, larger particles sink to the bottom. Agitation of the unit may cause issues with precipitation, transport of particles to the bottom of the vessel, and increased calcium loss. It is unknown exactly how the unit would function under these conditions and further experiments are suggested.

Motion is less likely to cause issues for SS DAC process, as the capture does not rely on different phases, and the solid particles are packed tightly within the contactor. Typical configurations [42, 48] are comprised of porous filter material placed on the top and bottom containing a thin (1cm) sheet of spherical adsorbent particles. Sheets are seen to be arranged in an accordion style arrangement, with alternating horizontal sheets and air flow channel gaps. Particles are packed tightly, and cannot move freely with motion. If the unit is placed in an orientation of significant constant tilt, particles may move due to gravity, forming areas near the bottom with more particles, and areas near the top with fewer particles. These thinner areas could create holes, where a lower pressure drop would be experienced [48]. If so, air would preferentially pass through these zones, reducing sorbent usage efficiency, resulting in increased rate of loss of sorbent capacity causing sorbents to be retired pre-maturely.

Ongoing work is being completed by Avellaneda Domene [124] to analyze stability of floating offshore wind turbine platforms with integrated DAC units installed on-board. This work is mostly about analyzing the impacts DAC will impose on the turbine performance, but will provide insight to the extent of motion that is will be experienced by the DAC units.

3.4.3 Offshore operation and maintenance

Operation and maintenance (O&M) contribute significantly to costs of offshore equipment. As of 2022, estimates for offshore wind O&M costs are estimated in the range of $59-89 USD/kW-yr [125], and onshore O&M is estimated on the order of $33-59 USD/kW-y [93]. In other words, offshore O&M costs are estimated to be 51-79% greater than onshore for wind power. All though cost estimates do not exist for DAC offshore, a similar or greater relationship is expected. Distance to shore, and degradation of components cause significant operational challenges. The interval at which equipment's needs to be serviced/replaced adds significant cost for the parts, but also the labor and transport. Maintenance staff must be transported to and from site, which require vessels and crew. This requires extensive planning and scheduling. Sorbents used for direct air capture have a finite lifetime before needing replacement, with current estimates on the order of 0.5-2 years. Depending on the modularity/size of the sorbent cartridges, offloading equipment such as cranes and winches are likely required. Further, delivering large pieces of equipment to floating structures comes with additional complexity to secure vessels for safe offloading. Significant logistical

impacts occur as a result of offshore operation. Costs of offshore wind power are quickly decreasing, and knowledge of offshore O&M can likely be transferred and adapted to offshore DAC. Tools, such as WOMBAT [126], developed by the National Renewable Energy Laboratory (NREL) are available for evaluating O&M costs for offshore wind. Ongoing work is being conducted at the University of Victoria to explore adding DAC modules to the current modelling.

3.4.4 Alternate configurations

Different configurations for installing DAC units offshore can be envisioned. Two conceptual designs are proposed in figure 3.6. One configuration mounts DAC units directly on the decks supporting structures of wind turbines shown in figure 3.6a, and a central hub concept (figure 3.6b) mounting many DAC units on a single platform, powered using nearby wind turbines.

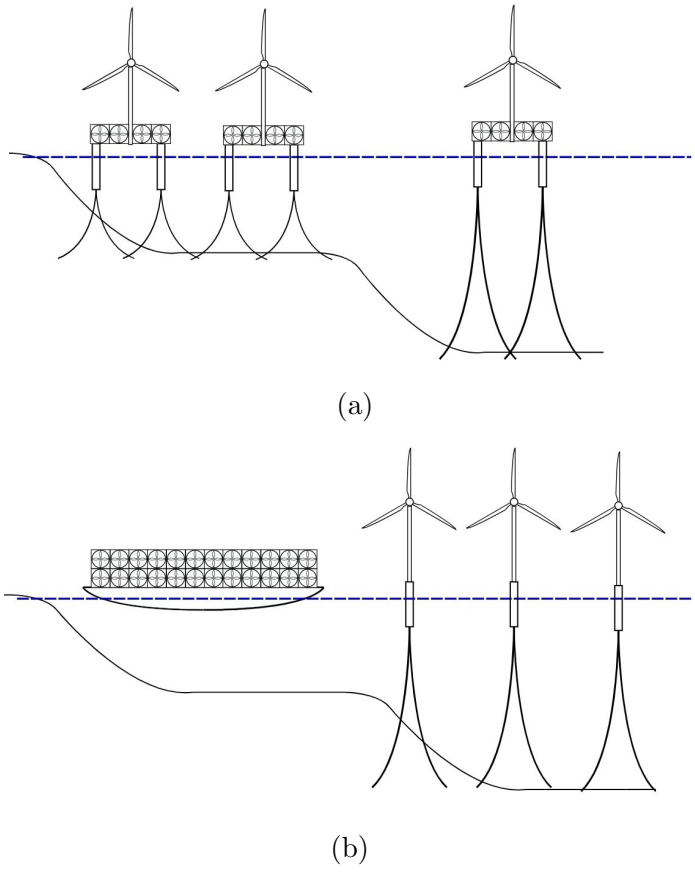

(a)

(b)

Figure 3.6: Alternate design configurations for installation of DAC units offshore. Concept of an a) integrated wind turbine with DAC units mounted directly on deck, and a b) central hub of DAC units powered by nearby turbines. Original artwork completed by P.Connolly [127, 128].

The integrated DAC concept (figure 3.6a) utilizes power generated by each individual turbine. Due to space constraints this configuration is likely only applicable to modular type DAC, such as SS DAC, or future generation LS DAC. There is also risk that on an integrated floating platform, increased motion may be encountered, further strengthening the argument for modular SS DAC. A benefit of this configuration is that power does not need to be transported from each individual turbine to a central location. However, if the goal is to capture CO_2 for sequestration, injection is likely to occur at a central location, requiring CO_2 to be transported from the integrated turbine DAC units. This may be done through pipe interconnections, or through vessel transport. If CO_2 is captured for utilization, perhaps converted to synthetic fuels; storage will need to be included for CO_2, H_2, and produced synthetic fuel.

The central hub, "mothership" concept allows all DAC units to be installed on a central platform, allowing units to share pieces of infrastructure, and reduce the need to transport CO_2 to the injection location. Infrastructure that has been retired from other purposes, such as offshore oil and gas platforms, or large vessels, may be able to be re-purposed. This could generate costs savings due to platform infrastructure already being mostly paid for, with potentially minor upgrades to use for the new purpose. This also has potential to lower the life cycle emissions as recycling of exiting infrastructure saves material and construction emissions.

3.4.5 Knowledge gaps, open questions and suggestions of future work

Currently, no studies have considered the performance losses due to operating in marine environments. As discussed, issues are likely to arise from interactions with salt particles contained in the air, or induced motions. Further experimental work is suggested to fill this knowledge gap

Salt particles contained in sea air are more likely to effect SS DAC based approaches. It is expected the thermal energy, adsorption kinetics,and sorbent degradation will all be effected. As such, experimental work exposing solid sorbents to conditions with increased salt content in the air is pertinent. This should be studied from an equilibrium loading, as well as a dynamic loading perspective to highlight adsorption rates. Data should be obtained at temperature and humidity levels applicable to an ocean environment, and adsorption measured for both CO_2 and H_2O. Degradation studies should also be completed to understand how the lifetime of the sorbent, a major cost driver of the process, is effected by salty sea air.

Motion studies have been conducted for other similar chemical processes, however, none have considered impacts on DAC. LS DAC is likely to be more effected by motion, and as such, experimental studies investigating the impacts of yaw, pitch, and roll on the processes of LS DAC would be beneficial for further development. Experiments should be targeted to each sub process, specifically the air contactor and pellet reactor, as well as the system as a whole.

3.5 Conclusions

This study has explored key areas for consideration when building DAC offshore exposed to marine environments. The two main DAC processes, solid sorbent and liquid solvent, have been summarized and their key areas of uncertainty highlighted. Parallels are drawn to other technologies that have undergone similar development, such as point source capture onboard ships, marine based engines, and floating chemical processing plants. Solid sorbent DAC is hypothesized to be more susceptible to issues caused by aerosol salt particles, and liquid solvent DAC more sensitive to induced motion of floating platforms. Due to the modularity and size, as well as feed stock requirement, Solid sorbent based DAC appears to be a better candidate for far offshore, such as onboard floating wind turbine platforms. Liquid solvent DAC requires feed stocks such as natural gas, chemical make-up, as well as freshwater. Further, waste products would need to be transported from site for disposal. This leads to the conclusion that LS DAC is likely only applicable in near shore/shore side applications. A baseline energy calculation is conducted assuming air must first be pre-treated using wire mesh demister pads prior to entering the air contactor. Demister pads increase overall pressure drop by 20-28% for solid sorbents, and 79% for aqueous based DAC, resulting in an additional fan energy requirement of 38.1 kWh/t-CO_2 and 194.44 kWh/t-CO_2 respectively. It is hypothesized that air pre-treatment is more prudent in the case of solid sorbents, however in either case, further experimental studies exposing the processes to salty sea air are required fully understand the impacts. Future work should conduct experimental analysis at a lab scale, as well as demo projects offshore to test under real world conditions.

Chapter 4

Conclusions

The work outlined in this thesis aims to contribute towards moving direct air capture offshore into a marine based environments. To date, only land based implementations have been considered, and as such, there lies a great deal of uncertainty when moving offshore. It is certain that costs will be higher, and changes will need to be made to the designs and operational methodology, but to what extent is still widely unknown. Assumptions that can be applied to land based approaches require modification for ocean based installations.

Equipment will likely be placed in close proximity to one another due to space constraints, which has further performance implications. DAC removes CO_2 directly from the atmosphere, which is fundamentally an energy expensive process based on the laws of thermodynamics. This large energy demand is further exaggerated by depleted CO_2 concentrations entering downstream units as a result of the close proximity of devices. This effect is explored in chapter 2, as well as the extent to which ambient wind conditions can lessen the impact. Further, ambient wind conditions are analyzed from the view of reductions to fan work required to pass large volumes of air through direct air capture units. A design is proposed to place solid sorbent DAC units onboard a floating offshore wind turbine. As wind turbines are typically located in regions with high average wind speeds, there lies an opportunity to reduce overall energy demand by reduction in fan work assisted by ambient wind. At very high wind speeds, above 24m/s at hub height (150m), upstream fans are able to be turned off, allowing ambient wind to passively drive air through the DAC units. The thermal energy demand is seen to decrease with increasing ambient wind speed, as a result of

higher CO_2 mixing, thus higher concentrations entering downstream units. Pressure loss through air capture units is commonly discussed and optimized for. Many have designed devices for optimal air flow to reduce pressure loss, but little information is publicly available for units at commercial scale. CFD was used to obtain pressure loss curves through realistic solid sorbent air contactors for a range of adsorbent materials.

Building DAC offshore comes with a whole suite of changes that may be necessary in order to ascertain the design works as it should on land. Chapter 3 discusses the necessary design changes that may need to be considered, and conducts a baseline energy estimate assuming a pre-treatment of air to remove aerosol salt particles contained in sea air. In the case of aqueous base DAC, the additional pressure loss induced by the pre-treatment is more significant than for solid sorbent based DAC. A 79% increase in overall pressure drop, and an additional 194.4 kWh/t-CO_2 is required as a result of the air pre-treatment. It is proposed that air pre-treatment is likely more necessary in the case of solid sorbent DAC, which sees an a 20-28% increase in overall pressure drop, and an additional 38.1kWh-t-CO_2 as a result. It is proposed that aqueous based DAC is more susceptible to issues caused by motion, drawn from parallels from similar technologies implemented in floating offshore environments. It is further concluded that due to size, modularity, and feed stock/waste transport requirements, aqueous based DAC is limited to nearshore/shore side applications. Solid sorbent DAC units appear attractive from a modularity, size, and temperature requirement for implementation in far offshore (floating) installations.

4.1 Future work

Many questions remain to be answered to better understand the implications of operating DAC in an offshore environment. This includes, but is not limited to:

1. Experimental testing of DAC capture materials under a range of operational conditions applicable to environments in close proximity to the ocean. Section 4.1.1.

2. Experimental work exposing DAC systems to motion. Section 4.1.1.

3. Further CFD analysis including a rotor at the top of the turbine tower. Section 4.1.2.

4. Further CFD analysis to observe alternate arrangements/configurations of DAC units. Section 4.1.2.

5. Phasing air contactors on/off and optimization based on wind conditions. Section 4.1.2.

6. Stability and power performance analysis of floating turbine design with DAC units on board. Section 4.1.3.

7. Detailed techno-economic analysis of converged design. Section 4.1.4.

8. Life cycle analysis of converged design. Section 4.1.4.

4.1.1 Experimental

As exemplified in chapter 3, there is much experimental work required to better understand sorbent performance when introduced to conditions experienced near the ocean. Such as experimental work introducing solid sorbents to a range of operating conditions including: humidity; salt and other contaminant content; and temperatures in an environmental chamber. This is likely the most pressing future work, as it has downstream impacts to further modelling/understanding of the system implications. Dr. Crawford's research group is actively pursuing this route, and hopes to conduct sorbent experimental work in the near future.

As discussed in chapter 3, motion is likely to change performance of aqueous based DAC systems. Experimental work introducing changes of orientation, as well as vibrations to these systems is pertinent to understand the extent of these impacts. This has an downstream impacts on overall feasibility, performance, and cost.

4.1.2 CFD analysis

The current CFD study in chapter 2 did not include rotor impacts to local wind flow and CO_2 mixing. It was deemed insignificant and beyond the scope of the current study, but future analysis could verify this assumption. A simplified rotor could be included as a rotating zone, to avoid detailed meshing of turbine blades.

One configuration of air contactors was studied in chapter 2. This could be elaborated by simulating alternate arrangements of contactors. There were clear impacts to the flow patterns and CO_2 mixing as a result of obstruction caused by the DAC units.

Alternate arrangements may show improvements to flow by channeling/re-directing winds in a more favorable manner. This may mean increased CO_2 mixing, or further decreasing fan work required. Further, DAC units could be mounted on different structures, such as re-purposed oil and gas platforms, or re-tired vessels. There is mention of these concepts in chapter 3, but detailed analysis was beyond the scope of the current study.

The study conducted in chapter 2 assumed a worst case scenario, where all contactors are in adsorption mode at once. This was meant to serve as baseline, but in reality, contactors would be in different phases of their cycle. Future analysis could take a detailed look at phasing contactors on and off. This could be done from a steady state analysis, or dynamic analysis. Further, optimization studies could be completed to understand the best operational configuration to maximize CO_2 output. This could look into selectively choosing whether to turn on fans, or direct all power to desorption, while in times with low power availability.

4.1.3 Turbine performance impacts

Beyond CFD simulations for impact on DAC units, analysis should be conducted on the performance impacts to the turbine itself as a result of having additional equipment on board. Studies examining the stability/buoyancy, and power performance are necessary. Current designs for offshore floating wind turbines do not account for additional weight on board. In present designs, there are commonly no decks/catwalks installed between floats supporting the turbine components. Re-design would need to be done to include this, or at minimum, have the flexibility to be adapted if required. With DAC units below the rotor plane, power production may be impacted. All though DAC units should be installed in a manner to not interfere with incoming flow upstream, they may change the overall boundary layer wind profile by increasing surface roughness. If less power is produced as a result, fewer DAC units can be supported based on the energy demand. Iteration needs to be done to the design to ensure power demand is balanced with power produced.

4.1.4 TEA and LCA

Once the design space has converged slightly and more detailed configurations are conceptualized, detailed techno-economic analysis will shine light to which arrangements

are most cost effective. Furthermore, detailed life cycle analysis should be conducted to ensure negative emissions are probable. This should be used as a go/no-go decision on any design related to CDR, because if not likely achievable, the project has no positive climate benefit.

Addressing climate change is one of the most pressing issues of today, and requires a global effort to tackle it. Carbon dioxide must be removed from the atmosphere, alongside aggressive emission reductions. The methods to best achieve this are still being explored today. One thing that is certain, is that no solution one will get us all the way there; rather, a broad portfolio of solutions will be required to meet the scale necessary.

Bibliography

[1] D. Chen, M. Rojas, B. Samset, K. Cobb, A. D. Niang, P. Edwards, S. Emori, S. Faria, E. Hawkins, P. Hope, P. Huybrechts, M. Meinshausen, S. Mustafa, G.-K. Plattner, and A.-M. Tréguier, "Chapter 1: Framing, Context and Methods," tech. rep., Cambridge University Press, Cambridge, United Kingdom and New York, NY, USA, 2021.

[2] C. Bloch, R. Kahsar, J. Newcomb, G. Wohl, and E. Hanson, "Scoping the Potential Need for Direct Air Capture- Near-Term Support is Critical to De-Risk Scalable Solutions," tech. rep., RMI, Feb. 2022.

[3] "Climate Change: Atmospheric Carbon Dioxide — NOAA Climate.gov." http://www.climate.gov/news-features/understanding-climate/climate-change-atmospheric-carbon-dioxide.

[4] National Academy of Science, Board on Atmospheric Sciences and Climate, Board on Energy and Environmental Systems, Board on Agriculture and Natural Resources, Board on Earth Sciences and Resources, Board on Chemical Sciences and Technology, Ocean Studies Board, Division on Earth and Life Studies, and National Academies of Sciences, Engineering, and Medicine, *Negative Emissions Technologies and Reliable Sequestration: A Research Agenda*. Washington, D.C.: National Academies Press, Mar. 2019.

[5] J. Wilcox, B. Kolosz, and J. Freeman, eds., *CDR Primer*. 2021.

[6] D. Todd, "Survive and Thrive- Why BC needs a CO2 removal strategy now," tech. rep., Pacific Institute For Climate Solutions, Oct. 2022.

[7] H. Ishaq, R. Foxall, and C. Crawford, "Performance assessment of offshore wind energy integrated monoethanolamine synthesis system for post-combustion and

potential direct air capture," *Journal of CO2 Utilization*, vol. 64, p. 102154, Oct. 2022.

[8] N. McQueen, K. V. Gomes, C. McCormick, K. Blumanthal, M. Pisciotta, and J. Wilcox, "A review of direct air capture (DAC): Scaling up commercial technologies and innovating for the future," *Progress in Energy*, vol. 3, p. 032001, July 2021.

[9] D. W. Keith, G. Holmes, D. St. Angelo, and K. Heidel, "A Process for Capturing CO2 from the Atmosphere," *Joule*, vol. 2, pp. 1573–1594, Aug. 2018.

[10] K. Lebling, H. Leslie-Bole, Z. Byrum, and L. Bridgwater, "6 Things to Know About Direct Air Capture." https://www.wri.org/insights/direct-air-capture-resource-considerations-and-costs-carbon-removal, Mon, 05/02/2022 - 16:40.

[11] A. Sinha and M. J. Realff, "A parametric study of the techno-economics of direct CO2 air capture systems using solid adsorbents," *AIChE Journal*, vol. 65, p. e16607, Apr. 2019.

[12] S. Deutz and A. Bardow, "Life-cycle assessment of an industrial direct air capture process based on temperature–vacuum swing adsorption," *Nature Energy*, pp. 1–11, Feb. 2021.

[13] A. Garcia-Teruel, G. Rinaldi, P. R. Thies, L. Johanning, and H. Jeffrey, "Life cycle assessment of floating offshore wind farms: An evaluation of operation and maintenance," *Applied Energy*, vol. 307, p. 118067, Feb. 2022.

[14] S. Ó. Snæbjörnsdóttir, B. Sigfússon, C. Marieni, D. Goldberg, S. R. Gislason, and E. H. Oelkers, "Carbon dioxide storage through mineral carbonation," *Nature Reviews Earth & Environment*, vol. 1, pp. 90–102, Feb. 2020.

[15] G. Dipple, P. Kelemen, and Caleb M. Woodall, "The Building Blocks of CDR Systrems: Mineralization," in *CDR Primer* (J. Wilcox, B. Kolosz, and J. Freeman, eds.), 2021.

[16] S. Ó. Snæbjörnsdóttir, S. Tómasdóttir, B. Sigfússon, E. S. Aradóttir, G. Gunnarsson, A. Niemi, F. Basirat, B. Dessirier, S. R. Gislason, E. H. Oelkers, and H. Franzson, "The geology and hydrology of the CarbFix2 site, SW-Iceland," *Energy Procedia*, vol. 146, pp. 146–157, July 2018.

[17] V. Gutknecht, S. Ó. Snæbjörnsdóttir, B. Sigfússon, E. S. Aradóttir, and L. Charles, "Creating a carbon dioxide removal solution by combining rapid mineralization of CO2 with direct air capture," *Energy Procedia*, vol. 146, pp. 129–134, July 2018.

[18] D. Goldberg, A. Bonneville, M. Stute, A. Fisher, A.-H. Park, M. Gerrard, K. Moran, K. Hnottavange-Telleen, A. Slagle, I. Demirkanli, M. White, M. Scherwath, M. Heesemann, L. Aston, R. Webb, E. Hsu, C. Evans, and L. Zahn, "Integrated pre-feasibility study for CO2 geological storage in the Cascadia Basin, offshore Washington State, British Columbia," Tech. Rep. DE-LDEO-FE0029219-1, Columbia Univ., New York, NY (United States), Dec. 2018.

[19] "SolidCarbon-A rock-solid climate solution." https://solidcarbon.ca/.

[20] B. Pirenne, K. Khandelwal, K. Moran, and M. Scherwath, "Durable Sequestration of Carbon- The Ocean to the Rescue," *The Journal of Ocean Technology*, vol. 17, no. 1, pp. 1–7, 2022.

[21] D. Goldberg and K. Moran, "Offshore Wind Energy, Direct Air Capture, and Carbon Sequestration in Basalt- Solutions to Atmopsheric CO2 Reduction," *The Journal of Ocean Technology*, vol. 17, no. 1, pp. 30–36, 2022.

[22] B. M. Tutolo, A. Awolayo, and C. Brown, "Alkalinity Generation Constraints on Basalt Carbonation for Carbon Dioxide Removal at the Gigaton-per-Year Scale," *Environmental Science & Technology*, vol. 55, pp. 11906–11915, Sept. 2021.

[23] A. N. Awolayo, C. T. Laureijs, J. Byng, A. J. Luhmann, R. Lauer, and B. M. Tutolo, "Mineral surface area accessibility and sensitivity constraints on carbon mineralization in basaltic aquifers," *Geochimica et Cosmochimica Acta*, vol. 334, pp. 293–315, Oct. 2022.

[24] A. N. Awolayo and B. M. Tutolo, "PyGeochemCalc: A Python package for geochemical thermodynamic calculations from ambient to deep Earth conditions," *Chemical Geology*, vol. 606, p. 120984, Sept. 2022.

[25] H. Ishaq and C. Crawford, "Potential of offshore wind energy for direct air capture," *International Journal of Energy Research*, vol. 46, no. 13, pp. 18919–

18927, 2022.

[26] P. Connolly and C. Crawford, "Analytical modelling of power production from Un-moored Floating Offshore Wind Turbines," *Ocean Engineering*, vol. 259, p. 111794, Sept. 2022.

[27] S. R. Cooley, S. Klinsky, D. R. Morrow, and T. Satterfield, "Sociotechnical Considerations About Ocean Carbon Dioxide Removal," *Annual Review of Marine Science*, vol. 15, no. 1, p. null, 2023.

[28] R. Foxall and C. Crawford, "Ambient Wind Conditions Impact on Energy Requirements of an Offshore Direct Air Capture Plant," *Journal TBD*, Jan. 2023.

[29] D. S. Goldberg, K. S. Lackner, P. Han, A. L. Slagle, and T. Wang, "Co-Location of Air Capture, Subseafloor CO $_2$ Sequestration, and Energy Production on the Kerguelen Plateau," *Environmental Science & Technology*, vol. 47, pp. 7521–7529, July 2013.

[30] S. K. White, F. A. Spane, H. T. Schaef, Q. R. S. Miller, M. D. White, J. A. Horner, and B. P. McGrail, "Quantification of CO2 Mineralization at the Wallula Basalt Pilot Project," *Environmental Science & Technology*, vol. 54, pp. 14609–14616, Nov. 2020.

[31] "How it works - Carbfix." https://www.carbfix.com/how-it-works.

[32] H. Pilorgé, B. Kolosz, G. C. Wu, J. Freeman, and J. Wilcox, "Global mapping of CDR opportunities," in *CDR Primer*, 2021.

[33] M. J. Bos, S. R. A. Kersten, and D. W. F. Brilman, "Wind power to methanol: Renewable methanol production using electricity, electrolysis of water and CO2 air capture," *Applied Energy*, vol. 264, p. 114672, Apr. 2020.

[34] A. Sinha, L. A. Darunte, C. W. Jones, M. J. Realff, and Y. Kawajiri, "Systems Design and Economic Analysis of Direct Air Capture of CO2 through Temperature Vacuum Swing Adsorption Using MIL-101(Cr)-PEI-800 and mmen-Mg2(dobpdc) MOF Adsorbents," *Industrial & Engineering Chemistry Research*, vol. 56, pp. 750–764, Jan. 2017.

[35] F. Sabatino, A. Grimm, F. Gallucci, M. van Sint Annaland, G. J. Kramer, and M. Gazzani, "A comparative energy and costs assessment and optimization for direct air capture technologies," *Joule*, vol. 5, pp. 2047–2076, Aug. 2021.

[36] N. McQueen, P. Psarras, H. Pilorgé, S. Liguori, J. He, M. Yuan, C. M. Woodall, K. Kian, L. Pierpoint, J. Jurewicz, J. M. Lucas, R. Jacobson, N. Deich, and J. Wilcox, "Cost Analysis of Direct Air Capture and Sequestration Coupled to Low-Carbon Thermal Energy in the United States," *Environmental Science & Technology*, vol. 54, pp. 7542–7551, June 2020.

[37] NREL, "Annual Technology Baseline -Offshore Wind." https://atb.nrel.gov/electricity/2022/offshore_wind, 2022.

[38] "Orca - the world's first large-scale direct air capture and storage plant." https://climeworks.com/orca, 2021.

[39] R. Long-Innes, *Thermodynamic Analysis of a Direct Air Carbon Capture Plant with Directions for Energy Efficiency Improvements*. PhD thesis, The University of Victoria, Victoria, BC, 2021.

[40] J. L. Merrill, "Electric kiln," Oct. 1931.

[41] Coolbrook, "Coolbrook- Technology- RDH – RotoDynamic Heater." https://coolbrook.com/technology/, 2022.

[42] C. Gebald, J. A. Wurzbacher, A. Borgschulte, T. Zimmermann, and A. Steinfeld, "Single-Component and Binary CO2 and H2O Adsorption of Amine-Functionalized Cellulose," *Environmental Science & Technology*, vol. 48, pp. 2497–2504, Feb. 2014.

[43] Y. Belmabkhout, R. Serna-Guerrero, and A. Sayari, "Adsorption of CO $_2$ -Containing Gas Mixtures over Amine-Bearing Pore-Expanded MCM-41 Silica: Application for Gas Purification," *Industrial & Engineering Chemistry Research*, vol. 49, pp. 359–365, Jan. 2010.

[44] L. A. Darunte, A. D. Oetomo, K. S. Walton, D. S. Sholl, and C. W. Jones, "Direct Air Capture of CO2 Using Amine Functionalized MIL-101(Cr)," *ACS Sustainable Chemistry & Engineering*, vol. 4, pp. 5761–5768, Oct. 2016.

[45] R. Veneman, N. Frigka, W. Zhao, Z. Li, S. Kersten, and W. Brilman, "Adsorption of H2O and CO2 on supported amine sorbents," *International Journal of Greenhouse Gas Control*, vol. 41, pp. 268–275, Oct. 2015.

[46] M. J. Bos, T. Kreuger, S. R. A. Kersten, and D. W. F. Brilman, "Study on transport phenomena and intrinsic kinetics for CO2 adsorption in solid amine sorbent," *Chemical Engineering Journal*, vol. 377, p. 120374, Dec. 2019.

[47] C. Gebald, N. Piatkowski, T. Ruesch, and J. andre Wurzbacher, "Low pressure drop structure of particle adsorbent bed for adsorption gas separation process," Oct. 2014.

[48] S. Sauerbeck, C. Gebald, and J. A. Wurzbacher, "Improved low-pressure drop structure of particle adsorbent bed for adsorption gas separation process," Nov. 2018.

[49] C. J. E. Bajamundi, J. Koponen, V. Ruuskanen, J. Elfving, A. Kosonen, J. Kauppinen, and J. Ahola, "Capturing CO2 from air: Technical performance and process control improvement," *Journal of CO2 Utilization*, vol. 30, pp. 232–239, Mar. 2019.

[50] V. Stampi-Bombelli, M. van der Spek, and M. Mazzotti, "Analysis of direct capture of CO2 from ambient air via steam-assisted temperature–vacuum swing adsorption," *Adsorption*, vol. 26, pp. 1183–1197, Oct. 2020.

[51] C. Drechsler and D. W. Agar, "Investigation of water co-adsorption on the energy balance of solid sorbent based direct air capture processes," *Energy*, vol. 192, p. 116587, Feb. 2020.

[52] J. A. Wurzbacher, C. Gebald, N. Piatkowski, and A. Steinfeld, "Concurrent Separation of CO2 and H2O from Air by a Temperature-Vacuum Swing Adsorption/Desorption Cycle," *Environmental Science & Technology*, vol. 46, pp. 9191–9198, Aug. 2012.

[53] J. A. Wurzbacher, C. Gebald, S. Brunner, and A. Steinfeld, "Heat and mass transfer of temperature–vacuum swing desorption for CO2 capture from air," *Chemical Engineering Journal*, vol. 283, pp. 1329–1338, Jan. 2016.

[54] J. Elfving, C. Bajamundi, J. Kauppinen, and T. Sainio, "Modelling of equilibrium working capacity of PSA, TSA and TVSA processes for CO2 adsorption under direct air capture conditions," *Journal of CO2 Utilization*, vol. 22, pp. 270–277, Dec. 2017.

[55] E. S. Sanz-Pérez, C. R. Murdock, S. A. Didas, and C. W. Jones, "Direct Capture of CO $_2$ from Ambient Air," *Chemical Reviews*, vol. 116, pp. 11840–11876, Oct. 2016.

[56] B. Blocken, "Computational Wind Engineering: Theory and Applications," in *Environmental Wind Engineering and Design of Wind Energy Structures* (C. C. Baniotopoulos, C. Borri, and T. Stathopoulos, eds.), CISM Courses and Lectures, pp. 55–93, Vienna: Springer, 2011.

[57] N. Holmes and L. Morawska, "A review of dispersion modelling and its application to the dispersion of particles: An overview of different dispersion models available," *Atmospheric Environment*, vol. 40, pp. 5902–5928, Sept. 2006.

[58] M. Loomans and T. Lemaire, "Particle concentration calculations using CFD," *Indoor Air*, p. 4, Jan. 2002.

[59] Carl von Linde Strasse, "Safety advice- Carbon Dioxide," 2017.

[60] M. T. Markiewicz, "A Review Of Models For The Atmospheric Dispersion Of Heavy Gases. Part Ii. Model Quality Evaluation," *Ecological Chemistry and Engineering S*, vol. 20, pp. 763–782, Dec. 2013.

[61] J. Labovský and Ľ. Jelemenský, "CFD-based atmospheric dispersion modeling in real urban environments," *Chemical Papers*, vol. 67, Jan. 2013.

[62] R. Ramponi, B. Blocken, L. B. de Coo, and W. D. Janseen, "CFD simulation of outdoor ventilation of generic urban configurations with different urban densities and equal and unequal street widths," *Building and Environment*, vol. 92, pp. 152–166, Oct. 2015.

[63] A. Nottrott, J. Kleissl, and R. Keeling, "Modeling passive scalar dispersion in the atmospheric boundary layer with WRF large-eddy simulation," *Atmospheric Environment*, vol. 82, pp. 172–182, Jan. 2014.

[64] E. Gaertner, J. Rinker, L. Sethuraman, F. Zahle, B. Anderson, G. Barter, N. Abbas, F. Meng, P. Bortolotti, W. Skrzypinski, G. Scott, R. Feil, Henrik Bredmose, K. Dykes, Matt Shields, C. Allen, and A. Viselli, "Definition of the IEA Wind 15-Megawatt Offshore Reference Wind Turbine," Tech. Rep. NREL/TP-5000-75698, National Renewable Energy Labratory, Golden,CO, 2020.

[65] C. Allen, A. Viscelli, H. Dagher, A. Goupee, E. Gaertner, N. Abbas, M. Hall, and G. Barter, "Definition of the UMaine VolturnUS-S Reference Platform Developed for the IEA Wind 15-Megawatt Offshore Reference Wind Turbine," Tech. Rep. NREL/TP-5000-76773, 1660012, MainId:9434, July 2020.

[66] IEA, "Offshore Wind Outlook 2019 – Analysis," tech. rep., Paris, Nov. 2019.

[67] S. Hameer and J. L. van Niekerk, "A review of large-scale electrical energy storage," *International Journal of Energy Research*, vol. 39, no. 9, pp. 1179–1195, 2015.

[68] "What We Do — Carbon Capture Inc.." https://www.carboncapture.com/what-we-do.

[69] "Our Technology-types of plants." https://carbonengineering.com/our-technology/.

[70] T. Uchida, Y. Taniyama, Y. Fukatani, M. Nakano, Z. Bai, T. Yoshida, and M. Inui, "A New Wind Turbine CFD Modeling Method Based on a Porous Disk Approach for Practical Wind Farm Design," *Energies*, vol. 13, p. 3197, Jan. 2020.

[71] "Porosity & Porous Media — Advanced Concepts." https://www.simscale.com/docs/simulation-setup/advanced-concepts/porous-media/.

[72] Y. Cengel and J. Cimbala, *Fluid Mechanics Fundamentals and Applications*. New York, NY, USA: McGraw-Hill, 1st ed., 2006.

[73] B. Blocken, R. Vervoort, and T. van Hooff, "Reduction of outdoor particulate matter concentrations by local removal in semi-enclosed parking garages: A

preliminary case study for Eindhoven city center," *Journal of Wind Engineering and Industrial Aerodynamics*, vol. 159, pp. 80–98, Dec. 2016.

[74] B. Blocken, T. Stathopoulos, and J. Carmeliet, "CFD simulation of the atmospheric boundary layer: Wall function problems," *Atmospheric Environment*, vol. 41, pp. 238–252, Jan. 2007.

[75] J. Labovský and L. Jelemenský, "Verification of CFD pollution dispersion modelling based on experimental data," *Journal of Loss Prevention in the Process Industries*, vol. 24, pp. 166–177, Mar. 2011.

[76] Simscale, "Momentum Sources — Advanced Concepts Documentation." https://www.simscale.com/docs/simulation-setup/advanced-concepts/momentum-sources/, Jan. 2023.

[77] "SimScale Documentation- Passive Scalar Sources." https://www.simscale.com/docs/simulation-setup/advanced-concepts/passive-scalar-sources/, Nov. 2021.

[78] F. Sabatino, M. Mehta, A. Grimm, M. Gazzani, F. Gallucci, G. J. Kramer, and M. van Sint Annaland, "Evaluation of a Direct Air Capture Process Combining Wet Scrubbing and Bipolar Membrane Electrodialysis," *Industrial & Engineering Chemistry Research*, vol. 59, pp. 7007–7020, Apr. 2020.

[79] "Air - Diffusion Coefficients of Gases in Excess of Air." https://www.engineeringtoolbox.com/air-diffusion-coefficient-gas-mixture-temperature-d_2010.html.

[80] Y. Abu-Zidan, P. Mendis, and T. Gunawardena, "Optimising the computational domain size in CFD simulations of tall buildings," *Heliyon*, vol. 7, p. e06723, Apr. 2021.

[81] J. Franke, A. Hellsten, K. H. Schlunzen, and B. Carissimo, "The COST 732 Best Practice Guideline for CFD simulation of flows in the urban environment: A summary," *International Journal of Environment and Pollution*, vol. 44, no. 1/2/3/4, p. 419, 2011.

[82] M. Golbazi and C. L. Archer, "Surface roughness for offshore wind energy," *Journal of Physics: Conference Series*, vol. 1452, p. 012024, Jan. 2020.

[83] H. Struchtrup, *Thermodynamics and Energy Conversion*. Berlin, Heidelberg: Springer Berlin Heidelberg, 2014.

[84] R. Long-Innes and H. Struchtrup, "Thermodynamic loss analysis of a liquid-sorbent direct air carbon capture plant," *Cell Reports Physical Science*, vol. 3, p. 100791, Mar. 2022.

[85] M. W. Chase, "NIST Chemistry WebBook, SRD 69-Carbon dioxide." https://webbook.nist.gov/cgi/cbook.cgi?ID=C124389&Mask=1&Type=JANAFG&Table=or 1998.

[86] "Water - Heat of Vaporization vs. Temperature." https://www.engineeringtoolbox.com/water-properties-d_1573.html, 2010.

[87] EIA, "How much electricity does an American home use?." https://www.eia.gov/tools/faqs/faq.php, Oct. 2021.

[88] "Average monthly humidity in Victoria (British Columbia), Canada." https://weather-and-climate.com:80/average-monthly-Humidity-perc,victoria,Canada.

[89] Christoph Gebald, N. Repond, Jan Andre Wurzbacher, Anca Elena Timofte, Isvan Meszaros, and Benjamin Keusch, "Method And Device For Adsorption/Desorption Of Carbon Dioxide From Gas Streams With Heat Recovery Unit," Dec. 2019.

[90] R. Foxall and C. Crawford, "Marinisation for offshore direct air capture- Design evaluation for air pre-treatment to remove aerosolized salt particles," *Journal TBD*, Jan. 2023.

[91] P. Smith, P. J. Gregory, D. van Vuuren, M. Obersteiner, P. Havlík, M. Rounsevell, J. Woods, E. Stehfest, and J. Bellarby, "Competition for land," *Philosophical Transactions of the Royal Society B: Biological Sciences*, vol. 365, pp. 2941–2957, Sept. 2010.

[92] H. Pilorgé, B. Kolosz, G. C. Wu, and J. Freeman, "Global mapping of CDR systems," in *CDR Primer* (J. Wilcox, B. Kolosz, and J. Freeman, eds.), 2021.

[93] R. Wiser, M. Bolinger, B. Hoen, D. Millstein, J. Rand, G. Barbose, N. Darghouth, W. Gorman, S. Jeong, and B. Paulos, "Land-Based Wind Market Report: 2022 Edition," tech. rep., U.S. Department of Energy, 2022.

[94] B. Songhurst, "The Outlook for Floating Storage and Regasification Units (FSRUs)," tech. rep., Oxford Institute for Energy Studies, July 2017.

[95] "Marinisation," *Wikipedia*, Oct. 2022.

[96] "Ocean-Based Carbon Dioxide Removal: Road Maps." https://www2.oceanvisions.org/roadmaps/, May 2021.

[97] I. A. Digdaya, I. Sullivan, M. Lin, L. Han, W.-H. Cheng, H. A. Atwater, and C. Xiang, "A direct coupled electrochemical system for capture and conversion of CO2 from oceanwater," *Nature Communications*, vol. 11, p. 4412, Dec. 2020.

[98] M. D. Eisaman, C.-F. de Lannoy, A. Jose, S. D. Karnitz, R. W. DeVaul, K. Hannun, and J. L. Rivest, "Indirect ocean capture of atmospheric CO2: Part II. Understanding the cost of negative emissions," *International Journal of Greenhouse Gas Control*, vol. 70, pp. 254–261, Mar. 2018.

[99] C.-F. de Lannoy, M. D. Eisaman, A. Jose, S. D. Karnitz, R. W. DeVaul, K. Hannun, and J. L. Rivest, "Indirect ocean capture of atmospheric CO2: Part I. Prototype of a negative emissions technology," *International Journal of Greenhouse Gas Control*, vol. 70, pp. 243–253, Mar. 2018.

[100] M. D. Eisaman, "Negative Emissions Technologies: The Tradeoffs of Air-Capture Economics," *Joule*, vol. 4, pp. 516–520, Mar. 2020.

[101] P. B. Kelemen, N. McQueen, J. Wilcox, P. Renforth, G. Dipple, and A. P. Vankeuren, "Engineered carbon mineralization in ultramafic rocks for CO2 removal from air: Review and new insights," *Chemical Geology*, vol. 550, p. 119628, Sept. 2020.

[102] X. Lu, K. J. Carroll, C. C. Turvey, and G. M. Dipple, "Rate and capacity of cation release from ultramafic mine tailings for carbon capture and storage," *Applied Geochemistry*, vol. 140, p. 105285, May 2022.

[103] E. Wynands, *Carbon Mineralization in Ultramafic Mine Tailings via CO_2 Injection*. PhD thesis, University of British Columbia, 2021.

[104] C. F. A. Sondak, P. O. Ang, J. Beardall, A. Bellgrove, S. M. Boo, G. S. Gerung, C. D. Hepburn, D. D. Hong, Z. Hu, H. Kawai, D. Largo, J. A. Lee, P.-E. Lim, J. Mayakun, W. A. Nelson, J. H. Oak, S.-M. Phang, D. Sahoo, Y. Peerapornpis, Y. Yang, and I. K. Chung, "Carbon dioxide mitigation potential of seaweed aquaculture beds (SABs)," *Journal of Applied Phycology*, vol. 29, pp. 2363–2373, Oct. 2017.

[105] National Academies of Sciences, Engineering, and Medicine, Committee on A Research Strategy for Ocean-based Carbon Dioxide Removal and Sequestration, and Division on Earth and Life Studies, *A Research Strategy for Ocean-based Carbon Dioxide Removal and Sequestration*. Washington, D.C.: National Academies Press, 2021.

[106] Carbon Engineering, "News and updates: Occidental, 1PointFive to Begin Construction of World's Largest Direct Air Capture Plant in the Texas Permian Basin." https://carbonengineering.com/news-updates/construction-direct-air-capture-texas/, Aug. 2022.

[107] J. F. Wiegner, A. Grimm, L. Weimann, and M. Gazzani, "Optimal Design and Operation of Solid Sorbent Direct Air Capture Processes at Varying Ambient Conditions," *Industrial & Engineering Chemistry Research*, vol. 61, pp. 12649–12667, Aug. 2022.

[108] J. Elfving and T. Sainio, "Kinetic approach to modelling CO2 adsorption from humid air using amine-functionalized resin: Equilibrium isotherms and column dynamics," *Chemical Engineering Science*, vol. 246, p. 116885, Dec. 2021.

[109] R. P. Wijesiri, G. P. Knowles, H. Yeasmin, A. F. A. Hoadley, and A. L. Chaffee, "Technoeconomic Evaluation of a Process Capturing CO2 Directly from Air," *Processes*, vol. 7, p. 503, Aug. 2019.

[110] N. Casas, J. Schell, R. Blom, and M. Mazzotti, "MOF and UiO-67/MCM-41 adsorbents for pre-combustion CO2 capture by PSA: Breakthrough experiments and process design," *Separation and Purification Technology*, vol. 112, pp. 34–48, July 2013.

[111] G. Rim, F. Kong, M. Song, C. Rosu, P. Priyadarshini, R. P. Lively, and C. W. Jones, "Sub-Ambient Temperature Direct Air Capture of CO $_2$ using

Amine-Impregnated MIL-101(Cr) Enables Ambient Temperature CO $_2$ Recovery," *JACS Au*, vol. 2, pp. 380–393, Feb. 2022.

[112] K. An, A. Farooqui, and S. T. McCoy, "The impact of climate on solvent-based direct air capture systems," *Applied Energy*, vol. 325, p. 119895, Nov. 2022.

[113] Naval Sea Systems Command- Department of the Navy, "Marine Gas Turbines," Aug. 1988.

[114] A. M. Dashliborun, J. Zhang, S. M. Taghavi, and F. Larachi, "110th Anniversary: Marinization of Multiphase Reactors through the Prism of Chemical Engineers," in *Industrial & Engineering Chemistry Research*, vol. 58, pp. 2607–2630, Feb. 2019.

[115] A. M. Dashliborun, F. Larachi, and S. M. Taghavi, "Gas-liquid mass-transfer behavior of packed-bed scrubbers for floating/offshore CO2 capture," *Chemical Engineering Journal*, vol. 377, p. 119236, Dec. 2019.

[116] M. Issa, P. Beaulac, Universite du Quebec a Rimouski, department of engineering, Rimouski, Canada., H. Ibrahim, Institut Maritime du Quebec, Department of applied sciences, Rimouski, Canada., A. Ilinca., and Institut Technologique de Maintenance Industrielle (ITMI), Sept-Iles, Canada., "Marinization Of A Two-Stage Mixed Structured Packing Scrubber For Sox Abatement And CO2 Capture," *International Journal of Advanced Research*, vol. 7, pp. 73–82, Apr. 2019.

[117] M. Schultes, J. Brauer, P. Chen, and S. Doong, "Marinization of Mass Transfer Columns for FLNG Applications," in *Day 3 Wed, May 02, 2018*, (Houston, Texas, USA), p. D032S092R010, OTC, Apr. 2018.

[118] "Air - Density, Specific Weight and Thermal Expansion Coefficient vs. Temperature and Pressure." https://www.engineeringtoolbox.com/air-density-specific-weight-d_600.html, 2003.

[119] R. Rahimi and D. Abbaspour, "Determination of pressure drop in wire mesh mist eliminator by CFD," *Chemical Engineering and Processing*, p. 5, 2008.

[120] H. T. El-Dessouky, I. M. Alatiqi, H. M. Ettouney, and N. S. Al-Deffeeri, "Performance of wire mesh mist eliminator," *Chemical Engineering and Processing:*

Process Intensification, vol. 39, pp. 129–139, Mar. 2000.

[121] A. A. Al-Dughaither, A. A. Ibrahim, and W. A. Al-Masry, "Investigating pressure drop across wire mesh mist eliminators in bubble column," *Journal of Saudi Chemical Society*, vol. 15, pp. 1–9, Jan. 2011.

[122] K. Li, J. D. Kress, and D. S. Mebane, "The Mechanism of CO2 Adsorption under Dry and Humid Conditions in Mesoporous Silica-Supported Amine Sorbents," *The Journal of Physical Chemistry C*, vol. 120, pp. 23683–23691, Oct. 2016.

[123] R. H. Weiland and N. A. Hatcher, "Acidic and basic contaminants in amine treating," *Optimized Gas Treating, Inc.*, p. 9, June 2014.

[124] G. Avellaneda Domene, "Static and dynamic stability analysis of a floating wind turbine with on-board direct air capture system," Sept. 2022.

[125] W. Musial, P. Spitsen, P. Duffy, P. Beiter, M. Marquis, R. Hammond, and M. Shields, "Offshore Wind Market Report: 2022 Edition," tech. rep., U.S. Department of Energy, 2022.

[126] R. Hammond, A. Cooperman, A. Barker, A. Key, M. Shields, and A. Eberle, "WOMBAT - Windfarm Operations and Maintenance cost-Benefit Analysis Tool — WOMBAT v0.5.1." https://wisdem.github.io/WOMBAT/, 2022.

[127] P. Connolly, "Direct air capture units installed directly on the deck of offshore wind turbines," 2021.

[128] P. Connolly, "Direct air capture units mounted on a central hub platform powered by nearby offshore wind turbines," 2021.

[129] J. Gutiérrez, "How does "Momentum Source" work? - SimScale," Mar. 2022.

[130] Q. Yu and D. Brilman, "Design Strategy for CO2 Adsorption from Ambient Air Using a Supported Amine Based Sorbent in a Fixed Bed Reactor," *Energy Procedia*, vol. 114, pp. 6102–6114, July 2017.

[131] The Engineering ToolBox, "Moist Air - Properties." https://www.engineeringtoolbox.com/moist-air-properties-d_1256.html, 2009.

[132] "Water - Heat of Vaporization vs. Temperature." https://www.engineeringtoolbox.com/water-properties-d_1573.html, 2010.

Appendix A

CFD setup: Reynolds Averaged Navier Stokes Equations

The Reynolds Averaged Navier Stoked Equations are commonly referred to as RANS equations [129]. These are the governing equations being solved internally by the CFD solver. They describe the mass continuity and momentum conservation. They are described for the x, y, and z-directions in eq. (A.1), and eqs. (A.2) to (A.4).

Continuity:

$$\frac{\partial U_x}{\partial x} + \frac{\partial U_y}{\partial y} + \frac{\partial U_z}{\partial z} = 0 \tag{A.1}$$

Momentum:

$$\rho\left(\frac{\partial U_x}{\partial \tau} + U_x\frac{\partial U_x}{\partial x} + U_y\frac{\partial U_x}{\partial y} + U_z\frac{\partial U_x}{\partial z}\right) = \\ -\frac{\partial P}{\partial x} + \frac{\partial}{\partial x}\left[(\mu+\mu_t)\frac{\partial U_x}{\partial x}\right] + \frac{\partial}{\partial y}\left[(\mu+\mu_t)\frac{\partial U_x}{\partial y}\right] + \frac{\partial}{\partial z}\left[(\mu+\mu_t)\frac{\partial U_x}{\partial z}\right] + S_x \tag{A.2}$$

$$\rho\left(\frac{\partial U_y}{\partial \tau} + U_x\frac{\partial U_y}{\partial x} + U_y\frac{\partial U_y}{\partial y} + U_z\frac{\partial U_y}{\partial z}\right) = \\ -\frac{\partial P}{\partial y} + \frac{\partial}{\partial x}\left[(\mu+\mu_t)\frac{\partial U_y}{\partial x}\right] + \frac{\partial}{\partial y}\left[(\mu+\mu_t)\frac{\partial U_y}{\partial y}\right] + \frac{\partial}{\partial z}\left[(\mu+\mu_t)\frac{\partial U_y}{\partial z}\right] + S_y \tag{A.3}$$

$$\rho\left(\frac{\partial U_z}{\partial \tau}+U_x\frac{\partial U_z}{\partial x}+U_y\frac{\partial U_z}{\partial y}+U_z\frac{\partial U_z}{\partial z}\right)= \\ -\frac{\partial P}{\partial z}+\frac{\partial}{\partial x}\left[(\mu+\mu_t)\frac{\partial U_z}{\partial x}\right]+\frac{\partial}{\partial y}\left[(\mu+\mu_t)\frac{\partial U_z}{\partial y}\right]+\frac{\partial}{\partial z}\left[(\mu+\mu_t)\frac{\partial U_z}{\partial z}\right]+S_z \quad \text{(A.4)}$$

2D CFD setup: Sorbent physical properties

The sorbent physical properties are adapted from Sabatino et al. [35] for the solid sorbents APDES-NFC, Tri-PE-MCM, MIL-101(Cr)-PEI-800, and Lewatit VP OC 106 as described in the text body. These parameters are used to determine the coeffiecients for the fixed coefficient porous media model in the 2D CFD modelling section.

	APDES-NFC	Tri-PE-MCM	MIL-101(Cr)-PEI-800	Lewatit VP OC 106
μ	1.813×10^{-5}	1.813×10^{-5}	1.813×10^{-5}	1.813×10^{-5}
D_p	1.3×10^{-3}	1×10^{-3}	9.96×10^{-4}	6.88×10^{-4}
ϕ	0.6	0.6	0.6	0.6
ρ	1.204	1.204	1.204	1.204
$C_{p,sorbent}$	2070	1000	892.5	1580

Table A.1: Physical properties of sorbents to determine pressure drop through solid sorbent air contactor.

Here μ is the dynamic viscosity$[kg/m \cdot s]$, D_p the particle diameter [m], ϕ the void fraction, ρ is the fluid density [kg/m^3], and $C_{p,sorbent}$ is the specific heat capacity of each sorbent [J/kg-K]. At 20°C, $\rho_{air} = 1.204\ kg/m^3$.

2D CFD set-up: Fixed coefficient pressure drop model coefficients

Coefficients A, and B inputs to the fixed coefficient porous media model in the 2D CFD analysis are summarized in table A.2. The method for solving these coefficients is outlined in the body of the text using the physical properties for each sorbent outlined in table A.1. These values were directly input into the commercial CFD software.

	APDES-NFC	Tri-PE-MCM	MIL-101(Cr)-PEI-800	Lewatit VP OC 106
A	990.02	1673.13	1686.59	3534.69
B	2492.88	3240.74	3253.76	4710.38

Table A.2: Calculated A and B coefficients for sorbents used as input for the fixed coefficient porous media model

2D CFD setup: Domain dimensions

The domain dimensions are shown for all 2D modelling simulations. First, the domain for a single vertical sheet to verify the coefficients obtained through comparison with the Ergun equation. This is shown in fig. A.1. Second, the lab scale air contactor employing multiple horizontal sheets, in order to verify the CFD model produces similar pressure drops compared with the patent results. This is shown in fig. A.2. Third, the scaled up geometry to obtain pressure loss information for a variety of sorbents is shown in fig. A.3.

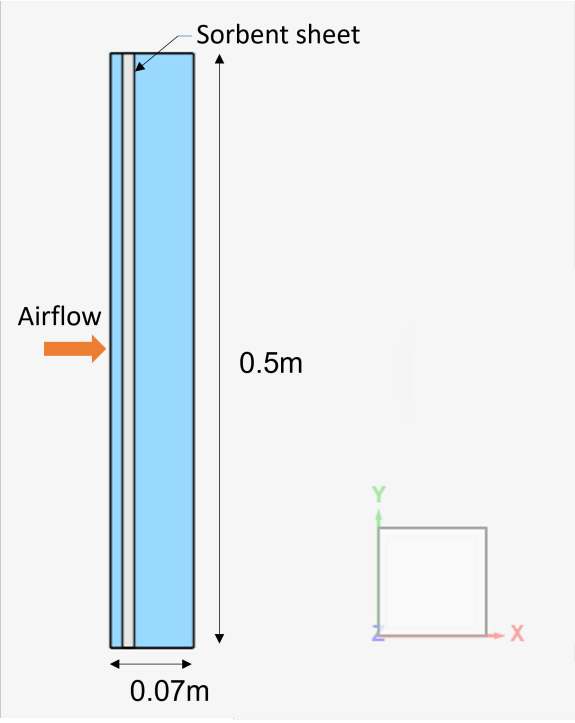

Figure A.1: Domain size for 2D CFD simulation to verify Ergun equation. 1cm thick sheet, with height of 0.5m. Flow enters at the left boundary, and flows left to right.

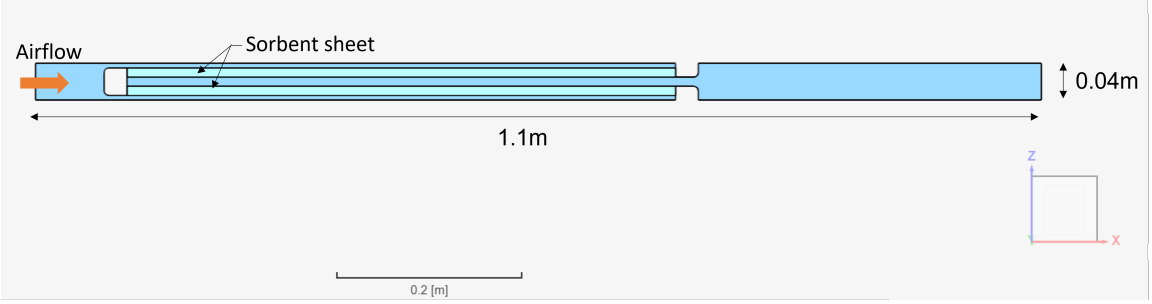

Figure A.2: Domain size for 2D CFD simulation of 0.5m contactor. 1cm thick sorbent sheets, and 1cm wide flow channels. Flow enters at the left boundary, and flows left to right.

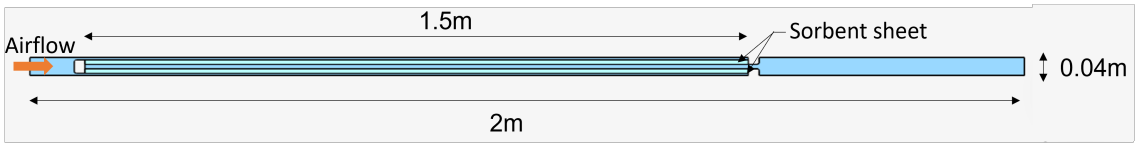

Figure A.3: Domain size for 2D CFD simulation of 1.5m contactor. 1cm thick sorbent sheets, and 1cm wide flow channels. Flow enters at the left boundary, and flows left to right.

2D CFD result: Ergun equation verification using a single vertical sheet of porous media

The result of 2D simulation number 1 is compared with the Ergun equation. The comparison of expected results to the results obtained in the 2D CFD model of a single vertical sheet are shown in table A.3.

Sorbent	Ergun equation ΔP (Pa)	Fixed Coefficient Result ΔP (Pa)
APDES-NFC	24.95	24.38
Tri-PE-MCM	35.86	35.10
MIL-101(Cr)-PEI-800	36.06	35.30
Lewatit VP OC 106	61.87	60.95
Exemplary	36.06	35.30

Table A.3: Porous media pressure drop model verification using the Ergun equation and the Fixed Coefficient Porous media model in SimScale. All simulations run at 0.73 m/s, through a vertical sheet with thickness of 1cm, height of 0.5m shown in figure A.1.

3D CFD setup: Domain dimensions

The 3D domain used for wind angles 91-180° is shown below. Angles 0-90° are shown in the main body of the report.

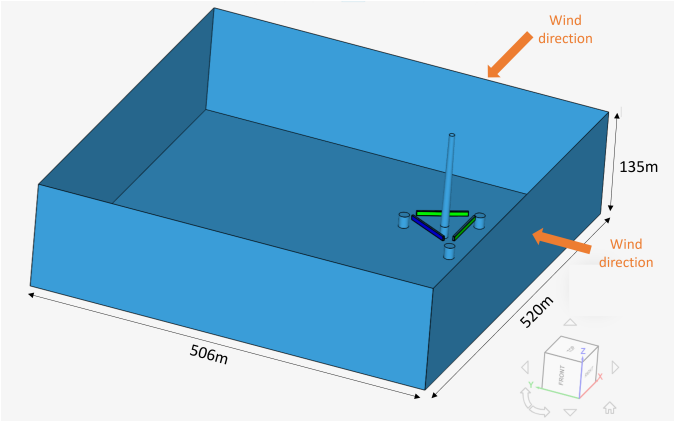

Figure A.4: Domain size used for 3D CFD simulations from 91-180 °wind angles

3D CFD setup: Fan off configuration

This section describes which fans are turned off at cut-out wind speeds (25m/s) based on the inflow wind direction. Fans roughly perpendicular to flow can be turned off, and other fans are directed in the predominant wind direction to avoid blowing upstream, which would result in an additional, unnecessary energy expense.

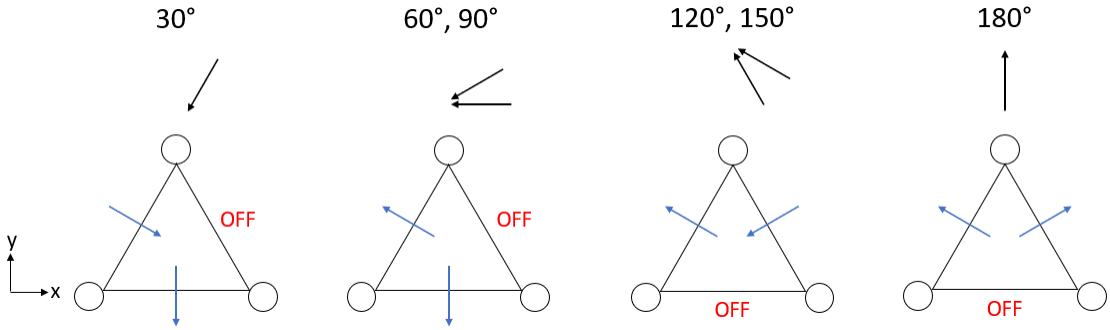

Figure A.5: Fan off configuration at cut-out wind speed of 25 m/s.

3D CFD result: No fan contactor outlet velocity mounted at ground level

Below is a result shown, fig. A.6, if contactors were to be mounted at ground level. In the report, units are mounted with a contactor center height of 17.9m. This result is shown to allow comparison with other implementations where contactors may be mounted directly at ground height. At this height, sufficient wind speed is not reached to allow turning off any fans completely.

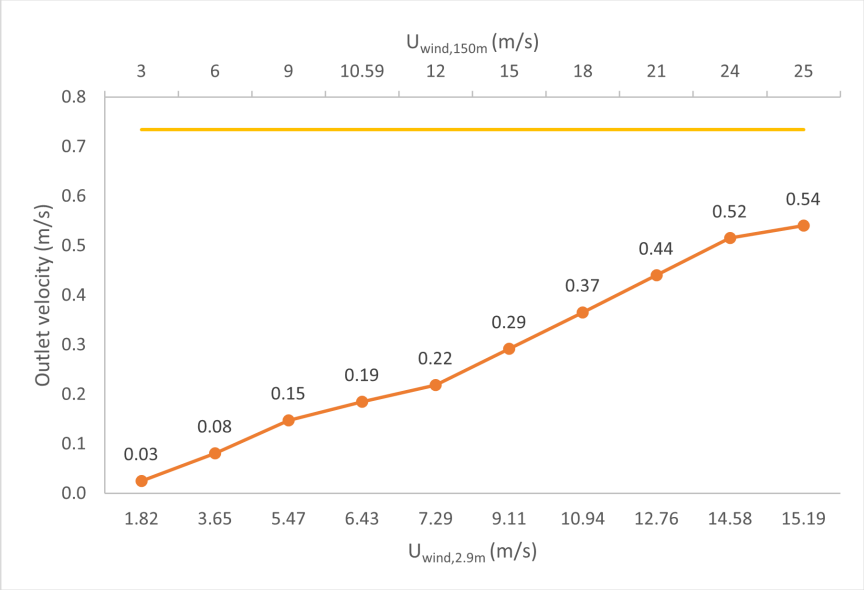

Figure A.6: Porous zone output velocity as a function of wind speed with a contactor bank mounted at ground level. Wind speed is measured using an upstream probe point at a height of 2.9m, the center of the contactor bank. Target throughput velocity is 0.7346 m/s, shown with the horizontal yellow line.

3D CFD result background: CFD cutting planes

The cutting planes used to display the CFD outputs are shown in figs. A.7 and A.8.

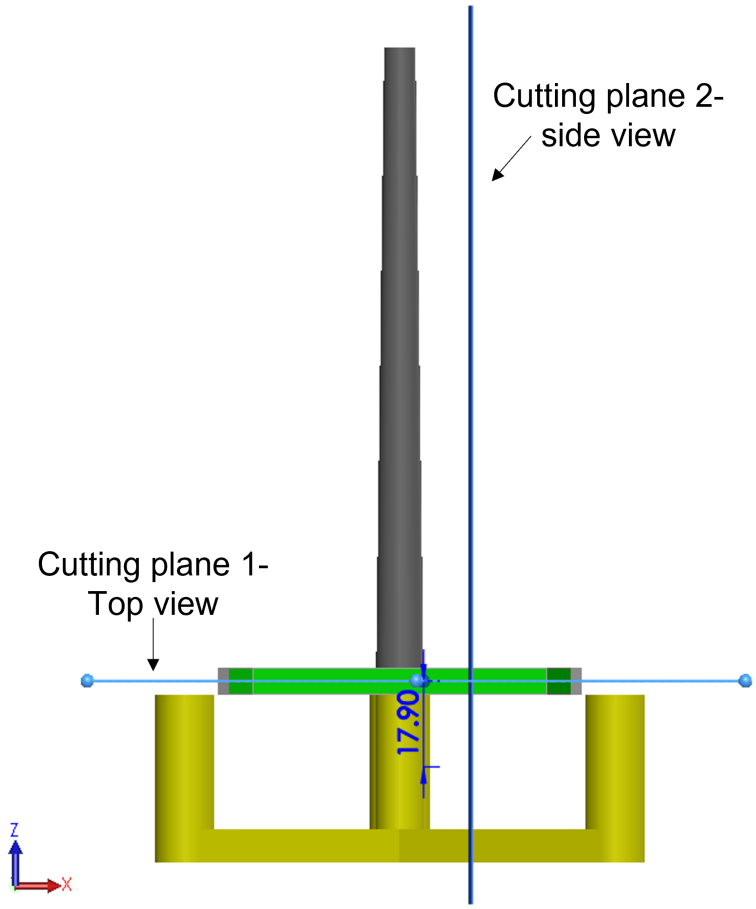

Figure A.7: Cutting planes for CFD output shown from the front view. Highlighted dimension shows that the top view cutting plane is placed 17.9m in the positive y-direction, and has direction normal to the z-axis

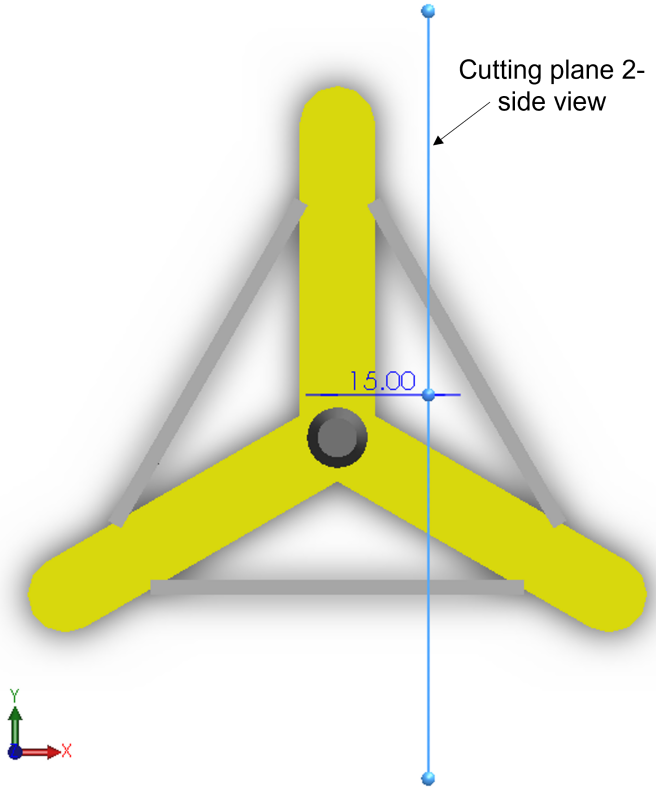

Figure A.8: Cutting planes for CFD output shown from the top view. Highlighted dimension shows that the side view cutting plane is placed 15m in the positive x direction, and has direction normal to the x-axis

3D CFD result: Additional plots showing CO_2 concentration change with wind speed

Additional figures showing CO_2 dispersion with increasing wind speed from 3m/s, 10.59m/s, and 25m/s at angles 0°, 90°, and 180°. It can be seen that with increasing wind speed, CO_2 dispersion increases, allowing downstream units to have higher inlet concentrations.

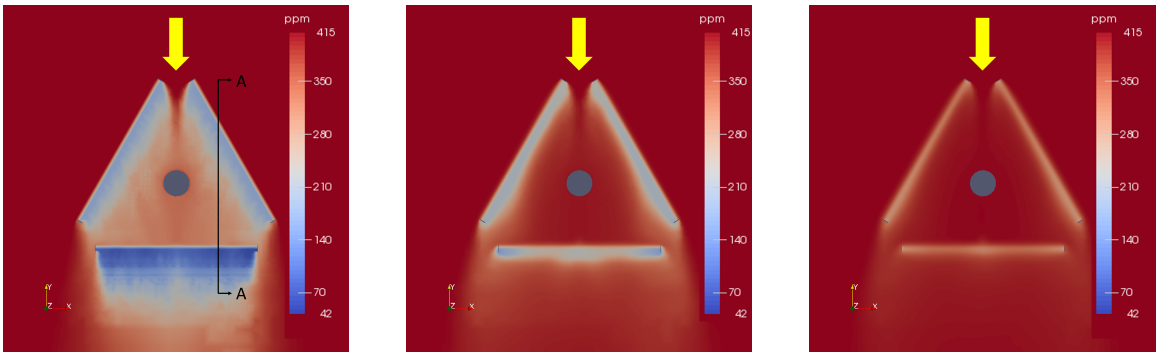

(a) (b) (c)

Figure A.9: CFD result showing dispersion of CO2 at 0°at a) cut in wind speed (3 m/s), b) rated wind speed (10.59m/s), and c) cut-out wind speed (25m/s). Wind direction shown with yellow arrow. Shown projected on the top plane (x-y plane) through the center of the air contactor bank, at height z = 17.9m as shown in figure A.7.

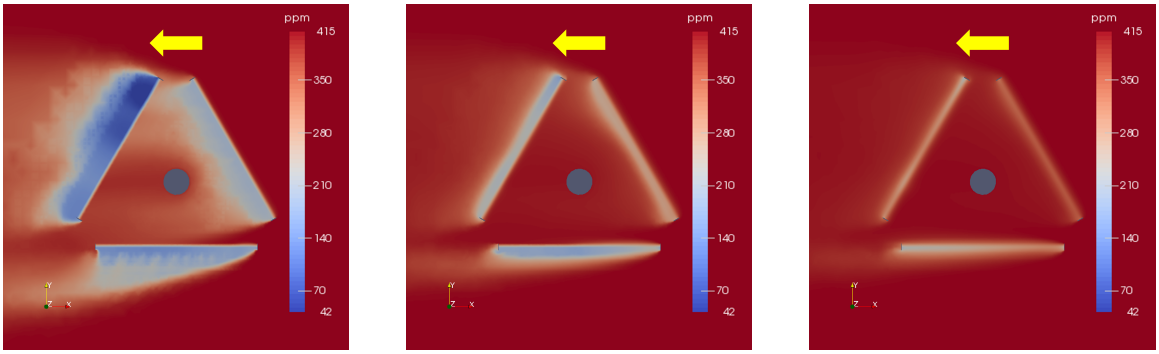

(a) (b) (c)

Figure A.10: CFD result showing dispersion of CO2 at 90°at a) cut in wind speed (3 m/s), b)rated wind speed (10.59m/s), and c)cut-out wind speed (25m/s). Wind direction shown with yellow arrow. Shown projected on the top plane (x-y plane) through the center of the air contactor bank, at height z = 17.9m as shown in figure A.7.

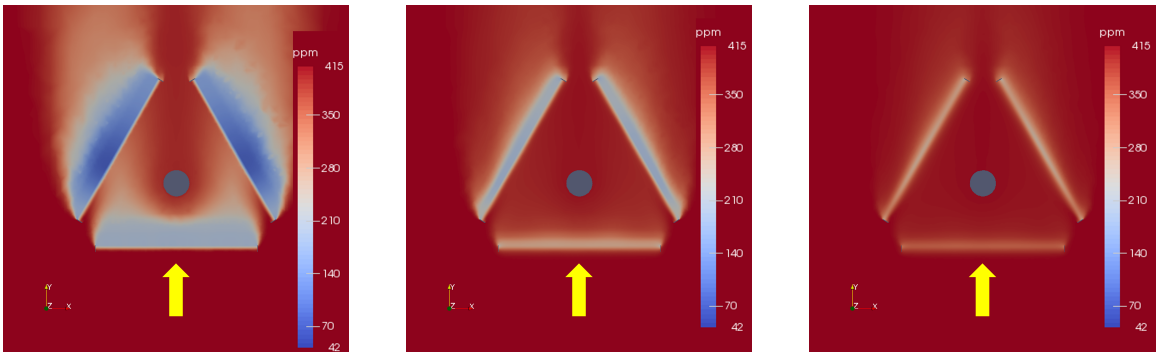

(a) (b) (c)

Figure A.11: CFD result showing dispersion of CO2 at 180°at a) cut in wind speed (3 m/s), b)rated wind speed (10.59m/s), and c)cut-out wind speed (25m/s). Wind direction shown with yellow arrow. Shown projected on the top plane (x-y plane) through the center of the air contactor bank, at height z = 17.9m as shown in figure A.7.

3D CFD result background: Concentration unit conversion sample calculation

Concentration (c) of passive scalars can be stated in any units. Atmospheric concentrations are typically described in parts per million (ppm). Using units for c of mg/m^3 made simulation setup much more straightforward. A sample calculation for conversion from ppm to mg/m^3 is shown below:

The unit ppm, represents 1 part CO_2 (moles) per million parts (moles) air. This is represented as follows:

$$\text{ppm-CO}_2 = \frac{1 \text{ mols-}CO_2}{1 \times 10^6 \text{ mols-air}}$$

Using this relationship, we can cancel units to compute the concentration, c, from ppm into mg-CO_2/m^3. We assume that air density, $\rho_{air} = 1.204 kg/m^3$ at 20 °C, and the molar mass of air, $M_{air} = 28.97$g/mol [118].

$$c = \frac{414.72 \text{ mols-}CO_2}{1 \times 10^6 \text{ mols-air}} \cdot \frac{44.01\text{g-}CO_2}{1 \text{ mol-CO}_2} \cdot \frac{1 \text{ mol-air}}{28.97\text{g-air}} \cdot \frac{1000\text{g-air}}{1\text{kg-air}} \cdot \frac{1.204\text{kg-air}}{1m^3\text{-air}} \cdot \frac{1000\text{mg-CO}_2}{1\text{g-CO}_2}$$

$$c = 758.55\text{mg-}CO_2/m^3\text{-air}$$

3D CFD result: ABL velocity profile in empty domain

Developing a homogeneous Atmospheric boundary layer (ABL) profile is key to ensuring accurate CFD results for large external domain. Shown in fig. A.12, is a simulation run with no obstacles present. This highlights that a homogeneous ABL profile was obtained.

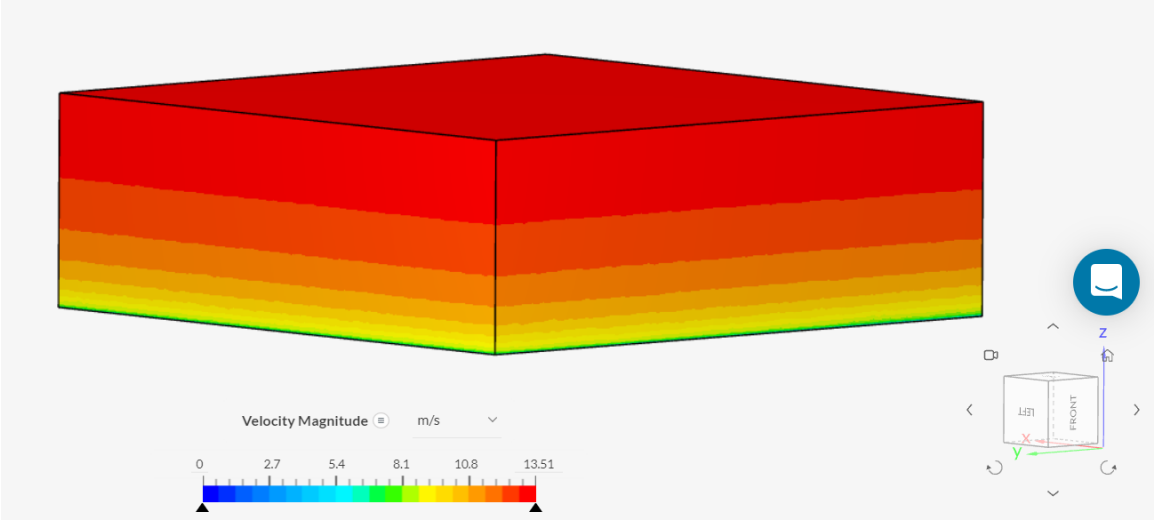

Figure A.12: ABL velocity profile applied to an empty domain to verify horizontal homogeneity

Energy model setup: Plant operating parameters

Table A.4 summarizes the constant design operating conditions used in the plant analysis. These parameters are used in the energy modelling section, within the isotherm method proposed.

Design operating parameter	Value	Units
T_{ads}	293.15	K
T_{des}	368.15	K
p_{des}	0.005	MPa
RH	66	%
η_{s,CO_2}	57	%
η_{s,H_2O}	55	%

Table A.4: Plant wide constant design operating parameters

Here, T_{ads} is the adsorption temperature, T_{des} is the desorption temperature, p_{des} is the desorption pressure, RH is the relative humidity, and η_{s,CO_2} and η_{s,H_2O} are the solid efficiency of the process. The solid efficiency shows the approach of working capacity, or in other words the actual adsorption encountered, to the equilibrium working capacity. This method is outlined further by Bos et al. [33], and Yu et al. [130].

Energy model setup: Isotherm method- Equilibrium loading capacities

Equilibrium loading capacities The equilibrium loading capacities, Δq_{CO_2} and Δq_{H_2O} of the sorbents are calculated using experimental data fitted using Langmuir isotherm models. The sorbent chosen for analysis in this study is the APDES-NFC sorbent, which has seen significant experimental work, and includes isotherms for CO_2 and H_2O, in both dry and humid conditions. H_2O loading is first calculated using the Guggenhein-Anderson de Boer (GAB) shown in equation A.5, and CO_2 adsorption is described using a modified version of the Toth isotherm equation shown in equation A.10. The calculation of the equilibrium capacities for each is discussed in the following paragraphs.

H_2O loading The H_2O loading is described using the GAB to model q_{H_2O} as a function of relative humidity (RH) shown in eq. (A.5). RH is the ratio between the partial pressure of water (p_{H_2O}), and the saturated vapor pressure of water described by eqs. (A.14) and (A.16). H_2O adsorption parameters from Wurzbacher et

al [53] were used in this analysis, with GAB isotherm model parameters summarized table A.5.

$$q_{H_2O}(RH) = C_m \frac{C_G K_{ads} RH}{(1 - K_{ads} RH)\,(1 + (C_G - 1)\,K_{ads} RH)} \tag{A.5}$$

GAB Parameter	Value	Units
C_G	0.1489	-
K_{ads}	0.5751	-
C_m	36.48	mol/kg

Table A.5: GAB H_2O isotherm parameters from Stampi-Bombelli et al. [50]

CO_2 loading The CO_2 equilibrium capacity is modelled using previous fitted values of the modified Toth model completed by Stampi-Bombelli et al. [50], with parameters from experimental studies by Wurzbacher et al [47, 53]. The loading is a function of CO_2 partial pressure during adsorption, $p_{CO_2,ads}$, and desorption, $p_{CO_2,des}$ described in the following paragraph. The enhancing effect of water on CO_2 adsorption is captured by embedding the water isotherm directly in the CO_2 isotherm. The traditional Toth isotherm is described in eqs. (A.6) to (A.9).

$$q_{CO_2}(p_{CO_2}, T) = \left[\frac{n_s b p_{CO_2}}{\left(1 + (b p_{CO_2})^t\right)^{1/t}} \right] \tag{A.6}$$

$$n_s(T) = n_{s0} exp\left[\chi \left(1 - \frac{T_0}{T} \right) \right] \tag{A.7}$$

$$b(T) = b_0 exp\left[\frac{\Delta H}{R T_0} \left(\frac{T_0}{T} - 1 \right) \right] \tag{A.8}$$

$$t(T) = t_0 + \alpha \left(1 - \frac{T_0}{T} \right) \tag{A.9}$$

The CO_2 loading capacity is enhanced by increased water uptake, however, multi-component isotherms are not available in literature for the sorbents at hand. Majority

of literature to date has ignored this phenomenon, however, it has a significant impact on the overall energy demand and capture capacity of a plant. Various methods have been presented in literature to capture the enhancing effect with the presence of increased humidity. Wurzbacher et al [53] used an enhancing factor to increase the equilibrium loading based on empirical results, however, this was only accurate within a small range of values, and produced errors beyond the bounds of the experiments. Stampi-Bombelli improved this by embedding the water loading within the CO_2 isotherm. The methods of Stampi-Bombelli are used in the current analysis shown in eqs. (A.10) to (A.12).

$$q_{CO_2}(T, P_{CO_2}, q_{H_2O}) = n_s(T, q_{H_2O}) \frac{b(T, q_{H_2O}) p_{CO_2}}{\left[1 + \left(b(T, q_{H_2O}) p_{CO_2}\right)^{t(T)}\right]^{1/t(T)}} \tag{A.10}$$

$$n_s(T, q_{H_2O}) = n_s(T) \left[\frac{1}{1 - \gamma q_{H_2O}}\right] \tag{A.11}$$

$$b(T, q_{H_2O}) = b(T) \left(1 + \beta q_{H_2O}\right) \tag{A.12}$$

The modified Toth parameters used in this study are summarized in table A.6 below.

Toth Parameter	Value	Units
T_0	296	K
b_0	7.074×10^8	1/MPa
ΔH	-5.7047×10^4	J/mol
t_0	0.4148	-
α	-1.606	-
n_{s0}	2.38	mol/kg
X	0.0	-
γ	0.0061	kg/mol
β	28.907	kg/mol

Table A.6: Modified Toth CO_2 isotherm parameters from Stampi-Bombelli et al. [50]

Computing composition during adsorption and desorption The isotherm models discussed above require the partial pressure of gasses, as well as the temperature of the process. The partial pressure of each species can be computed for adsorption and desorption.

To find the adsorption concentrations as a partial pressure, equation A.13 and equation A.14 are used.

$$P_{CO_2,ads} = \frac{c_{CO_2}}{p_0 \cdot 1 \times 10^6} = \frac{400ppm}{101325\text{Pa} \cdot 1 \times 10^6} = 40.53\text{Pa} \tag{A.13}$$

$$RH = \frac{P_{H_2O,ads}}{P_{H_2O,sat}} \cdot 100\% \Longrightarrow P_{H_2O,ads} = \frac{RH \cdot P_{H_2O,sat}}{100} \tag{A.14}$$

Here $P_{H_2O,sat}$ is the saturated water vapor pressure which can be found from Psychrometric tables for moist air [131]. At 25 °C, $P_{H_2O,sat}$ is 3167 Pa.

To obtain the partial pressure during desorption, it is assumed that all the CO_2 and H_2O that is adsorbed will be desorbed. The purity is between 94-99%, with water being the main impurity. This means that once the adsorption capacity ($q_{ads,i}$), for both CO_2 and H_2O are known, the desorption composition (ie. partial pressures of CO_2 and H_2O) can be computed. It is important to note that during the desorption phase, the chamber is under vacuum conditions so Daltons law of partial pressures is used, expressed in equation A.15 and equation A.16.

$$p_{total} = p_{gas,1} + p_{gas,2} + ...p_{gas,n} \tag{A.15}$$

$$p_{gas,i} = x_i p_{total} \tag{A.16}$$

Where p_{total} is the total pressure of the chamber, $p_{gas,i}$ is the partial pressure of each species, and x_i is the mole fraction of the respective species.

Based on the assumption that all CO_2 and H_20 adsorbed will be subsequently desorbed allows for the solving of the number of moles of each species, then to the mole fraction, and finally the partial pressures using equation A.17.

$$n_{i,ads} = q_{i,ads} \cdot m_{sorbent} \tag{A.17}$$

$$n_{total} = \sum_{i}^{n} n_{i,ads} \tag{A.18}$$

$$x_i = \frac{n_{i,ads}}{n_{total}} \tag{A.19}$$

Heat of reaction The isoteric heat of adsorption can be calculated from the Van't Hoff equation, also known as the Clausius-Clapeyron equation, as per the work of gebald et al. [42], shown in equation A.20. They derive specific equations for the heat of adsorption for CO_2 and H_2O as a function of the Toth and GAB parameters. Here, a relationship based on the partial pressures during adsorption and desorption is used shown in equation A.21.

$$\left(\frac{\partial(ln(p_{CO_2}))}{\partial T}\right)_{q_{eq}} = \frac{-\Delta H_{iso}}{RT^2} \tag{A.20}$$

This can also be written in in the form as per equation A.21.

$$ln\left(\frac{p_2}{p_1}\right) = \frac{\Delta H_{iso}}{R}\left(\frac{T_2 - T_1}{T_1 T_2}\right) \tag{A.21}$$

Here, state 2 is desorption, state 1 is adsorption, and p is the partial pressure at each state, R is the universal gas constant, and T is the temperature at each state. The heat of adsorption, ΔH_{iso}, can be solved for both CO_2 and H_2O using equation A.21.

Adsorbed H_2O undergoes condensation, so the resulting heat of reaction for H_2O (ΔH_{H_2O}) is the sum of the isoteric heat of reaction ($\Delta H_{iso,CO_2}$) and the heat of vaporization (ΔH_{vap}) as shown in equation A.22. The heat of vaporization can be interpolated from the heat of vaporization versus temperature chart [132].

$$\Delta H_{H_2O} = \Delta H_{iso,H_2O} + \Delta H_{vap} \tag{A.22}$$

Appendix B

Sorbent physical properties

Described in the following tables are the physical properties of four solid sorbents of interest adapted from Sabatino et al. [35]. These values are used to calculate the pressure drop through a an air contactor comprised of horizontal sheets of packed spherical particles. 2D computational fluid dynamics was used to determine the pressure drop by applying a fixed coefficient porous media model, and solving for the coefficients by comparing terms with the Ergun equation.

	APDES-NFC	Tri-PE-MCM	MIL-101(Cr)-PEI-800	Lewatit VP OC 106
μ	1.813×10^{-5}	1.813×10^{-5}	1.813×10^{-5}	1.813×10^{-5}
D_p	1.3×10^{-3}	1×10^{-3}	9.96×10^{-4}	6.88×10^{-4}
ϵ	0.6	0.6	0.6	0.6
ρ	1.204	1.204	1.204	1.204

Table B.1: Physical properties of sorbents to determine pressure drop through solid sorbent air contactor.

where μ is the dynamic viscosity$[kg/m \cdot s]$, D_p the particle diameter [m], ϵ the void fraction, and ρ is the fluid density [kg/m^3]. At 20°C, $\rho_{air} = 1.204\ kg/m^3$.

SS DAC- Equilibrium adsorption isotherms

The equilibrium adsorption capacity Δq_i for CO_2 and H_2O is the difference between the amount adsorbed during adsorption and desorption. The adsorbed quantity can

be computed using the Toth isotherm model, the modified Toth isotherm model, and the GAB model below:

The steady state Toth equilibrium equations are described below. Equation B.1 describes the equilibrium loading of CO_2 during adsorption and desorption.

$$q_i(p,T) = \left[\frac{n_s b p_i}{\left(1+(bp_i)^t\right)^{1/t}}\right] \tag{B.1}$$

with

$$n_s(T) = n_{s0} exp\left[\chi\left(1-\frac{T_0}{T}\right)\right] \tag{B.2}$$

$$b(T) = b_0 exp\left[\frac{\Delta H}{RT_0}\left(\frac{T_0}{T}-1\right)\right] \tag{B.3}$$

$$t(T) = t_0 + \alpha\left(1-\frac{T_0}{T}\right) \tag{B.4}$$

The modified Toth equations from Stampi-bombelli et al. [50] are shown below:

$$q_{CO_2}(T,p_{CO_2},q_{H_2O}) = n_s(T,q_{H_2O})\frac{b(T,q_{H_2O})p_{CO_2}}{\left[1+\left(b(T,q_{H_2O})p_{CO_2}\right)^{t(T)}\right]^{1/t(T)}} \tag{B.5}$$

with

$$n_s(T,q_{H_2O}) = n_s(T)\left[\frac{1}{1-\gamma q_{H_2O}}\right] \tag{B.6}$$

$$b(T,q_{H_2O}) = b(T)\left(1+\beta q_{H_2O}\right) \tag{B.7}$$

The GAB equations are described below:

$$q_{H_2O}(RH) = c_m \frac{c_G K_{ads} RH}{\left(1-K_{ads}RH\right)\left(1+\left(C_G-1\right)K_{ads}RH\right)} \tag{B.8}$$

with

$$C_G(T) = C_{G,0} exp\left(\frac{\Delta H_C}{RT}\right) \tag{B.9}$$

$$K_{ads}(T) = K_0 exp\left(\frac{\Delta H_K}{RT}\right) \tag{B.10}$$

$$C_m(T) = C_{m,0} exp\left(\frac{\beta}{T}\right) \tag{B.11}$$

SS DAC- Dynamic energy modelling

The following common dynamic adsorption models for CO_2 on amine based capture materials are summarized by Bos et al. [46].

Pseudo-first order LDF model:

$$\frac{\delta q}{\delta t} = k_{LDF1} p_{CO_2} (q_e - q) \tag{B.12}$$

Pseudo-second order LDF model:

$$\frac{\delta q}{\delta t} = k_{LDF2} p_{CO_2} (q_e - q)^2 \tag{B.13}$$

Toth rate equation:

$$\frac{\delta q}{\delta t} = k_{toth} \left[p_{CO_2} \left[1 - \left(\frac{q}{q_s}\right)^{t_h} \right]^{\frac{1}{t_h}} - \frac{1}{b}\frac{q}{q_s} \right] \tag{B.14}$$